UNIVERSITY OF OKLAHOMA

GRADUATE COLLEGE

HOT SURFACE IGNITION PROPERTIES OF PRE-VAPORIZED JET-A AND BIODIESELS

A THESIS

SUBMITTED TO THE GRADUATE FACULTY

in partial fulfillment of the requirements for the

Degree of

MASTER OF SCIENCE

By

ALEXANDER SPENS
Norman, Oklahoma
2017

HOT SURFACE IGNITION PROPERTIES OF PRE-VAPORIZED JET-A AND BIODIESELS

A THESIS APPROVED FOR THE
SCHOOL OF AEROSPACE AND MECHANICAL ENGINEERING

BY

_____
Dr. Ramkumar Parthasarathy, Co-Chair

_____
Dr. Subramanyam Gollahalli, Co-Chair

_____
Dr. Jivtesh Garg

I dedicate this thesis to my friends and family,

in appreciation for their company and support.

"For once you have tasted flight

you will walk the earth with your eyes turned skywards,

for there you have been

and there you will long to return."

Leonardo da Vinci

Acknowledgements

Many people helped get me to this point, and I would like to thank a few of them in particular and give them recognition.

First, I would like to thank Dr. Parthasarathy and Dr. Gollahalli for their aid and mentoring. This would not be possible without their support and guidance. I would also like to thank Dr. Garg for taking the time to be a part of my thesis committee.

Next, I would like to thank those who worked with me, building and running the setup: Scott Carter, for his initial construction of the system; Jesse Harter, for his aid in completing the setup and running of the first experiments; James Icenogle and Johnathan McClary, for their assistance gathering and analyzing data as well as perfecting the procedures; and Bach Duong, for continuing to use the setup with new fuels. A thank you also goes out to the aerospace and mechanical engineering machine shop at OU for their assistance in the construction and maintenance of the setup.

I would like to thank my lab mates, Arun Balakrishnan, Flavio Moreno, and Tonči Maleta for their humor, knowledge, and assistance during research. I enjoyed our many insightful discussions on all topics, both in and out of the lab.

A special thanks as well to Kristen Baird, for her help with proofreading and her encouragement.

Finally, I would like to thank my parents, Bill and Fabiola, for their love and support. As well as my brother, Nick, for always providing me with a challenge and competition.

Table of Contents

Acknowledgements iv

Table of Contents v

List of Tables viii

List of Figures ix

Abstract xiii

Chapter 1: Introduction 1

Chapter 2: Literature Review 4

2.1 Spark Ignition 4

2.2 Hot Surface / Wire / Gas Ignition 10

2.3 Biofuels and Traditional Fuel Comparisons 20

2.4 Current Research Objectives 23

Chapter 3: Experimental Setup and Measurements 24

3.1 Experimental Setup 24

3.1.1 Combustion Chamber 25

3.1.2 Ignitor 27

3.1.3 Air/Fuel Delivery System 28

3.2 Data Collection and Analyzation 30

3.2.1 Power and Energy Measurements 31

3.2.2 Mixture Temperature Measurements 33

3.2.3 Surface Temperature Measurements 35

3.2.4 Flame Front Velocity Measurements 36

3.2.5 Other Measurements 38
3.2.6 Uncertainties 39
3.3 Test Procedures 39
3.3.1 Heat-Up Phase 39
3.3.2 Filling Phase 40
3.3.3 Ignition Phase 41
3.3.4 Reset Phase 41
3.3.5 Periodic Procedures and Maintenance 42
3.4 Calibrations 42
3.4.1 Filling Time 42
3.4.2 Airflow Rate 43
3.5 Testing Conditions 43
3.5.1 Fuels and Equivalence Ratios Tested 43
3.5.2 Other Conditions 44
Chapter 4: Results and Discussion 56
4.1 Setup Calibration 56
4.1.1 Ignitor Temperature Calibration 56
4.1.2 Filling Duration 57
4.1.3 Airflow Rates 58
4.2 Example Data and Calculations 58
4.2.1 Example Data 58

4.2.2 Example Calculations 61

4.3 Setup verification 63

4.3.1 Ignition Temperature 63

4.3.2 Flame Velocities 64

4.3.3 Ignition Energy Trends 65

4.4 Results and Discussion 66

4.4.1 General Observations 66

4.4.2 Lower Flame Front Velocity 67

4.4.3 Upper Flame Front Velocity 68

4.4.4 Ignition Temperature 69

4.4.5 Time Interval for Ignition and Measured Ignition Energy 70

4.4.6 Adjusted Ignition Energy 72

4.4.7 Ignition Energy Discussion 72

Chapter 5: Summary and Conclusions 114

5.1 Recommendations 115

References 117

Appendix A: Nomenclature 120

List of Tables

Table 3.1: Equipment used 44

Table 3.2: Basic fuel properties 44

Table 3.3: Typical estimated experimental uncertainties 44

Table 3.4: Fuel flow rates for varying equivalence ratios 45

Table 4.1: Flame and ember velocities at various equivalence ratios for a trial of Jet A74

Table 4.2: Physical and thermal properties of Jet A/air mixtures at 670 K..... 75

Table 4.3: Physical and thermal properties of CME/air mixtures at 670 K 75

Table 4.4: Physical and thermal properties of SME/air mixtures at 670 K..... 76

Table 4.5: Physical and thermal properties of PME/air mixtures at 670 K..... 76

List of Figures

Figure 1.1: Total U.S. greenhouse gas emissions by sector in 2014 (United States Emvironmental Protection Agency, 2017) 3

Figure 3.1: Images of the setup 46

Figure 3.2: Images of the setup from the point of view of the high speed camera 47

Figure 3.3: Combustion chamber and tubing diagram 48

Figure 3.4: Combustion chamber diagram 49

Figure 3.5: Image of diffuser plate 50

Figure 3.6: Ignitor Schematic 51

Figure 3.7: Images of the ignitor mount and combustion chamber thermocouples 52

Figure 3.8: Air/fuel delivery system diagram 53

Figure 3.9: System diagram 54

Figure 3.10: LabVIEW and high speed camera user interfaces 55

Figure 4.1: Ignitor current at various temperatures 77

Figure 4.2: Ignitor temperatures as a function of current and change in current with time 78

Figure 4.3: Ignitor temperature varying with time 79

Figure 4.4: Adjusted ignition energy for Jet A, equivalence ratio 1.00, for varying fueling times at a fueling airflow rate of 30.3 L/min 80

Figure 4.5: Adjusted ignition energy for Jet A, equivalence ratio 1.00, for varying fuel times at a fueling airflow rate of 24 L/min 81

Figure 4.6: Temperatures recorded from a complete trial of Jet A at an equivalence ratio of 1.00 82

Figure 4.7: Temperatures during the fueling and ignition phases of a trial of Jet A at an equivalence ratio of 1.00 83
Figure 4.8: Temperature during the ignition phase of a trial of Jet A at an equivalence ratio of 1.00 84
Figure 4.9: Images captured by the high speed camera during a trial of Jet A at an equivalence ratio of 1.00 85
Figure 4.10: Ember position with respect to frame number for an ember in a trial of Jet A at an equivalence ratio of 1.00 86
Figure 4.11: Plot of Jet A ignition temperature with respect to equivalence ratio 87
Figure 4.12: Variation in ignition temperature with ignitor size, Kuchta et al. (1965) .. 88
Figure 4.13: Upper and lower flame front velocities of Jet A at various equivalence ratios 89
Figure 4.14: Flame velocity data for n-hexane as measured by Boettcher (2012) 90
Figure 4.15: Normalized ignition energy of Jet A for the current study and Lee (2001) 91
Figure 4.16: Flames of Jet A, CME, SME, and PME, at an equivalence ratio of 1.3 92
Figure 4.17: Images of Jet A flames at various equivalence ratios 93
Figure 4.18: Images of CME flames at various equivalence ratios 94
Figure 4.19: Images of SME flames at various equivalence ratios 95
Figure 4.20: Images of PME flames at various equivalence ratios 96
Figure 4.21: Residue left behind by CME, SME, and PME 97
Figure 4.22: Images of Jet A flame at an equivalence ratio of 1.3 98
Figure 4.23: Images of CME flame at an equivalence ratio of 1.3 99
Figure 4.24: Images of SME flame at an equivalence ratio of 1.3 100

Figure 4.25: Images of PME flame at an equivalence ratio of 1.3 101
Figure 4.26: Lower flame front velocity with respect to equivalence ratio for all tested fuels 102
Figure 4.27: Lower flame front velocities of CME and SME 103
Figure 4.28: Upper flame front velocity with respect to equivalence ratio for all tested fuels 104
Figure 4.29: Images of sparks following the flame of Jet A at an equivalence ratio of 1.4 105
Figure 4.30: Ignition temperature with respect to equivalence ratio for all tested fuels 106
Figure 4.31: Time interval for ignition with respect to equivalence ratio for all tested fuels 107
Figure 4.32: Measured ignition energy with respect to equivalence ratio for all tested fuels 108
Figure 4.33: Initial mixture temperature with respect to equivalence ratio for all tested fuels 109
Figure 4.34: Initial ignitor temperature with respect to equivalence ratio for all tested fuels 110
Figure 4.35: Adjusted ignition energy plotted with respect to equivalence ratio for all tested fuels 111
Figure 4.36: Equivalence ratio at which ignition energy is at a minimum, plotted with respect to the number of carbon atoms in the fuel for various fuels, from Lewis and von Elbe (1961) and Lee et al. (2001) data 112

Figure 4.37: Representation of the mixture temperature with respect to distance from the ignitor, for various ignitor temperatures at x=0..... 113

Abstract

In the search for more environmentally friendly energy sources, biofuels have emerged as an attractive alternative to traditional petroleum fuels. In addition to being close to carbon-neutral and renewable, biofuels have similar properties to traditional hydrocarbon fuels, allowing them to be implemented in existing combustion engines with few changes to either the engines or supporting infrastructure. The fundamental ignition properties of petroleum fuels are reasonably understood. Although the engine properties such as ignition delay and pollutant emissions have been studied for biofuels, their fundamental ignition properties of these biofuels are still unknown. Studies of the fundamental ignition properties of biofuels are important for the safety and handling of these fuels. The objective of this study was to compare the fundamental hot surface ignition properties of biofuels relative to petroleum fuels. Properties included in this study are: ignition energy, time interval for ignition, ignition surface temperature, and flame front velocities. The fuels studied were Jet A, as the petroleum fuel, and canola methyl ester (CME), soy methyl ester (SME), and palm methyl ester (PME), as the biofuels/biodiesels. Equivalence ratios of 0.75 through 2.00 were examined for each fuel. The fuels were studied as pre-vaporized mixtures in stagnant, constant pressure and constant volume conditions. The combustion chamber was approximately 1.56 L in size with a 5 cm by 23 cm window on one side and heated walls to prevent fuel condensation. A commercially available silicon carbide dryer ignitor was used as an ignition source and was located in the center of the combustion chamber. A high speed camera recorded the propagation of the flame following ignition, allowing for the calculation of the flame front velocity. K-type thermocouples measured the temperature of the mixture at selected

points inside the combustion chamber. A current transformer, shunt resistor, and voltage meter were used to calculate the current and power supplied to the ignitor, which could then be used to calculate the ignitor temperature and ignition energy. The setup can be used to study the relative differences in ignition properties of pre-vaporized fuel/air mixtures.

Both Jet A and the biofuel flames were blue in color across all equivalence ratios. Equivalence ratios near 1.3 produced the brightest flames, while equivalence ratios near 0.5 and 2.0 produced dim flames which propagated slowly. The ignitor temperature increased linearly at a rate of 110 K/s. Ignition temperature of the fuel/air mixture was determined to be nearly constant at 630°C for all examined equivalence ratios and fuels. Ignition energy was found to be six orders of magnitude greater than that in spark ignition energies due to thermal energy diffusion, aided by natural convection effects and a larger volume of mixture to heat near the ignitor. The ignition energies and time intervals of ignition of the biodiesel fuels were comparable to that of Jet A, and decreased with increased equivalence ratios. Flame velocities peaked near an equivalence ratio of 1.3 for both Jet A and the biofuels. The flame velocities for CME, SME, and PME were only 70-83% of those of Jet A, in agreement with results found in literature.

Chapter 1: Introduction

Petroleum fuels provide 95% of the energy used by the transportation industry in the United States (Kahn, et al., 2007). Both internal combustion engines and gas turbines use these fuels for the moving of people and freight every day. Unfortunately, as displayed in Figure 1.1, the transportation industry is also a major contributor to climate change, responsible for 26% of all greenhouse gas emissions in the United States in 2014. Most of these harmful emissions come from combustion engines, which produce CO_2, a major contributor to climate change (United States Emvironmental Protection Agency, 2017). Traditionally, hydrocarbon fuels come from petroleum products obtained from beneath the earth's surface. However, this supply of fuels is limited. With the growing market of transportation and threat of climate change, alternative "greener" fuels are being sought after to power the world's transportation industry.

Biodiesels are created from the transesterification of vegetable or other crop oils. Biofuels, such as canola methyl ester (CME), soy methyl ester (SME), and palm methyl ester (PME), provide an attractive alternative to traditional fossil fuels because of their ability to be easily integrated into current infrastructure, without making extensive changes to combustion engines. Biofuels are also more environmentally friendly than traditional fuels through their ability to be close to carbon-neutral. By absorbing the carbon they emit during combustion in the crop growing process, the net release of carbon into the atmosphere is maintained at near-zero values.

As evidenced in literature review, the fundamental combustion properties of petroleum fuels have been well documented. However, the combustion properties of biofuels are still not well understood and form a topic of many new research studies in

the field. Ignition is a basic combustion parameter whose understanding will aid in the understanding of biofuel combustion.

Hot surface ignition has been thoroughly studied for hydrocarbon fuels by a variety of agencies and researchers. By using hot surfaces or wires as an ignition source, the temperature at which a fuel and air mixture ignites can be easily measured for a given ignitor setup. This is often used in determining safety parameters for transporting and handling a fuel, and to prevent unwanted fires in the event of a crash (Botteri, et al., 1979). The ignition energy can be determined by monitoring the energy provided to the ignitor. Flame velocities can be used to provide insight into the differences in the reaction rates and ignition energies between fuel types. By using pre-vaporized fuel, exact equivalence ratios can be determined and the differences between them observed. Stagnant, constant pressure and constant volume conditions eliminate a few of the many variables in the ignition process, helping to measure only the basic fundamental properties of a fuel.

Although the emissions of biodiesel flames have been extensively studied, many of the fundamental ignition properties are still unknown. Ignition temperature, energy, and delay, as well as flame velocities, are useful for designing reliable combustion engines as well as safety standards for the storage and transportation of biofuels. By designing a setup to study these properties, future work can also be performed on the properties of different biofuels and biofuel blends with traditional fuels.

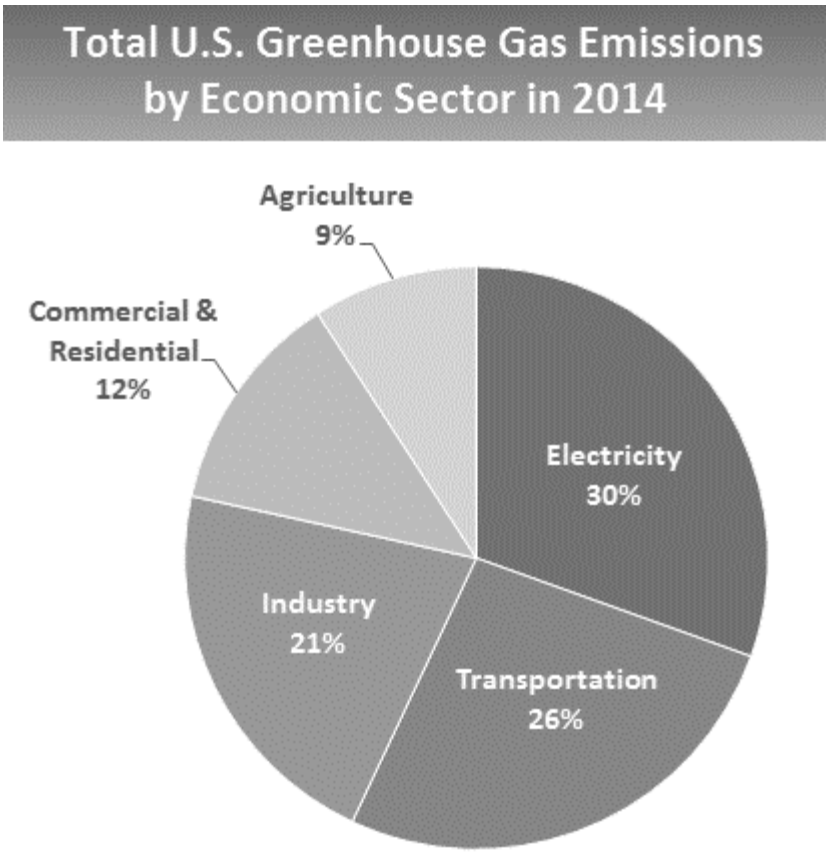

U.S. Environmental Protection Agency (2014).
U.S. Greenhouse Gas Inventory Report: 1990-2014.

Figure 1.1: Total U.S. greenhouse gas emissions by sector in 2014 (United States Emvironmental Protection Agency, 2017)

Chapter 2: Literature Review

This chapter reviews the past experimental research related to the combustion of hydrocarbons. Many ignition methods are covered, including: spark ignition by lasers and electrodes, hot surface, wire, and gas ignition, as well as shock tube ignition. Combustion is a complex phenomenon, and each of these ignition methods provides insight into the extent of which a mixture's characteristics and environment influence its combustion. Finally, the scope of this research is presented at the end of the chapter.

2.1 Spark Ignition

Spark ignition relies on a small, quick spark to initiate a mixture. These occur in practice both unintentionally, with fuel leaks near electronics, and intentionally with the spark plugs in an internal combustion engine. As such, it is important to know the amount of energy required for a spark to ignite a mixture. Differences in type of spark as well as fuel, equivalence ratio, and pressure can influence the amount of energy needed for a spark to create a sustainable ignition. There are two types of spark ignition methods covered in this section, electrode and laser sparks. Electrode sparks are created by maintaining a voltage difference across a short gap between two metal rods. The spark occurs when current arcs across them for a short period of time. Laser sparks require the use of a laser focused on a surface to create sparks, which in turn ignite the mixture.

Lewis and von Elbe (1961) measured the minimum ignition energies of methane and heptane type fuels using a capacitance discharge powered electrode spark. The bomb type combustion chamber had an inner diameter of 5 inches, and the electrodes were located at the center. Glass flanges of diameter 1 inch were added to the electrodes. The minimum ignition energy of natural gas (approximate composition 83% CH_4 and 17%

C_2H_6) and air was tested with varying electrode gap sizes. For a stoichiometric mixture of natural gas and air, at atmospheric pressure and a gap width of 0.01 inch, the required ignition energy was 8 mJ. For increasing gap widths up to the tested 0.09 inches, the ignition energy decreased, to 1 mJ. Various hydrocarbon type fuels (methane, ethane, propane, butane, hexane, and heptane) in air were also tested at various equivalence ratios. Each fuel had a parabolic relationship between equivalence ratio and ignition energy. The ignition energy was at a minimum for a certain equivalence ratio, and grew as the equivalence ratio increased or decreased. As the carbon chain length and molecular weight increased, the equivalence ratio of the absolute minimum ignition energy for a fuel also increased. Methane, with a carbon chain length of one, required a minimum of 0.3 mJ for ignition, at an equivalence ratio of 0.9. Heptane, with a larger carbon chain length of 7, required a minimum ignition energy of 0.9 mJ at an equivalence ratio of 1.8.

Between 1961 and 1991, spark ignition was continuously studied and of interest. Common topics focused on spark ignition in internal combustion engines, which were not relevant to the current study.

Ko et al. (1991) observed the spark ignition of propane at low equivalence ratios near minimum ignition energies. A bomb style constant volume combustion chamber of diameter 83 mm was filled with propane and air mixtures and ignited using 0.5 mm diameter spark electrodes. A laser schlieren system and high speed camera were used to observe the combustion. The gap between the electrodes was set between 0.5 and 2.0 mm and the spark power level and duration controlled. Propane and air mixtures of equivalence ratios 0.6 through 0.8 were tested. Decreasing the electrode gap distance from 2.0 mm to 0.5 mm caused a drastic increase in minimum ignition energy from 2.6

mJ to 35.0 mJ at the equivalence ratio of 0.7. Decreasing equivalence ratios from 0.8 to 0.7 (1 mm electrode gap) and from 0.7 to 0.6 (2 mm electrode gap) also caused an increase in minimum ignition energy, of 2.9 mJ and 54.4 mJ respectively. This was due to the large increase in kernel radius before an ignition would be self-sustaining. An increase in critical kernel radius required an increase in ignition energy as a larger amount of mixture needed to be heated. The spark ignition energies for propane were found to range between 2.6 and 57.0 mJ for varying electrode gap distances between 0.5 and 2 mm and equivalence ratios between 0.6 and 0.8.

Sheperd et al. (1999) examined the spark ignition characteristics of Jet A at low pressures and moderate heat, which simulated the conditions of an aircraft fuel tank at altitude. The combustion chamber consisted of a cube with a 14 cm side length and volume of 1.8 L. Circular windows were added to the front and back to allow the combustion to be visually observed and recorded using a schlieren method. Heating pads and thermocouples on the sides of the setup controlled the chamber temperature, while a K-type thermocouple measured the internal gaseous mixture temperature. The initial pressure was measured using a pressure transducer and the pressure rise was measured using a Kulite XT-190 gauge. Liquid fuel was injected through the top using a pipet. The electrodes consisted of two 3.2 mm diameter rods with rounded edges spaced 3.3 mm apart in the center of the chamber. The chamber temperature was varied between 20°C and 55°C. Two fuel loadings were used in the chamber corresponding to 3 kg of fuel per cubic meter and 200 kg of fuel per cubic meter. Estimates of the equivalence ratio were made using the vapor pressure of Jet A (Coordinating Research Council, 1983). For the fuel level corresponding to 3 kg/m^3, the spark minimum ignition energy decreased

exponentially from 100 J at an initial temperature of 30°C (estimated equivalence ratio of 0.77) to 2 mJ at an initial temperature of 55°C (estimated equivalence ratio of 2.8). Although the authors give no reason for the drop in ignition energy, it is likely that the change in equivalence ratio due to the temperature difference caused the decrease. The peak pressure was at a maximum of 4.5 bar at temperatures of 55°C. The burning speed, similar to flame velocity, increased as well with increasing temperature from 0.15 m/s at 40°C to 0.5 m/s at 55°C. Similar trends were noted for the fuel loading of 200 kg/m^3, with ignition energies decreasing from 20 J at a temperature of 35°C (estimated equivalence ratio of 1.0) to 1 mJ at temperatures of 55°C (estimated equivalence ratio of 2.8). The peak pressure reached a maximum of 4.2 bar at temperatures of 55°C. Additionally, the burning speed showed a linear increase with temperature, from 0.1 m/s at 35°C to 0.3 m/s at 55°C.

Phuoc and White (1999) investigated the laser-induced spark ignition of methane and air mixtures at atmospheric pressure and room temperature. A cylinder of inner diameter 62.5 mm and length 37.5 mm was used as the combustion chamber. The ends of the chamber were clear and allowed for a high speed camera to record the ignition process. Other measurements included the pressure of the mixture, using a piezoelectric transducer, as well as the ignition energy produced by the laser spark, measured with a pyroelectric energy meter. Fuel was injected via a needle valve, and pressures of the fuel and air during fueling were used to determine the mixture composition. A 5.5 ns laser pulse of wavelength 1064 nm was used to ignite the mixture. Ignition was achieved for mixtures with equivalence ratios between 0.61 and 1.95, with the minimum ignition energies of 3 mJ near an equivalence ratio of 1.3, and ignition energies of 40 mJ and 70

mJ for equivalence ratios of 0.61 and 1.95. Ignition energies varied with equivalence ratio parabolically, similar to the variation recorded by Lewis and von Elbe (1961), with minimum ignition energies of 3 to 4 mJ required for the ignition of equivalence ratios between 1.06 and 1.68. These minimum values for ignition energies were an order of magnitude higher than those reported by Lewis and von Elbe (1961) using electrode spark ignition methods. Laser sparks were theorized to require a higher ignition energy due to their shorter spark duration and more focused nature compared to electrode sparks. The shorter duration and more focused spark increased the thermal gradients within the mixture, which resulted in a quicker dissipation of energy, requiring a higher ignition energy. More extreme equivalence ratios, such as 0.66 and 1.95, required a large increase in minimum ignition energies, 40 mJ and 70 mJ respectively.

Lee et al. (2001) examined the minimum ignition energies of hydrocarbon fuels using laser-induced sparks. A 100 mm diameter by 270 mm length chamber was temperature and pressure controlled to simulate different equivalence ratios and atmospheric pressures. A 532 nm laser with a pulse duration of 10 ns was used to ignite the mixtures. Pyroelectric energy meters were used to measure the laser spark energy. The fuels tested were propane, dodecane, and Jet A. A method of partial pressures was used to fill the combustion chamber and determine the equivalence ratios of propane. For the liquid fuels, the fuel was first added to the chamber and then heated to various temperatures within 40°F of 114.8°F. The chamber was then evacuated to the desired pressure. For dodecane, phase-equilibrium calculations were used to make an estimate of the gaseous equivalence ratio. Jet A results were only reported as a function of temperature (relative to the flash point of 114.8F) and pressure. Estimates of the

equivalence ratio were made using the vapor pressure of Jet A (Coordinating Research Council, 1983). The minimum ignition energy of propane followed a parabolic trend with respect to equivalence ratio with a minimum of 0.6 mJ at a pressure of 1 atm and an equivalence ratio of 1.2. The ignition energy increased to 8 mJ at equivalence ratios of 0.6 and 2.0. These ignition energy values were a factor of 2 larger than the minimum ignition energy values reported by Lewis and von Elbe (1961) for electrode spark ignition under similar conditions. Differences between the two ignition energies were due to the size and duration of the sparks. The laser sparks were smaller and of shorter duration than the electrode sparks. As a result, higher ignition energies were required to overcome the diffusion of energy caused by the large temperature gradient created by smaller, quicker sparks. Dodecane had a similar parabolic trend as propane, with minimum ignition energy of 1 mJ at a pressure of 1 atm and an equivalence ratio of 3.5. The ignition energy of Jet A varied with temperature in a parabolic fashion as well. Minimum ignition energies of 2 mJ were recorded for all tested temperature values. As pressure increased, the temperature at which the ignition energy was at a minimum also increased, from 5°F below the flashpoint at 0.4 atm (estimated equivalence ratio of 1.8) to 25°F above the flashpoint at 1 atm (estimated equivalence ratio of 1.98). Higher temperatures increased the vapor pressure of Jet A, increasing the equivalence ratio of the mixture. The increase in total pressure reduced the equivalence ratio of Jet A at a constant vapor pressure. To keep near the optimum equivalence ratio for minimum ignition energy, the temperature had to increase with increasing total pressure.

Many trends were consistent across various works. Both Lewis and von Elbe (1961) and Ko et al. (1991) noted that the energy required for electrode spark ignitions

depended heavily on the distance between the electrodes. As the gap between the electrodes increased, the minimum ignition energy decreased, due to smaller temperature gradients which reduced the thermal energy dissipation and a larger portion of the initial flame kernel being heated. The minimum ignition energy was also determined to be heavily dependent on the fuel equivalence ratio. Lewis and von Elbe (1961), Phuoc and White (1999), and Lee et al. (2001) observed a parabolic relationship (concave upward) between equivalence ratio and required ignition energy. Lewis and von Elbe (1961) noted that the equivalence ratio at which the ignition energy was at a minimum for a fuel was correlated to the length of the carbon chain, with longer carbon chains having a higher equivalence ratio for the minimum ignition energy.

2.2 Hot Surface / Wire / Gas Ignition

Hot surfaces, wires, and gases can ignite a mixture through direct contact. For safety reasons, it is important to know under what thermal conditions, similar to the conditions simulated by the hot surface, wire, and gas ignition methods, a fuel will ignite. Precautions can then be implemented in fuel tanks and near fuel lines to ensure that high temperature parts or exhaust gases will not come in contact with the fuel. The minimum temperature at which a fuel mixture will ignite in a setup with specific conditions is of interest for each type of heated surface. Hot surface ignition occurs through the heating of a relatively large surface in a fuel/air mixture, and is also used to determine the auto-ignition temperature of a fuel, the temperature at which the container or large surface must be to cause the fuel inside to ignite. During hotwire ignition, a thin wire or tube is heated and comes in contact with a fuel/oxidizer mixture inside a chamber, resulting in combustion. Hot gas ignition uses a high temperature gas to ignite a stream of vaporized

fuel and air. The ignition temperatures associated with each of these ignition methods varies depending on the exact conditions of fluid flow, equivalence ratio, size of the ignitor, as well as container surface temperatures.

Zabetakis et al. (1954) measured the minimum ignition temperature of various hydrocarbons in air under atmospheric conditions, using the hot surface ignition/auto-ignition method. A 1200 W electric crucible heater was used to heat a 200 cc Erlenmeyer flask to a desired temperature. Thermocouples located at various intervals along the flask ensured that there was a uniform temperature distribution, within 1°C. The flask was capped and fuel was injected using a syringe and needle. After fuel was injected, an electronic stopwatch was started, and stopped when ignition was observed visually, to determine ignition delay. If ignition did not occur within 5 minutes, the flask was emptied and cleaned out with dry air. The volume of the fuel added varied between 0.25 ml and 1.00 ml to determine the critical volume for minimum ignition temperature. The critical volume for each fuel was not reported in this paper. The spontaneous ignition temperature of the paraffin hydrocarbons was plotted with respect to the length of their carbon chains. It was found that longer carbon chains required a lower minimum temperature for ignition. Methane, with a chain length of 1, had an ignition temperature of 537°C, whereas n-hexadecane, with an average carbon chain length of 16, had an ignition temperature of 205°C. A similar trend was noticed for the paraffin hydrocarbons between ignition temperature and ignition delay. As the ignition temperature increased from 200°C to 300-400°C, the time lag before ignition decreased from 140 s to 5 s. The ignition temperature of JP-4 was reported at 1 atm to be 242°C with a time lag of 185 s.

Kuchta and Cato (1966) studied the hot gas ignition of hydrocarbon fuel vapor-air mixtures, including JP-6. The combustion chamber was constructed from a 4 inch diameter by 26 inch long Pyrex pipe. A ceramic tube wrapped in platinum-rhodium wire was used to heat the incoming air. The vapor-air mixture was added to the chamber via a mixing ring in a bed of ceramic beads, to aid with heating. The temperature of the inlet airflow was measured by a platinum-rhodium thermocouple located one-fourth of an inch above the base of the jet. The fuel vapor-air mixture temperature was measured with three evenly spaced chromel-alumel thermocouples. Various diameter jets were used, ranging from 1/8 inch to 1/2 inch. The ignition temperature was found to decrease with increasing jet diameter for all fuels tested. For JP-6, an ignition temperature of 1985°F was required for the 1/8 inch diameter jet, which decreased to 1290°F for the 3/4 inch diameter jet. High flow rates for the vapor air mixture, 365 in^3/min, and low jet flow rates, 185 in^3/min, proved to be optimal for ignition, preventing too much dilution from the jets. Varying fuel to air mass ratios above 0.3, maximum of 0.7, had little effect on the hot gas ignition temperatures of JP-6, or any of the other tested fuel. Fuel to air ratios below 0.3 resulted in approximately a 5% increase in ignition temperature. It was theorized that the unusually high fuel-to-air ratios were ignitable due to the dilution caused by the hot air jet. When compared to similar type setups with different ignition methods, hot gas ignition occurred at temperatures around 200°F higher than heated wire, and 300°F higher than ignition by heated vessels (Kuchta, et al., 1965). Differences in the ignition temperature between the hot gas and other ignition methods was predicted to be due to the differences in the length of the heated gas and wire, as well as a difference in actual ignition temperature and measured ignition temperature of the hot gas. A shorted hot gas

length, compared to the heated wire ignition, would require a larger ignition temperature. The hot gas temperature was measured at the base of the heated gas jet, the ignition occurred further along the gas jet, which would have resulted in a lower ignition temperature, more similar to that of the hot wire and hot vessel ignition temperatures.

Myronuk (1981) compared the hot surface ignition temperatures between various aircraft fuels subject to airflows. The outer surface of a 7.62 cm diameter by 1 meter long pipe, which heated internally by a propane flame, was used as the test surface. A fuel trough was formed by welding two smaller pipes axially on the upper surface of the tube. Airflow occurred axially and was provided by a blower which could produce airflows in the range of 0 to 50 m/s. 15 cc of fuel was applied to the surface via high pressure sprayers in bursts of 1 second. Thermocouples attached to the surface were used to determine the surface temperatures. Because highly volatile fuels would quickly vaporize and be carried away from the heated surface by the airstream before igniting, cavities and conics on the surface were used to provide a stagnation region and allow vaporized fuel to come in prolonged contact with the hot surface. Ignition delays were reported on the order of 1 to 2 seconds for each of the aircraft fuels tested (JP-4, JP-5, Jet A, Jet TS, Jet A with a variety of anti-misting agents). The ignition temperature for each of the fuels increased logarithmically as a function of air velocity. Jet A was found to have a minimum ignition temperature of 650°C at the minimum tested air velocity of 0.8 m/s. At the maximum tested airflow rate of 40 m/s, the ignition temperature of Jet A increased to 850°C. This trend was repeated for JP-4 and JP-5 as well, whose ignition temperatures increased 200 and 350°C respectively from air velocities of 0.8 to 40 m/s. The increase in ignition

temperature was reported to be due to a decrease in contact time between the mixture and hot surface at higher velocities.

Laurendeau (1982) studied the relationship between ignition temperature and ignitor orientation and size. Using data collected by Rae et al. on methane air combustion, it was determined that natural log of the hot surface ignition was proportional to the activation energy and inversely proportional to the surface ignition temperature. Laurendeau also noted that the reaction rate of a fuel was exponentially related to the initial fuel mass fraction and density of a mixture. Rae et al. (1964) examined the effect of ignitor size and orientation on the hot surface ignition temperature of a 6% methane and air mixture. Ignitors of various sized platinum squares, ranging in area from 10 mm^2 to 325 mm^2, were attached to various locations inside a combustion chamber, wall, floor, and roof. The temperature of the ignitor surface was measured with an optical pyrometer. The ignitor surface was uncovered for 1 second, requiring the ignition delay to be less than a second. As the surface area of the ignitor was increased from 10 mm^2 to 325 mm^2, the ignition temperature decreased from 1400°C to 1175°C. This was theorized to be due to the increased amount of the mixture in contact with the heated surface, decreasing the energy loss due to temperature gradients. Similarly, the ignitor position influenced the ignition temperature of the fuel. For an ignitor size of 325 mm^2, at a location of the wall, roof, and floor, the ignition temperature was approximately 1175°C, 1700°C, and 1060°C respectively. Differences between ignition temperatures at various locations was due to the orientation of the surface and buoyancy forces which moved the mixture away from the ignitor. For locations with higher buoyancy forces, such as the wall, the ignition

temperature needed to be larger to compensate for the thermal energy lost by natural convection.

Colwell and Reza (2005) compared hot surface ignition temperatures with the published auto-ignition temperatures of various aviation and automotive fuels and fluids. A pipette was used to release droplets of fuel onto a 48 cm by 38 cm, temperature-controlled hot plate below. The temperature of the hot surface was measured using a K-type thermocouple and ignition was determined visually. The procedure was repeated 200 times over a range of temperatures to obtain probabilities for ignition at each temperature. Each fuel had a 10% ignition probability of at least 100°C to 300°C above their auto-ignition temperature. Jet A specifically had an auto-ignition temperature of 250°C and a hot surface ignition temperature ranging from 10% ignition probability at 550°C to 90% probable at 600°C.

The above studies indicate that hotwire ignition of a fuel involves a number of variables including wire dimensions, initial temperature and pressure, fuel-to-air ratio, and outer container temperature. Due to the many variables involved with hotwire ignition, many studies have focused on determining ways to generally classify or predict hotwire ignition temperatures based on ignitor size or container volume ratios. Kuchta and coworkers attempted to bridge the knowledge between hotwire ignition and hot surface ignition using these correlations with ignitor/hot surface size (Kuchta, et al., 1965).

Kuchta et al. (1965) examined the effect of heat source dimensions on hot surface and hotwire ignition of hydrocarbon fuel vapors and air. The hot surface containers were cylinders 15 cm long, and radii varying between 0.4 and 1.75 cm, along with spheres

varying between radii of 1.0 to 3.7 cm. These containers were placed in a modified auto-ignition setup used by Zabetakis (1954). Ignition tests were carried out at atmospheric pressure and ignition was determined visually. Fuels tested included n-hexane, n-octane, n-decane, JP-6, and an aircraft engine oil. The auto-ignition temperature was found to decrease with the molecular weight of the fuel, from 509°C for n-hexane with a molecular weight of 86 g/mol to 427°C for n-decane with a molecular weight of 142 g/mol in a sphere of volume 10 cm^3. Although the authors gave no explanation for this trend, they noted that it was similar to the relationship between auto-ignition temperature and fuel molecular weight. Each fuel was also found to have a decreased auto-ignition temperature with a decreased surface to volume ratio. This was expected because the heat loss depends on the wall surface area, while the amount of thermal energy required to heat the mixture to auto-ignition temperature is related to the volume. Vessels with a smaller surface area to volume ratio will lose less energy through the walls and require less thermal energy to reach the auto-ignition point. For JP-6 in the cylindrical container, the surface area to volume ratio decreased from 5.15 cm^{-1} to 1.25 cm^{-1} the ignition temperature decreased from 596°C to 242°C.

Changes in the ignitor size were also examined using a hotwire/surface ignition setup. A cylinder of inner diameter of 5 cm and length 20 cm was attached to a heated fuel and air inlet. The case was also heated to 150°C as measured by surface thermocouples. A hot nichrome wire, tube, or inconel tube were used as the ignitors. Ignitor radii ranged from 0.02 cm to 1.27 cm with a length of 5 cm. An optical pyrometer measured the temperature of the wires, while surface thermocouples measured the temperatures of the tubes. Two K-type thermocouples monitored the mixture temperature

2.5 cm above and below the ignitor. Initial temperatures of 150°C and flow rates of 290 cc, or 0.35 to 0.45 cm/s, were used. Fuel to air weight ratios were varied from 0.05 to 0.5, although they were determined to have a negligible effect on the ignition temperature. The ignition temperature was found to decrease logarithmically as a function of the increasing surface area of the heat source. Ignition was theorized to occur within the boundary layer of the ignitor. Larger boundary layers due to larger ignitors result in a lower required ignition temperature. As the surface area increased from 0.65 cm^2 to 40.5 cm^2, the ignition temperature of JP 6 decreased from 1026°C to 530°C.

Botteri et al. (1979) reviewed existing literature on the ignition of jet fuels. The ignition temperatures of vaporized Jet A in a heated sphere of radius 0.46 m with varying hot pipe ignitor sizes were reported (Macdonald and Cansdale, 1972) (Kuchta, et al., 1961). Ignition tests were carried out under atmospheric conditions with optimum fuel concentrations (actual fuel concentrations used were unreported). The ignition temperature of the fuel varied with both the pipe diameter and outer sphere temperature. As pipe diameter decreased from 152 mm to 19 mm, the ignition temperature increased, from 350°C to 700°C, for outer sphere temperatures of 25°C. Smaller pipe diameters were more influenced by changes to the outer sphere temperature. At outer sphere temperature of 200°C, the ignition temperature was 350°C for a pipe diameter of 19 mm, and 275°C for a pipe diameter of 152 mm. This difference in ignition temperatures with pipe diameter and sphere temperature was due to the temperature gradients created by the ignitor. At lower wall temperatures the heat produced by the ignitors more rapidly dissipates to the surrounding mixture due to large temperature gradients in the mixture. The smaller surface area on the smaller ignitor results in a larger required ignition

temperature, as studied previously by Kuchta and coworkers (Kuchta, et al., 1965). Higher sphere temperatures were closer to the ignitor temperature, which resulted in smaller temperature gradients throughout the mixture. Smaller temperature gradients reduced the rate of thermal energy flowing to the remainder of the mixture and away from the ignitor. As a result, the thin boundary layer near the ignitor could obtain a temperature closer to the ignitor temperature requiring a smaller ignition temperature for both sizes of ignitor.

Boettcher (2012) studied the hot surface ignition of n-hexane air mixtures in detail. The combustion chamber had a 2 L volume (11.4 cm x 11.4 cm x 17.1 cm), with windows on two sides to allow for a schlieren system to be used with a high speed camera to record the flame propagation following ignition. Two types of glow plugs were used as an ignition heat source: a specialized Bosh glow plug with a diameter of 3.1mm and a height of 6.9mm, and a commercial Autolite 1110 glow plug with a diameter of 5.1mm and a height of 9.3mm. Both glow plugs could reach a maximum temperature of approximately 1500 K. K-type thermocouples with 0.5 second response times were used to measure the top of the case as well as the glow plug temperatures. A pressure transducer on the top of the vessel measured the change in pressure during ignition. A partial pressures method was used to fill the initially evacuated chamber to the desired equivalence ratio and pressure. For equivalence ratios of 0.75 through 2.75, a near-constant temperature of 900 K was required to ignite the mixture. At equivalence ratios below 0.25 and above 2.75, the ignition temperature increased greatly to values near 1500 K, due to a closer proximity to the flammability limits of n-hexane. As the pressure in the chamber decreased from 101 kPa to 25 kPa, the ignition temperature increased from 925

K to 1100 K, for an equivalence ratio of 2.11. The flame velocities were determined for the top and sides using the images captured by the high speed camera and schlieren technique. The flame velocities reached a maximum at equivalence ratios of 1.2, with a top velocity of 5.5 m/s and the side velocities of 3.0 m/s. The top flame was theorized to have a higher velocity than the sides due to the convective flow in the plume above the glow plug. At a lower equivalence ratio of 0.75, the vertical velocity was 2.5 m/s and the horizontal velocity was 1 m/s. This was similar to the higher equivalence ratio, of 2.75, with velocities of 2.0 m/s in the vertical direction and 0.5 m/s in the horizontal. No reason was given for the difference in flame velocities between equivalence ratios except that it was expected based on models created by various other studies. A possible explanation for the flame velocity variation with equivalence ratio is that it is based on the reaction rates of the fuel air mixtures, with higher reaction rates resulting in a quicker flame velocities.

Most recently, Melguizo-Gavilanes et al. (2016) verified numerical models of hydrogen air glow plug ignitions at stoichiometric conditions. The 2 L volume (11.4 cm x 11.4 cm x 17.1 cm) rectangular prism combustion chamber setup was similar to that used by Boettcher (2012). The temperature field was measured using interferometry. A pyrometer was used to measure the temperature of the glow plug ignitor. Two ignitor heating profiles were tested, an 18 K/s ramp and a 190 K/s ramp. Three trials were conducted for each heating profile. The ignition temperature of the hydrogen air mixture was found to be 1052 K ± 52 K for the 18 K/s ramp, and 1028 K ± 53 K for the 190 K/s ramp.

Ignition temperature for hot surface and hotwire ignition was dependent on the fuel's molecular weight. Both Zabetakis et al. (1954) and Kuchta et al. (1965) noted that as the molecular weight of the fuel increased, the ignition temperature decreased. Similarly Kuchta et al. (1965), Kuchta and Cato (1966), and Botteri et al. (1979) noted that as the surface area or diameter of the ignition source was increased, the ignition temperature decreased. Unlike the fuel molecular weight or the ignitor size, the equivalence ratio or fuel to air ratio was observed by Kuchta et al. (1965), Kuchta and Cato (1966), and Boettcher (2012) to have negligible influence on the ignition temperature.

2.3 Biofuels and Traditional Fuel Comparisons

One of the main advantages of biofuels as an alternative energy source is their potential to directly replace existing hydrocarbon fuels without major changes to propulsion systems or other infrastructure. To determine what changes do need to be made, the differences between the ignition properties of traditional fuels and biofuels need to be studied.

An important property of compression ignition engines is the auto ignition temperature and ignition delay of a fuel. These properties can be characterized by the Cetane number of a fuel, which is a measure of a fuel's ignition delay and compression required for ignition. Larger Cetane numbers indicate a reduction in ignition delay in an internal combustion engine (Pulkrabek, 2004). Methyl ester biodiesels, similar to those used in the current study, were found to have higher Cetane numbers, 70-85, compared to diesel, 40, (Klopfenstein, 1985), decreasing their ignition delay and causing ignition

earlier in the engine cycle. As a result, slight adjustments would be needed to be made to combustion engines using biofuels to account for variations in ignition delay difference.

Gómez-Meyer (2012) compared the laminar flame velocities of Soy Methyl Ester and Canola Methyl Ester with diesel. A syringe pump was used to provide a constant flow of fuel into a heated airstream which vaporized the fuel. The temperature of the air/fuel mixture was kept at 350°C and burned at the exit of a Bunsen burner. A still picture camera was used to capture the shape and height of the flame at the burner exit. The flame velocity was computed using the mass flow rate of the mixture divided by the mixture density multiplied by the area of the outer flame cone. This process was repeated multiple times for equivalence ratios 1, 1.1, and 1.2 and the resulting velocities were found to agree with previous published values when corrected for the pre heating to vaporize the fuel. The flame velocities of CME and SME were found to be 12-15% lower than those of diesel for each measured equivalence ratio. Additionally, the flames had a maximum velocity of 128.5 cm/s for Diesel, 110.5 cm/s for CME and 107.5 cm/s for SME at an equivalence ratio of 1.1. These lower velocities for the biofuels were attributed to the lower reaction rates of methyl ester fuels.

One of the major propulsion systems for using biofuels is in diesel internal combustion engines. Shock tubes replicate the piston of an IC engine, allowing the combustion properties such as ignition delay and pressure rise to be compared between fuels.

Wang et al. (2014) studied auto-ignition of biodiesel using a shock tube. The shock tube had a 5.7 cm diameter, 2.59 m driver, and 4.11 m driven section. An electronic resistance system heated the tube to an initial temperature of 200°C, as measured by

thermocouples. Post shock conditions were calculated using normal shock relations. 5 piezoelectric pressure transducers located at various points along the length of the tube, were used to determine the shock velocity. Ignition was determined by a silicon photo detector which could detect the presence of electronically excited OH in the mixture following a combustion. The ignition delay was determined as the time between when the shock reached the end of the tube and when ignition occurred. Palmitate was tested for equivalence ratios of 0.25, 0.5, and 1.0. The ignition delay was found to decrease at post shock conditions of 1000 K, 12.5 milliseconds for an equivalence ratio of 0.25 to 11.0 milliseconds for an equivalence ratio of 1.0. This was predicted to be caused by a decrease in activation energy with increasing equivalence ratios from fuel lean conditions.

In recent years, much biofuel research has been focused on the topic of emissions. Hashimoto et al. (2008) studied the NO_X emissions of PME in a spray flame, in the search for an alternative fuel for gas turbine engines. While the adiabatic flame temperature of PME was similar to that of diesel, the NO_X emissions decreased by approximately 30% (actual concentration). Similarly, Sharon et al. (2012) studied PME and diesel blends in a direct injection diesel engine. CO emissions were measured to be 20-50% (actual concentration) lower for PME blends than pure diesel for similar loads. Additionally, NO_X concentrations were found to be unchanged.

To predict the NO_X emissions of other biofuels, such as canola methyl ester (CME), and soy methyl ester (SME), Love et al. (2009) studied the effect of iodine number on fuel in laminar flames. NO concentration was determined increase with increasing iodine number. Similarly, Balakrishnan et al. (2016) examined the correlation

between fuel unsaturation and NO_X emissions. Both petroleum and biofuels such as soy methyl ester, canola methyl ester, palm methyl ester, and rapeseed methyl ester were studied in a pre-vaporized laminar flame. The emissions index of NO was determined to increase with an increased degree of unsaturation of a fuel.

2.4 Current Research Objectives

The objective of this study was to compare the hot surface, constant volume, and constant pressure, vapor ignition properties of Canola Methyl Ester (CME), Soy Methyl Ester (SME), and Palm Methyl Ester (PME) to those of Jet A. By analyzing the differences between Jet A and the selected biofuels, it can be determined, for example, if safety procedures for storage and transportation are adequate or need to be updated, as well as provide information regarding the fundamental ignition properties of biofuels. In addition to variations between various fuels, the variations in ignition properties were also studied for changes in equivalence ratios between 0.75 and 2.00. This study also serves as a verification of the setup and experimental procedures, allowing for other types of biofuels or biofuel blends to be investigated in the future.

The following ignition properties were selected as objectives to be measured by the study: Ignition energy, time interval for ignition, ignition temperature, and flame front velocities (upward and downward). Each of these objectives is explained in more detail in Chapter 3. The independent variables in the study included the fuel type and equivalence ratio. Together, these properties define some of the differences between biofuels and traditional hydrocarbon fuels.

Chapter 3: Experimental Setup and Measurements

A fixed volume combustion setup was constructed to study the ignition properties of pre-vaporized liquid fuels. This chapter describes the setup design and data collection methods, as well as the experimental procedures and test conditions.

3.1 Experimental Setup

All experiments were conducted at the Combustion and Flame Dynamics Laboratory located at the University of Oklahoma main campus. The ambient pressure of the laboratory was maintained at slightly higher than atmospheric in order to provide a positive draft in the laboratory combustion chamber so that flue gases did not leak into the laboratory installations. In addition, the laboratory was equipped with a fume hood with an exhaust of diameter 20 cm, which was used in the present setup.

The setup was designed to heat and mix the air and fuel at controllable rates and to allow for the combustion chamber to be isolated prior to combustion. Additionally, measurements that were of interest included the temperature of the mixture, energy used by the ignitor, and flame front velocities. A National Instruments Data Acquisition Unit and a laptop computer running LabVIEW software were used for data acquisition. Figure 3.1 shows two images of the overall setup. The upper image includes the laptop computer running the LabVIEW interface for the experiment. The setup is on the left side of the image, next to the fume hood. The high speed camera is located on the red mat at the top center of the image. The syringe fuel pump is visible in the lower left corner. In the upper image, the exhaust from the combustion chamber is capped with an aluminum foil cap. In the lower image the combustion chamber exhaust is attached to the exhaust hose leading to the fume hood vent. Visible in both images is the combustion chamber sheath,

constructed from thin steel walls on the top half of the setup, filled with white insulation. Directly below the combustion chamber extending downward is the inflow tubing through which the fuel/air mixture entered the chamber. The lower image shows the location of the DAQ, mounted in a white metal case attached to the wood paneling below the combustion chamber. The combustion chamber itself is hidden in both images within the insulation. Figure 3.2 shows the view of the combustion chamber and combustion chamber window from the point of view of the high speed camera. The image on the left shows the insulation in place, and the image on the right shows the direct view to the window. Figure 3.3 shows a schematic diagram of the combustion chamber and inflow tubing. The furthest left depiction shows the same view as displayed in the lower image in Figure 3.1, with the exception of the pressure gauge and rotameter, which are drawn next to the process heater in the schematics for compactness. The pressure gauge and rotameter on the setup can be seen in Figure 3.1 mounted to the steel frame beneath the combustion chamber. At the top of the schematic diagram is the combustion chamber, described in Section 3.1.1. Inside the combustion chamber, visible in the center depiction, is the ignitor, which is discussed in Section 3.1.2. Beneath the ignitor are the heaters and tubing used to allow fuel and air to enter the combustion chamber. These are described further in Section 3.1.3. Table 3.1 contains a list of the equipment used, along with their specifications and manufacturer.

3.1.1 Combustion Chamber

The combustion chamber was constructed of steel and had internal dimensions of 7.0 cm by 7.0 cm by 32.0 cm tall, an approximate volume of 1.56 liters. A 1.3 cm diameter opening at the bottom of the chamber allowed for the fuel-air mixture to enter the

combustion chamber. On the outside of the chamber, two cartridge heaters were mounted in hollow steel tubes with inner diameters of 1.0 cm and wall thicknesses of 0.1 cm. These heaters were used to heat the walls of the chamber during runs. To aid in the heating of the chamber, a thin steel sheath was added around the outside of the chamber, leaving a 3.0 cm to 6.0 cm gap. The volume between the outside of the chamber and the inside of the sheath was filled with insulation. A schematic diagram of the combustion chamber is presented in Figure 3.4. The cutaway view A-A shows the inside of the chamber, including the locations of the diffuser plate, thermocouples, and ignitor.

A diffuser plate was attached directly above the chamber inlet to help facilitate the even mixing and distribution of the fuel-air mixture into the chamber. The diffuser plate was constructed using a steel circular plate with a diameter of 7.0 cm and thickness of 0.3 cm. Thirteen evenly spaced holes of diameter 0.5 cm were drilled into the plate to allow the fuel-air mixture to evenly pass through. An image of the diffuser is shown in Figure 3.5. The diffuser plate was raised 4.0 cm from the bottom of the chamber. The location of the diffuser is label in Figure 3.4 in the cross section A-A.

The front of the chamber contained a 5.0 cm by 23.0 cm by 0.5 cm thick window of high temperature rated glass, which allowed the ignition process to be visually observed. The window was held in place by a removable frame, to facilitate the cleaning of the glass and provide access to the interior of the chamber. During the heat-up, fueling, and reset phase of a trial, a steel box stuffed with insulation was placed in front of window to better insulate the setup and allow for shorted heating times.

Centered at the back of the chamber, a steel hollow cylinder of inner diameter 6.0 cm, thickness 0.1 cm, and depth 3.0 cm and a steel back plate of thickness 0.1 cm provided

a location for thermocouples and the ignitor to be mounted. A small hole of diameter 0.15 cm at the top of the chamber provided access for another thermocouple near the ignitor surface.

Along the back of the chamber, 3.0 cm from the top, a steel hollow cylinder of inner diameter 3.8 cm thickness 0.1 cm, and depth 13.0 cm was attached as an exhaust for the chamber. During the heat up and fueling phases, an exhaust hose, constructed of aluminum dryer tubing connected the chamber exhaust to the fume hood exhaust. During combustion trials, a fitted aluminum foil cap covered the end of the exhaust. This cap maintained a constant pressure and volume in the chamber. The increase in pressure during combustion would blow the cap off of the exhaust and prevented the glass on the front of the chamber from being shattered.

3.1.2 Ignitor

A commercially available dryer ignitor was used as an ignition surface. The ignitor was selected due to its ease of acquisition and uniform manufacturing. The ignitor was controlled by a relay which connected it to a standard 115-120 V power outlet. The heating element was constructed out of silicon carbide, with a specific heat of 670 J/ kg K and a density of 3.21 g/cm^3 (Gieck and Gieck, 1990). The volume of the exposed heating element was 1.45 cm^3 with a surface area of 17.8 cm^2. A schematic diagram of the ignitor can be found in Figure 3.6. The ignitor was mounted on an L bracket with a screw and bolt. The L bracket was welded to the back plate and allowed the ignitor to protrude into the approximate center of the combustion chamber. Figure 3.7 shows the ignitor mount from above (left image) and below (right image). The L bracket which supports the ignitor is visible below the ignitor ceramic in the right image, and the bolt

keeping the ignitor in place is visible at the back of the ignitor from above. The location of the ignitor is the combustion chamber is displayed in Figure 3.3 and Figure 3.4.

3.1.3 Air/Fuel Delivery System

Air provided by the laboratory compressor was used for both the heating up of the setup and for the combustion trials. A flexible plastic hose connected the laboratory air wall port to a pressure gauge. The pressure gauge was used to measure the backpressure of the system and to ensure that it remains at a constant 10 psi. Following the pressure gauge, the air flowed through a LO FLO 1/4-33-G-5 rotameter with a stainless steel ball float. The rotameter had a range of up to 38 L/min and was incremented in marks of 1% of maximum flow rate. Corrections were made to account for the higher pressure of the air resulting in a corrected maximum flow rate of 31.21 L/min (McCrometer, 1996). This value was checked using an electronic flow meter. The percentages of the corrected maximum were then used to measure the airflow rate into the setup.

Following the rotameter, the air passed through a process heater, which was located below the air inlet of the combustion chamber at the furthest end of the inflow tubing, approximately 1 meter below the combustion chamber. As the air flowed vertically upward through the process heater, it was heated up to a temperature of approximately 375°C. This temperature was slightly above the boiling points of the liquid fuels used in this study, displayed in Table 3.2, and was found to be sufficient to vaporize the fuel without any coking in the tubes (Balakrishnan et al., 2016). Liquid fuel was introduced into the airflow, using a syringe pump and injection needle, 7.0 cm downstream of the process heater. The fuel was contained in a 34 mm diameter syringe with a maximum volume 100 ml. The fuel flow rate was controlled by a Harvard

Apparatus brand electronic syringe pump. After exiting the syringe, the fuel passed through a small plastic tube to the injection needle. This injection needle was inserted through an airtight seal at a T-junction directly following the process heater. A wet cloth (that was periodically kept wetted with tap water) was wrapped around the fuel tube and needle interface in order to cool the plastic and prevent it from melting. Air flowed vertically past the fuel injection location carrying the liquid fuel upward while it vaporized. Above the T-junction, a 35.0 cm length steel tube of outer diameter 1.3 cm and thickness 0.1 cm carried the air toward the combustion chamber. Heating tape was wrapped around the tube to keep it at a high enough temperature, 375°C, to vaporize the fuel. Both the process heater and heating tape were controlled by relays connecting them to a 220 V AC wall power supply. The relays were controlled by the DAQ and LabVIEW program.

The vaporization tube connected to the bottom of a four way cross junction. The forward facing connection of the junction was sealed and a stainless steel sheathed, 0.15 cm diameter, K-type thermocouple was inserted to measure the temperature of the fuel air mixture. The rear facing junction connected to an uninsulated and unheated 1.3 cm outer diameter, 0.1 cm thick steel pipe with a manually operated valve on the end. When opened, this valve allowed air to exit the setup without entering the combustion chamber. The top of the junction led to a 1.3 cm diameter steel flapper valve. This valve ensured that flow only proceeded upward, preventing the pre-combustion mixture from escaping after the chamber had been isolated and the post-combustion exhaust gasses from flowing back into the inlet tube. Following the flapper valve, the mixture passed into the combustion chamber, and through the diffuser plate located in the bottom of the

combustion chamber (Section 3.1.1). During all phases except for the ignition phase, the excess gases exited the combustion chamber through the exhaust tube and out of the building through the fume hood vent. A diagram of the air/fuel delivery system is presented in Figure 3.8. The fuel and air inlets are labeled “fuel” and “air” and have arrows pointing into the setup. Conversely, the flow exits from the chamber are denoted with arrows pointing away from the setup.

3.2 Data Collection and Analyzation

All data collection, excluding the high speed images, was performed with a National Instruments Data Acquisition Unit, DAQ. The DAQ also contained controllable 5 V DC outputs, which were used to operate the relays and control the experiment. A laptop computer running LabVIEW was used to interact with the DAQ through a USB cable. LabVIEW was custom programmed for the experiment and provided a user interface from which to interact with and control the setup. Figure 3.9 provides an overview of the control system and data collection system used in the setup. A screenshot of the LabVIEW and high speed camera user interfaces can be found in Figure 3.10. Each of the seven graphs in LabVIEW correlates to a variable which was measured. The upper left graph shows the voltages, in Volts, measured across the shunt resistor which was connected via a current transformer to the ignitor and used to measure power usage. Below the ignitor voltage graph are the fuel injection temperature and case temperature graphs, which show the temperatures, in degrees Celsius of the inflow air and combustion chamber wall as measured by their respective thermocouples. On the right side, from the top down, are the 15 mm above ignitor, 1 mm above ignitor, and unused 15 mm below ignitor thermocouple temperature measurements in degrees Celsius. Due to a lack of entry

points into the combustion chamber, the 15 mm below ignitor thermocouple was not used in the experiments. Below the thermocouple temperature graphs, on the right side, is the camera trigger voltage, which was measured in Volts and used to determine when the high speed camera was triggered. Finally, on the right side of the screen next to the LabVIEW interface was the high speed camera user interface. The high speed camera interface was used to set the frame rate, exposure time, and recording style of the camera, and was also used to review the images captured after a combustion.

3.2.1 Power and Energy Measurements

The power used by the ignitor was measured using a current transformer and shunt resistor. A current transformer with 442 coils was attached to one of the power lines of the ignitor. The current transformer was connected to a 240 ohm shunt resistor. The voltage was measured on each side of the resistor by the DAQ. The current through the shunt resistor was first calculated as the root mean square of the measured voltage divided by the resistance of the shunt resistor. The stepped down current was then multiplied by the current transformer ratio of 442 to calculate the current through the ignitor. The ignitor was assumed to have a voltage of 120 Volts, which was multiplied by the current to determine the power. The shunt resistor voltages were measured at a rate of 1000 Hz using the voltage input ports on the DAQ. Calculations were performed by LabVIEW for every 100 samples.

Ignition energy was measured by integrating the power used in the ignitor with respect to time. The equation for calculating ignition energy is given by:

$$E_{ignition} = \int_{t_{0\ (ignitor\ enabled)}}^{t_{ignition}} P_{ignitor}\, dt \qquad 3.1$$

Where t is the time in seconds and P is the power supplied to the ignitor in Watts. The calculation was carried out numerically using trapezoidal Riemann sums. $E_{ignition}$ represents the calculated energy using only the raw data recorded by the DAQ and LabVIEW. A voltmeter connected across the ignitor showed that for the first 3 seconds, the voltage across the ignitor was not 120 V (as assumed), but a constant value of 115 V AC. This correction to the raw calculations of energy was made using the equation:

$$E_{115V} = E_{120V}\frac{115}{120} \tag{3.2}$$

Where E_{115V} is the energy calculated, in Joules, correctly using a wall voltage of 115 V and E_{120V} is the energy calculated, in Joules, incorrectly using a wall voltage of 120 V.

All of the energy consumed by the ignitor was not transferred to the fuel-air mixture; corrections must be made for the energy required to heat up the ignitor, as well as to the energy lost by radiation. The energy used to heat up the ignitor was calculated from using the initial and combustion temperatures of the ignitor as well as the ignitor's mass and specific heat. This value can be calculated from the equation:

$$E_{C\ (specific\ heat\ of\ ignitor)} = mC(\Delta T) \tag{3.3}$$

Where m is the mass of the ignitor in kilograms, C is the specific heat of the ignitor, which is a constant 690 (J/kg K), and ΔT is the difference in temperatures of the ignitor in °C or K. The energy lost to radiation can be calculated from the Stefan-Boltzmann law, for radiation power, integrated with respect to time (Wong, 2003). The emissivity of the material of the ignitor was assumed to be 1.0.

$$E_{R\ (radiation)} = \int_{t_{0\ (ignitor\ enabled)}}^{t_{ignition}} A\sigma[(T_i(t))^4 - (T_{case}(t))^4]\,dt \tag{3.4}$$

Where σ is the Stefan-Boltzmann constant 5.67 x 10^{-8} W/m^2 K^{-4}, A is the surface area of the ignitor, T_i is the temperature of the ignitor as a function of time in Kelvin, and T_{case} is the temperature of the case as a function of time in Kelvin, $t_{ignition}$ is the time of ignition in seconds and $t_{0\ (ignitor\ enabled)}$ is the time when the ignitor was enabled in seconds. As discussed further in 3.2.3, the ignitor temperature can be approximated as increasing linearly with time from the initial temperature to the temperature at combustion. The case temperature can be approximated as being constant and is set by the initial case thermocouple temperature. Combined, the values for energy loss due to heating of the ignitor and radiation can be subtracted from the ignition energy for the trial to obtain the adjusted ignition energy.

$$E_{adjusted} = E_{115V} - (E_{R\ (radiation)} + E_{C\ (specific\ heat\ of\ ignitor)}) \qquad 3.5$$

Where E_{115V} is the previously calculated ignition energy in Joules, adjusted for the correct wall voltage, $E_{R\ (radiation)}$ is the energy lost by radiation in Joules, and $E_{C\ (specific\ heat\ of\ ignitor)}$ is the energy lost to the ignitor, in Joules.

3.2.2 Mixture Temperature Measurements

The temperature of the mixture was measured at three different locations throughout the setup. The furthest upstream measurement is taken at the just prior to the mixture entering the combustion chamber. The other two measurements are taken from the center of the combustion chamber at various heights. All direct temperature measurements are taken using Omega brand K-type, chromel-alumel junction, thermocouples, with grounded stainless steel sheaths of diameter 1.5 mm. The locations of the thermocouples are discussed individually in the following paragraphs, and an

overview of their locations relative to the ignitor is displayed in Figure 3.4, cross section A-A.

The thermocouple located at the inflow to the combustion chamber, at the cross pipe connection, was used to help ensure that the mixture is at a high enough temperature to completely vaporize the fuel and acted as an input for the heating tape and process heater control system. If the inflow thermocouple sensed a temperature below 375°C, during the heating up, fueling, or resetting phase of a trial, the heating tape and process heater were turned on via a relay, quickly increasing the temperature of the inflow mixture. The control system was programmed using LabVIEW and the measurements and responsive actions were performed using the DAQ.

The lower combustion chamber thermocouple was positioned 1 mm above the center of the ignitor and is referred to as the 1 mm above ignitor thermocouple. The 1 mm above ignitor thermocouple was inserted from the top of the case through a small hole, and electrically insulated from the case using threading tape. During the ignition phase of a trial, temperature measurements were made using this thermocouple at a rate of 1000 Hz.

The higher combustion chamber thermocouple was positioned 15 mm above the center of the ignitor and is referred to as the 15 mm above ignitor thermocouple. The 15 mm above ignitor thermocouple was inserted from the back plate, above the ignitor mount location. Similar to the other chamber thermocouple, this thermocouple was insulated using threading tape and temperature data was recorded at a rate of 1000 Hz during the ignition phase of a trial. Together with the temperature measured by the lower chamber

thermocouple, these measurements could be used to estimate the magnitude of the temperature gradient of the mixture in the combustion chamber.

3.2.3 Surface Temperature Measurements

The temperature of the interior wall of the combustion chamber, as well as the temperature of the ignitor surface were measured.

The interior wall temperature was measured using an omega brand K-type thermocouple, inserted through the back plate near where the ignitor was mounted, and bent to touch the back wall at a point 5.5 cm below the ignitor. The measurements from the thermocouple were used to help ensure that the vaporized fuel in the combustion chamber did not condense onto the chamber wall, altering the equivalence ratio of the mixture. The control system for monitoring the temperature of the combustion chamber used the measurements from this thermocouple to control the relays for the cartridge case heaters. When the wall temperature dropped below 350°C during the heat-up, filling, or reset phases, the control system would activate the case heaters, heating up the combustion chamber.

The surface temperature of the ignitor was determined indirectly using the resistance of the ignitor which changed with temperature. Calibration tests were performed by heating stagnant air in the combustion chamber to various temperatures as measured by the two chamber thermocouples. After the air reached a constant temperature for 20 minutes, the ignitor was activated and the current measurements were recorded. The initial current flowing through the ignitor was used to calculate the resistance of the ignitor at the measured chamber temperature. This was repeated 68 times

over a variety of temperatures ranging from 22°C to 1100°C. Only the initial values of current and resistance were used in the calibration tests, because the self-heating of the ignitor would change its resistance. Since the voltage input from the wall electrical outlet was constant, and current and resistance are directly related to voltage, the measured current flowing through the ignitor at a set voltage was used in place of the ignitor's resistance to determine its temperature. The temperature was plotted, using excel, as a function of current and a best fit polynomial was determined. The resulting equations were used to determine the temperature of the ignitor at various instances during the ignition phase.

$$T_i(I) = 5.4\,I^5 - 94.3\,I^4 + 642.0\,I^3 - 2122.4\,I^2 + 3548.2\,I - 2234.5 \qquad 3.6$$

$$T_i(I) = -447.8\,I^2 + 4184.1\,I - 8684.3 \qquad 3.7$$

Where T_i is the temperature of the ignitor, in °C, and I is the instantaneous current flowing through the ignitor, in amps. Due to the nature of the current-temperature relations of the ignitor, Equation 3.6 was used for instances where current was steady or increasing with time, and Equation 3.7 was used for instances where current was decreasing with time. 700°C was the approximate ignitor temperature when the current began decreasing with time. When activated, it was found that the ignitor temperature increased linearly with time. This observation was used with Equation 3.4 to calculate the radiation energy emitted by the ignitor.

3.2.4 Flame Front Velocity Measurements

In addition to the power and temperature data, a high speed camera was used to record flame images during each trial. The high-speed camera is an IDT brand MotionPro X3 with a maximum frame rate at full resolution of 1000 frames per second. Located 60

cm from the viewing window, the camera was raised 17 cm in order to be level with the ignitor. The high speed camera was triggered through a 5 V voltage output from the DAQ. This trigger also connects back to the DAQ in order to allow the syncing of the camera frames with the temperature and power data. The high speed camera was used at a rate of 500 frames per second and an exposure of 1997 microseconds for the majority of the trials. Recording was done in a circular mode, which allowed for previous and future frames to be saved when the trigger button was pressed.

The high speed camera saved data as a set of images. These images were analyzed to determine the flame front velocities. A set of 1.0 cm sized markings was positioned on the left side of the combustion chamber window. This scale was used to determine the distance the flame front had traveled between frames. Flame velocities were calculated by using the change in distance and the change in time between the first appearance of a flame, and the furthest measureable distance. The upper and lower flame front velocities were calculated using the equation:

$$V_{flame\ front} = \frac{(h_2 - h_1)\,(fps)}{(n_2 - n_1)} \tag{3.8}$$

Where $V_{\text{flame front}}$ is the velocity of the flame front in m/s, h is the height of the flame, as measured as the absolute value of the distance from the ignitor to the flame front in meters, n is the frame number, and fps is the frame rate in frames per second. Equation 3.8 was used for both the upper and lower flame velocities.

A large difference was observed in the measured upper and lower flame velocities due to the significant buoyant forces acting on the gases inside the combustion chamber post combustion. It was also noticed that occasional specs of flammable particles inside the combustion chamber would be ignited by the passing flame and would glow brightly.

These glowing particles were used to determine the velocity of the gases inside the combustion chamber. The velocity of the airflow at a certain location within the combustion chamber (due to buoyancy) was calculated using the equation:

$$V_{gas} = \frac{\left(h_2 - h_1\right)(fps)}{\left(n_2 - n_1\right)} \quad 3.9$$

Where V_{gas} is the local velocity of the gas in m/s, h is the ember's height from the bottom of the viewing window, n is the frame number as captured by the high speed camera, and fps is the frame rate in frames per second.

3.2.5 Other Measurements

All of the measurements recorded required knowledge of when the ignition occurred. Ignition was defined to occur at the first visual presence of a flame, as captured by the high speed camera. The high speed camera was linked to the data gathered by the DAQ by the camera trigger. The camera was triggered by a drop voltage across two wires. These wires were also routed into the DAQ and their voltages were measured and recorded throughout the ignition phase of the trial. The time of ignition in the collected data could then by calculated by the equation:

$$t_{ignition} = t_{recording\ started} + \frac{n_{ignition}}{fps} \quad 3.10$$

Where $t_{ignition}$ is the time of ignition in seconds relative to the start of the DAQ data recording, $t_{recording\ started}$ is the time of triggering of the high speed camera in seconds relative to the start of the data recording, $n_{ignition}$ is the frame number of the first observed flame, and fps is the frame rate in frames per second.

The time interval for ignition was calculated using the difference between the time the ignitor was activated and ignition using the equation:

$$\Delta t_{for\ ignition} = t_{ignition} - t_{0\ (ignitor\ enabled)} \quad 3.11$$

Where $\Delta t_{\text{for ignition}}$ is the time interval for ignition in seconds, t_{ignition} is the time in seconds at which ignition occurred, and $t_{0\ \text{(ignitor enabled)}}$ is the time in seconds at which the ignitor was activated. The time interval for ignition was calculated during data analysis.

3.2.6 Uncertainties

The experiments were repeated at least four times at each condition. Uncertainties were calculated from the results using standard methods based on the Student-t distribution with a 95% confidence value. A table of typical uncertainties can be found in Table 3.3. Uncertainties are also marked as error bars in figures containing results.

3.3 Test Procedures

The fuels tested were Jet-A, canola methyl ester (CME), soy methyl ester (SME), and palm methyl ester (PME). Each fuel was tested at the equivalence ratios of 1.0 through 1.5 at intervals of 0.1. Additionally, equivalence ratios of 0.75, 1.75, and 2.00 were also tested. Prior to a fuel being tested, air and fuel flow values were calculated and recorded for later reference and use in trials.

3.3.1 Heat-Up Phase

Before each trial, the setup underwent a heat-up process, lasting approximately 30 minutes for the first heat-up and 5 minutes after a previous trial. During this heat-up process, the process heater and heating tape would raise the air in the inflow tube to a temperature of 375°C. Airflow was supplied through the inflow tube at a rate of 30.3 L/min to prevent the process heater from overheating and aid in the heating of the combustion chamber. Additionally during the heat-up process, the case heaters would heat the combustion chamber walls to a predetermined temperature of 350°C, to prevent

the condensation of the fuel on the walls during the fueling phase. The case heaters ran on a 60% duty cycle to keep them from overheating. The process heater and heating tape were controlled by a bang-bang control system, turning on when the temperature measured by the inflow thermocouple was below 375°C and off when the measured temperature exceed 375°C. During the heat-up process, the bypass valve was closed, glass insulation was in place, and the exhaust was uncapped and connected to the vent hood, but the vent hood fan remained off.

3.3.2 Filling Phase

After the completion of the heat-up process, the filling process began. The total filling time lasted 1 minute to ensure that the chamber was filled completely. Theoretically, the chamber should be filled after 5 seconds of filling, and it was found that there was no significant difference in results between filling times ranging from 30 seconds to 2 minutes. One minute allowed sufficient time for temperatures to re-stabilize and flow rates to be adjusted to ensure as similar as possible initial conditions for each trial. During the filling process, the fuel was injected into the inflow pipe, between the process heater and the heating tape. The fuel injection rate was controlled via a syringe pump and calculated prior the trial. The case heaters were disabled to eliminate the risk of auto ignition. The exhaust was uncapped and connected to the vent hood, and the exhaust fan was off. The bypass valve remained closed and the glass insulation also remained in place. Finally, the high speed camera recording was started during the filling process.

3.3.3 Ignition Phase

After filling, the ignition process began. Transitioning between the filling process and the ignition process required several actions to be performed simultaneously to best trap the fuel air mixture in the chamber: moving the exhaust hose from the chamber exhaust to the bypass pipe, capping the exhaust with the aluminum foil cap, and opening the exhaust valve to redirect the airflow from into the chamber to out of the bypass valve. After the chamber mixture had been isolated, the following actions were performed: the fuel pump was turned off, the airflow was decreased, and the glass insulation was removed. The heating tape and process heaters were also turned off to prevent them from melting. Next, the ignitor was turned on, automatically starting the data recording. When combustion was observed through visual means, the high speed camera recording was triggered manually, saving the previous 3 seconds and future 1 second of camera images. Finally, the ignitor was turned off, ending the data recording.

3.3.4 Reset Phase

At the end of each trial, a reset process was undertaken to ensure that the previous trial did not interfere with the next trial. This reset process began by reattaching the exhaust hose and enabling the vent hood fan. Next, the bypass valve was closed and air flow was reestablished at a rate of approximately 30.3 L/min. All the heaters were turned on and set to the “heat-up” conditions described earlier. 2 minutes were allowed for the reset period. This time was also used to trim the high speed camera footage by removing the frames before ignition and after flame propagation had completed. After the reset period ended, the vent hood fan was disabled, and the heat-up process was started for the next trial.

3.3.5 Periodic Procedures and Maintenance

Throughout trials, water would periodically need to be dripped onto the fuel injection needle, to keep it from heating up to a temperature which would melt the plastic hose leading from the syringe. Additionally, after each session of trials, equivalence ratios 0.75 to 2.00 tested, the glass view window would need to be removed and cleaned. A buildup of residue was observed for each of the biofuels, which was cleaned using glass stove top cleaner and a scotch bright pad. After cleaning, the glass was rinsed with water, thoroughly dried, and reinstalled into the setup.

3.4 Calibrations

3.4.1 Filling Time

In order to ensure an adequate amount of time was taken to fill the combustion chamber, a series of tests were carried out using Jet A at stoichiometric conditions. In theory, with a flow rate of 30.3 L/min of air at room temperature, the combustion chamber, with the approximate volume of 1.6 L, would take only 2.6 seconds to fill. However, this would assume for a perfect filling rate and neglects any remnants of the air in the combustion chamber mixing with the incoming fuel air mixture. To experimentally determine the filling times, four different filling times were used ranging from 30 seconds to 120 seconds. The results were then analyzed and compared to see if there was any noticeable difference between the four. A selection of one minute for filling times was then made on the basis of no significant differences in adjusted ignition energy (within a range of 17 J) and a duration which provided enough time for the system to come to a stabilized state and the filling procedures to be carried out consistently.

3.4.2 Airflow Rate

The airflow rate was also tested at two different rates to empirically determine the optimal airflow rate for consistent results. The calibration consisted of the same test as used above for the filling time calibration except at a lower airflow rate, and fuel flow rate to maintain stoichiometric conditions. The adjusted ignition energy results varied significantly between the various trials of lower flow rate (maximum range of 114 J) compared both to themselves and to the previous high flow rate trials (maximum range of 17 J). As a result, higher flow rates were chosen to be used during the filling phase of a trial.

3.5 Testing Conditions

3.5.1 Fuels and Equivalence Ratios Tested

The fuels tested in this study included Jet A, palm methyl ester, soy methyl ester, and canola methyl ester. A list of the basic fuel properties, including density, viscosity, and heating values can be found in Table 3.2. All the biofuels tested have a significant oxygen content, on average about 11% by mass, compared to Jet A. Additionally, the biofuels have a much higher density, on average 10% greater, and viscosity, on an average of 3.63 times greater, than that of Jet A. The upper boiling point of each of the fuels is greater than 300°C, with CME and SME having the highest of the biofuels at 405°C, and PME the lowest at 354°C, which is 44°C higher than Jet A.

In addition to testing various fuel, each fuel was also tested along a range of equivalence ratios. The tested equivalence ratios ranged from 1.00 to 1.50 at intervals of 0.10, and additional ratios of 0.75, 1.75, and 2.00. The flow rates for each of the fuels at each equivalence ratio can be found in Table 3.4. The airflow rate was kept constant and

the fuel flow rate was increased to raise the equivalence ratio value. Thus, the density of the fuel/air mixture and the mass fraction of fuel in the mixture increased with equivalence ratio.

3.5.2 Other Conditions

Because the experiment relied on laboratory supplied air, the ambient conditions were also recorded for each day. These conditions were used along with the results to ensure no outside influence affected the trial results.

Table 3.1: Equipment used

Equipment	Manufacturer	Version / Specifications
Laptop Computer	Sony	Vavio
Data Acquisition Unit	National Instruments	SCB-68
Rotameter	S.K. McCrometer	LO FLO ¼-33-G-5 with a Stainless Steel Float
Pressure Gauge	U.S. Gauge	-
Ignitor	Whirlpool	279311
Syringe Pump	Harvard Apparatus	55-2222

Table 3.2: Basic fuel properties

Fuel	Equivalent Molecular Formula	Density (kg/m^3)	Dynamic Viscosity (cP @22 °C)	Lower Heating Value (MJ/kg)	Boiling Point (°C)
Jet A	$C_{13}H_{23}$	796	1.54	42.8	145-310
Canola Methyl Ester (CME)	$C_{19}H_{36}O_2$	876	5.92	37.4	340-405
Soy Methyl Ester (SME)	$C_{18.8}H_{34.6}O_2$	887	5.25	37.0	351-405
Palm Methyl Ester (PME)	$C_{17.05}H_{32.9}O_2$	869	5.61	36.8	350-354

Table 3.3: Typical estimated experimental uncertainties

Measurement	Typical Uncertainty
Measured Ignition Energy	±117.3 J
Time Interval for Ignition	±0.22 s
Upper Flame Front Velocity	±1.07 m/s
Lower Flame Front Velocity	±0.45 m/s
Adjusted Ignition Energy	±42.9 J
Ignition Temperature	±20.1°C

Table 3.4: Fuel flow rates for varying equivalence ratios

Equivalence Ratio	Airflow Rate (L/min)	Jet A Flow Rate (mL/min)	CME Flow Rate (mL/min)	SME Flow Rate (mL/min)	PME Flow Rate (mL/min)
0.75	30.3	2.39	2.49	2.48	2.55
1.00	30.3	3.19	3.33	3.31	3.40
1.10	30.3	3.51	3.66	3.64	3.74
1.20	30.3	3.83	3.99	3.79	4.07
1.30	30.3	4.14	4.32	4.30	4.41
1.40	30.3	4.46	4.66	4.63	4.75
1.50	30.3	4.78	4.99	4.97	5.09
1.75	30.3	5.58	5.82	5.79	5.94
2.00	30.3	6.38	6.65	6.62	6.79

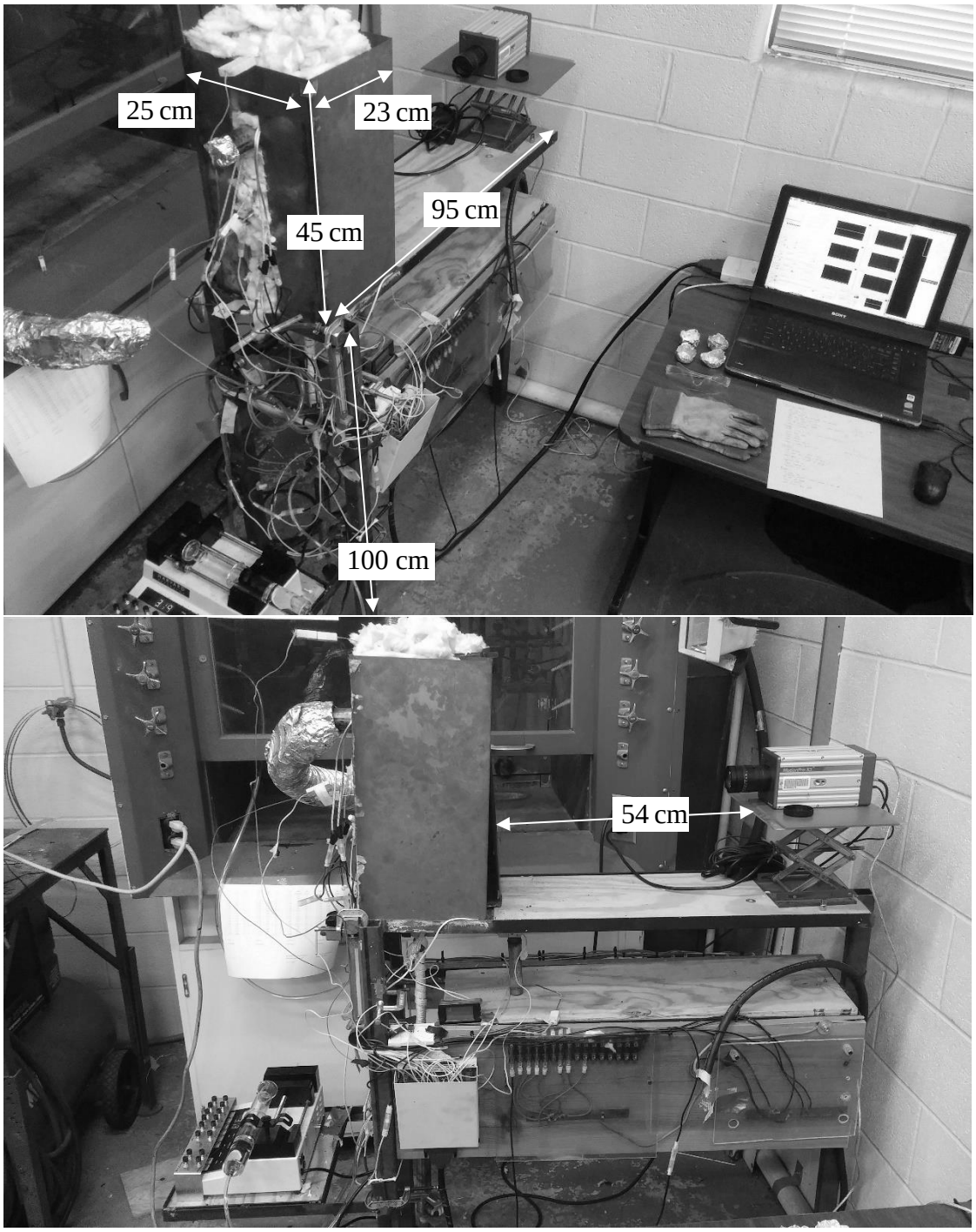

Figure 3.1: Images of the setup

Figure 3.2: Images of the setup from the point of view of the high speed camera

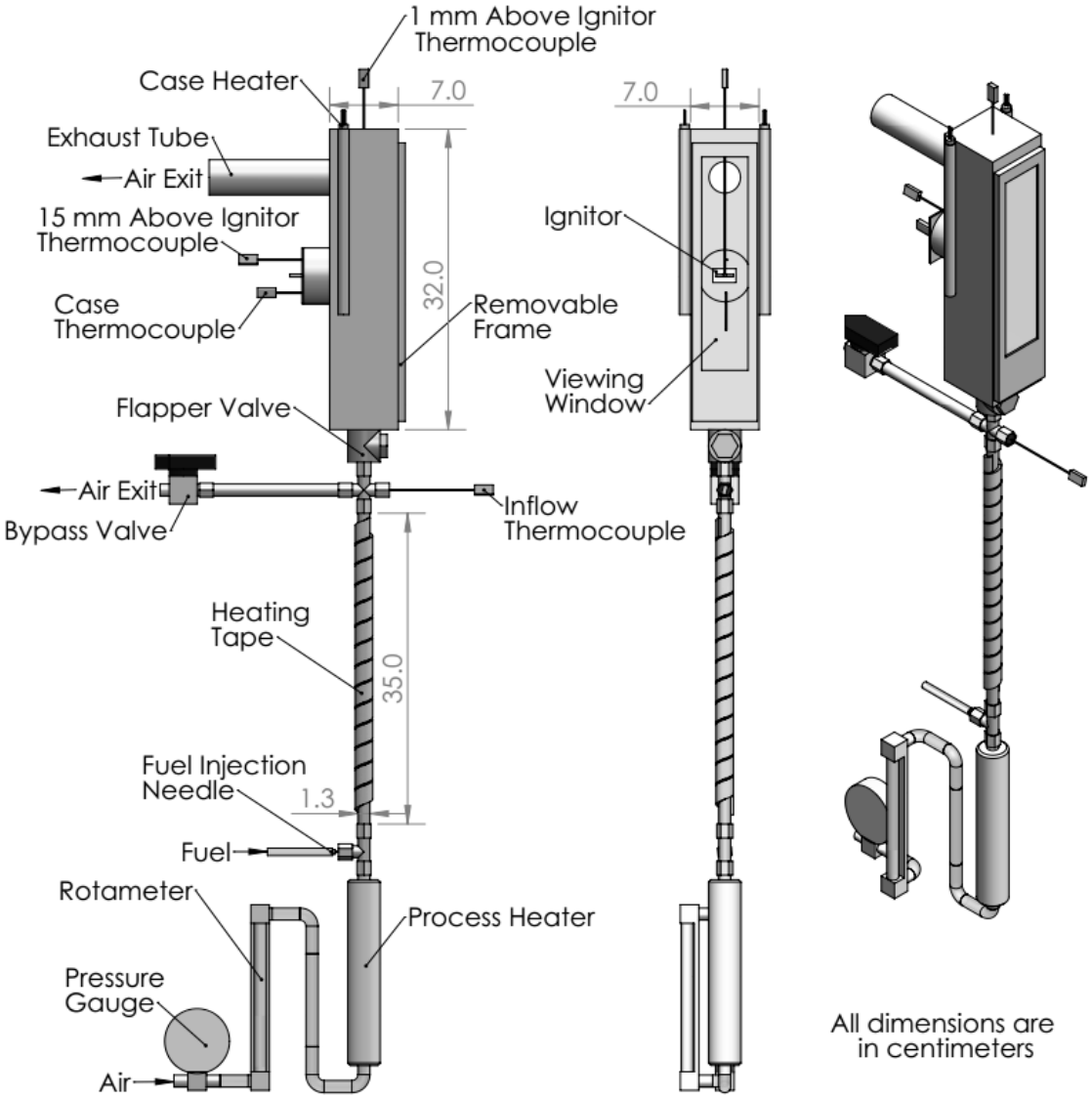

Figure 3.3: Combustion chamber and tubing diagram

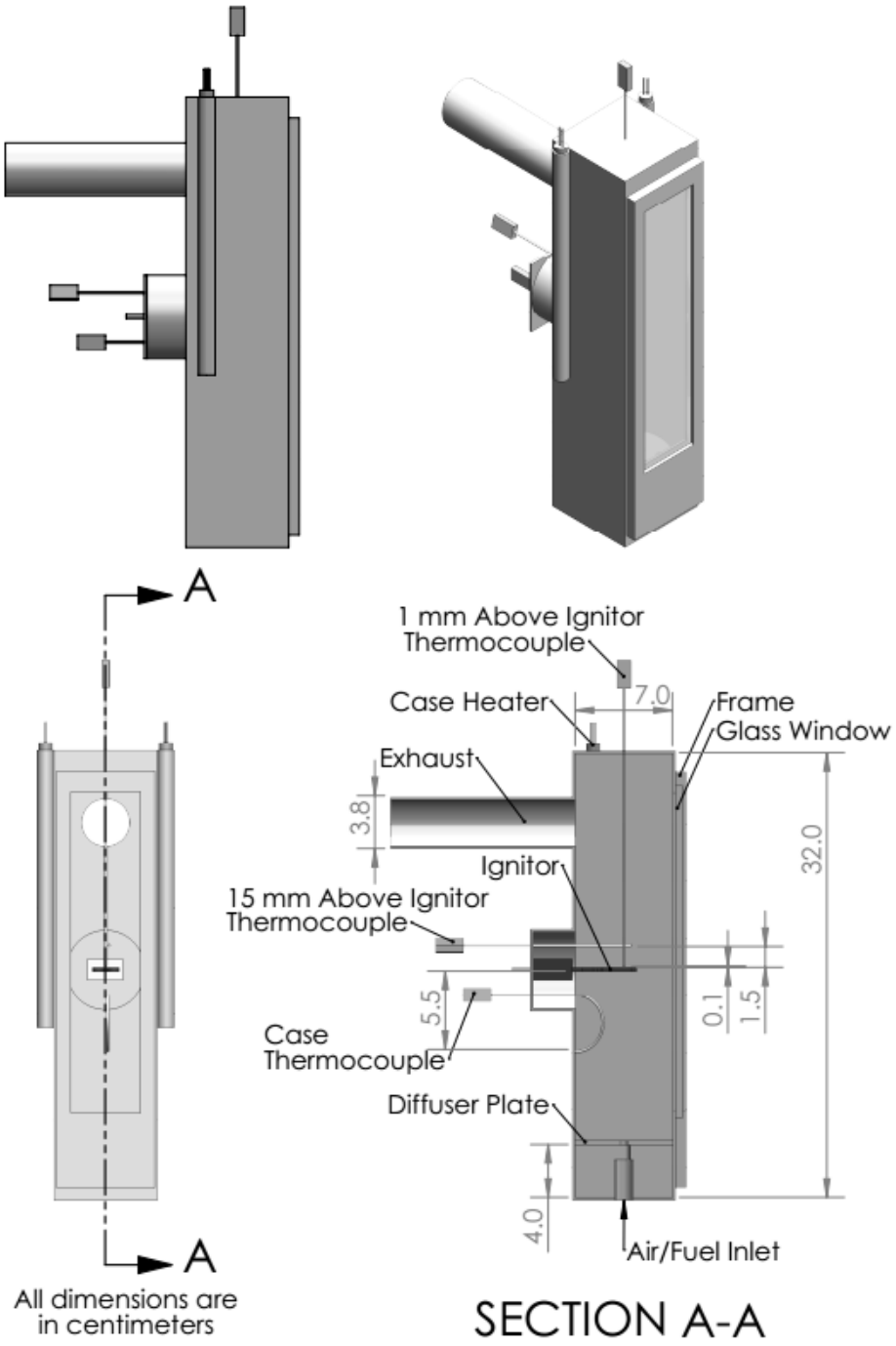

Figure 3.4: Combustion chamber diagram

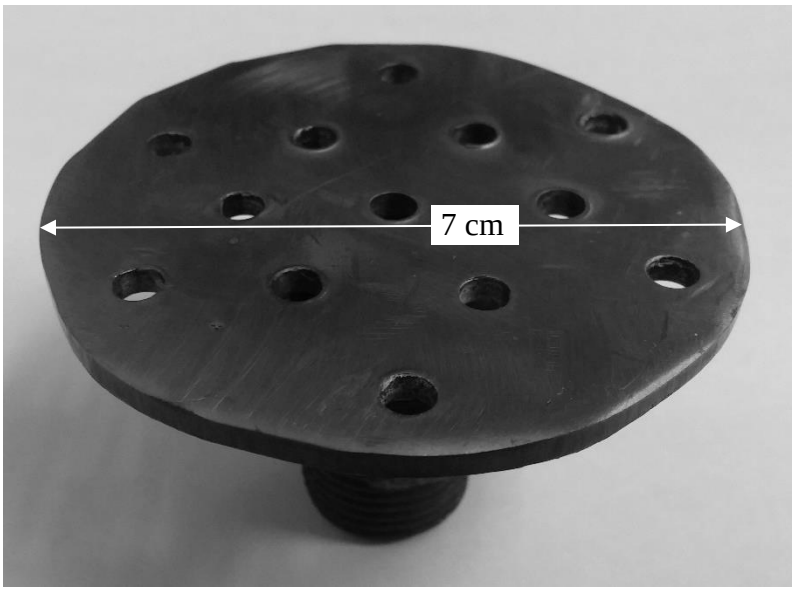

Figure 3.5: Image of diffuser plate

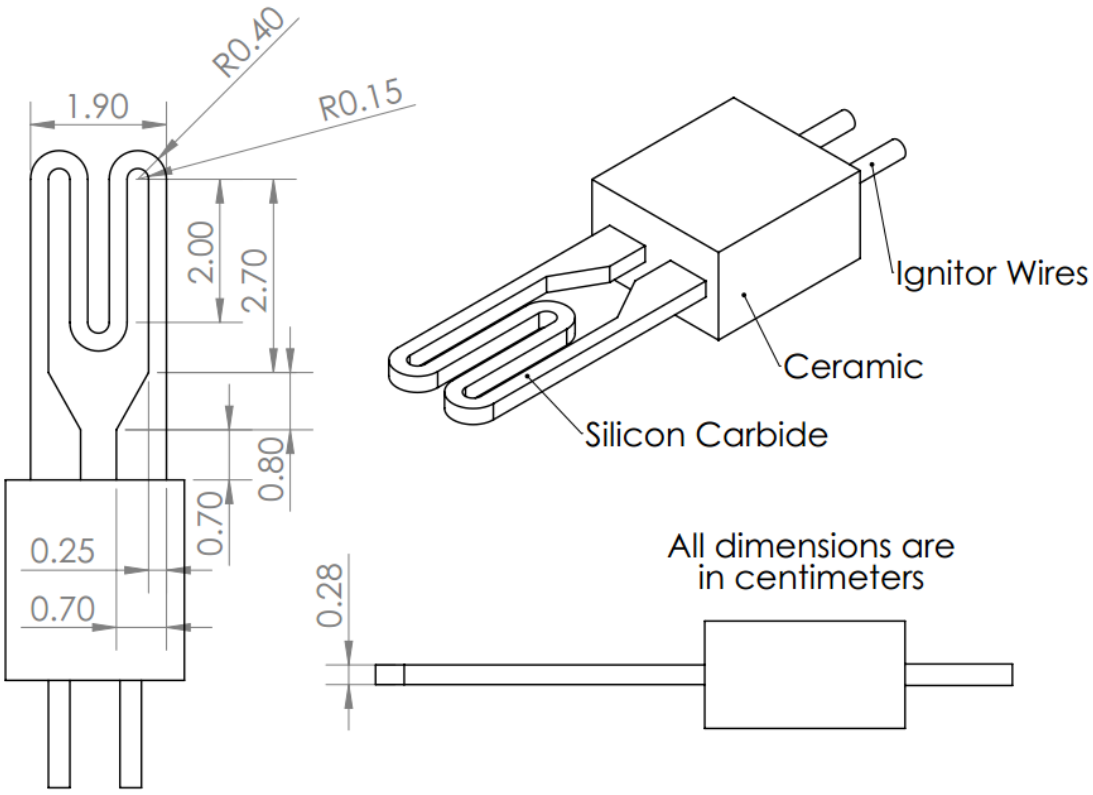

Figure 3.6: Ignitor Schematic

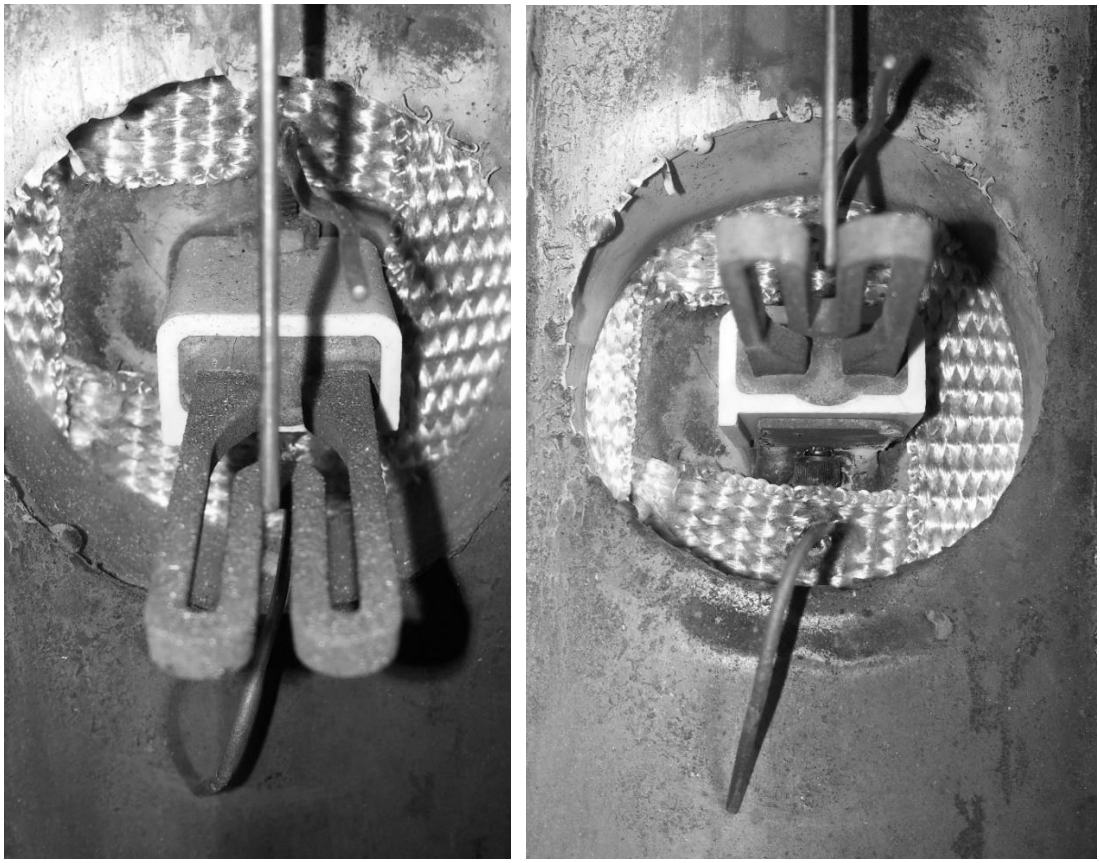

Figure 3.7: Images of the ignitor mount and combustion chamber thermocouples

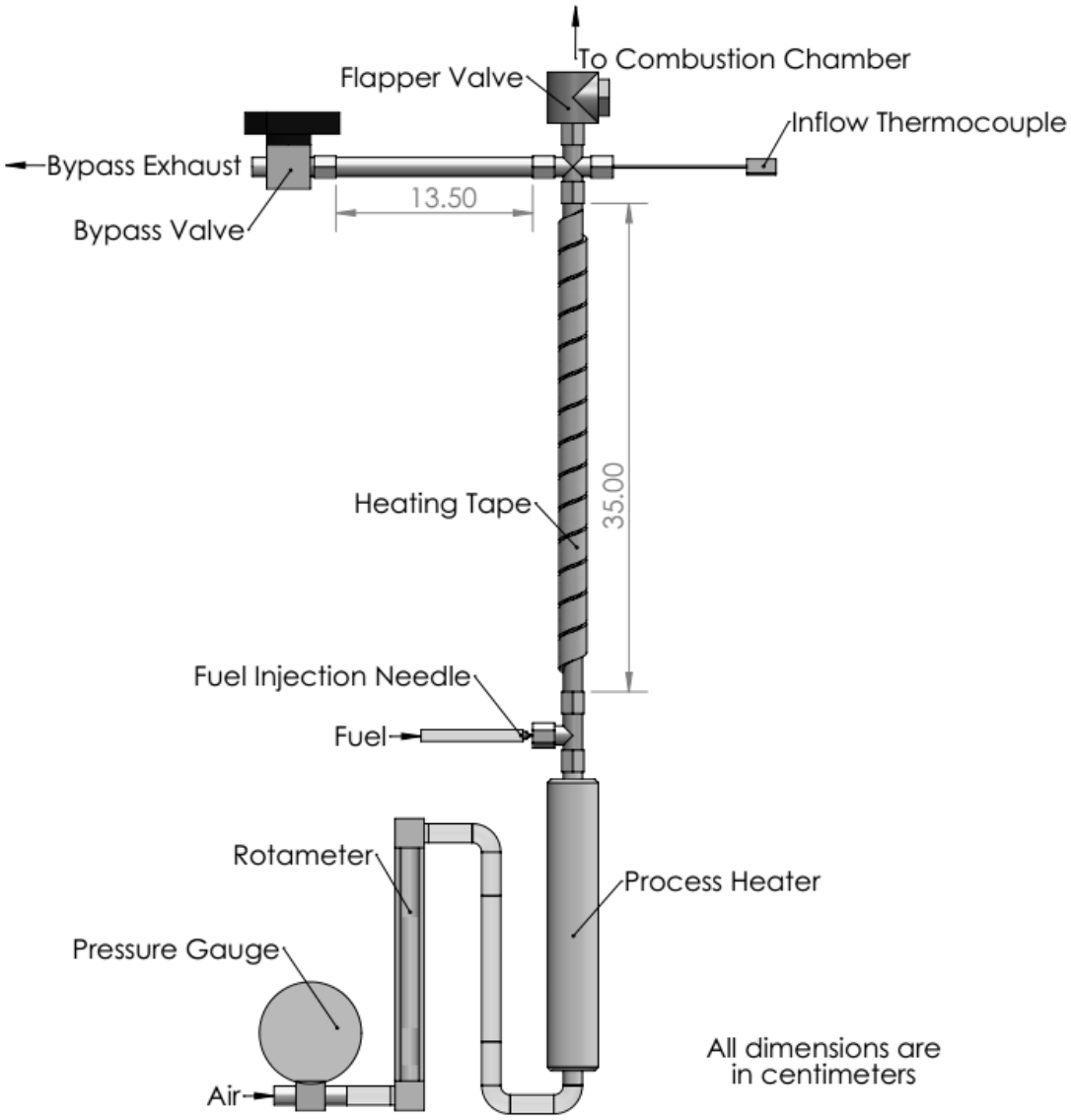

Figure 3.8: Air/fuel delivery system diagram

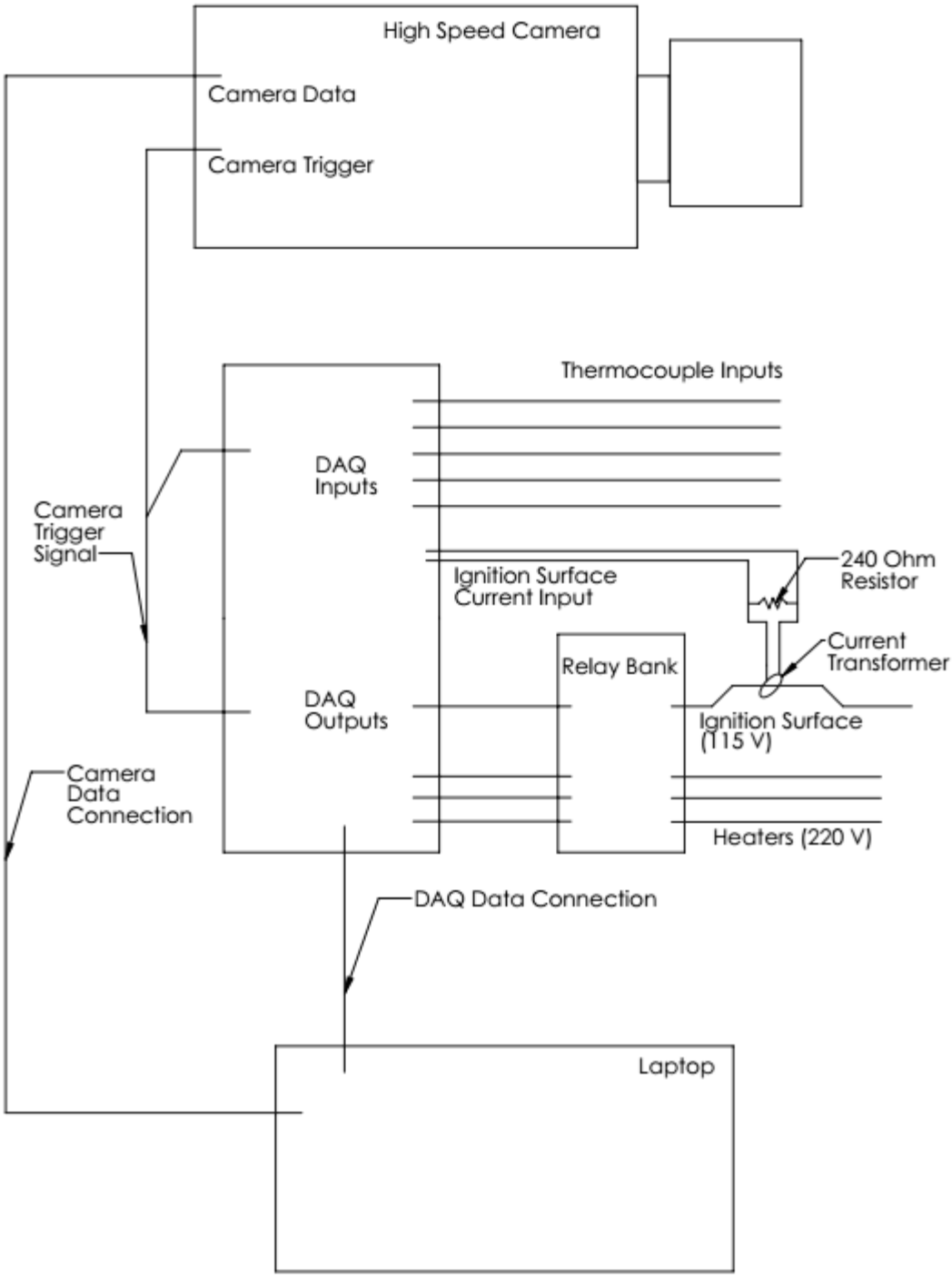

Figure 3.9: System diagram

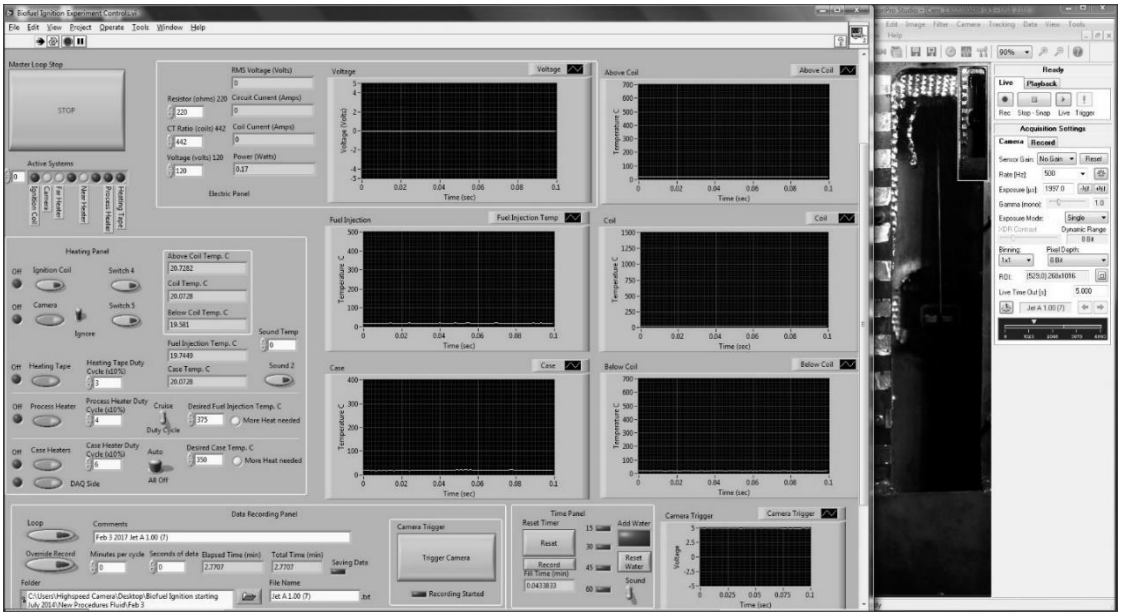

Figure 3.10: LabVIEW and high speed camera user interfaces

Chapter 4: Results and Discussion

The results and analysis of the various ignition properties of the tested fuels and equivalence ratios are presented in this chapter. First, the calibration results that were used to determine the temperature of the ignitor, filling time duration and airflow rate are discussed. Next, example results and calculations for a trial of Jet A are presented. The results for Jet A are then compared to previously published results found in literature for a variety of available measurements in order to validate the present results. Finally, the ignition temperature, energy, and delay, as well as the flame front velocities for the biofuels are presented and discussed.

4.1 Setup Calibration

4.1.1 Ignitor Temperature Calibration

Because the temperature of the ignitor was measured indirectly, a relationship was developed between the current flowing through the ignitor and the ignitor temperature, as previously discussed in Section 3.2.3. The ignitor was heated to various temperatures and the current flowing through the ignitor was measured to develop a relationship. The plot of current as a function of temperature is presented in Figure 4.1. The current flowing through the ignitor increased from 1.5 A to 5.5 A as the temperature increased from 20°C to 700°C. Between ignitor temperatures of 700°C to the maximum temperature of 1200°C, the ignitor current decreases gradually from 5.5 A to 4.5 A. The non-linear variation of current through the ignitor was due to the non-linear dependence of resistance of the ignitor on temperature.

To calculate the temperature, the current and temperature relations were broken into two graphs, as shown in Figure 4.2, which represent the temperature when the current

increased with time and when the current decreased with time. Best-fit polynomials were applied to each plot to obtain an equation for the temperature of the ignitor as a function of current. The equations are given as Equation 3.6, for instances of increasing current, and Equation 3.7, for decreasing current. The R squared values for each of the best fit lines was found to be 0.995 and 0.914 respectively, indicating that these equations were a good fit to the current variation with temperature.

To determine how the temperature of the ignitor varied over time, the temperatures were calculated and plotted with respect to time, shown in Figure 4.3. The ignitor temperature increased in a linear fashion, at a rate of approximately 114 K/s. Each circle represents the calculated instantaneous ignitor temperature using the ignitor current and Equations 3.6-3.7. Between the times of 2068.75 s and 2069.5 s, the current temperature relations are no longer valid as the current is not changing with temperature. However, the ignitor temperature through these times can be estimated by a linear trend of increasing temperature with time. The average rate of increase of temperature with respect to time was 110 K/s

4.1.2 Filling Duration

To determine an appropriate duration of time for filling the combustion chamber, described in Section 3.4.1, Jet A was tested at an equivalence ratio of 1.00 with multiple filling time durations. Filling times between 30 to 120 seconds, at 30 second intervals, were examined. The resulting adjusted ignition energy was plotted in Figure 4.4 using Equation 3.5 described in Section 3.2.1. The average adjusted ignition energy was nearly constant for each filling time at a value of approximately 278 J, with measurements ranging between 269 J and 286 J. To provide an adequate duration of time for temperature

and flowrate stabilization, as well as prerecording of the high speed camera, a filling time of 60 seconds was selected for the experiments.

4.1.3 Airflow Rates

To determine an appropriate volumetric airflow rate for the filling of the combustion chamber, described in Section 3.4.2, Jet A was tested under conditions similar to those of the prior filling time trial, but for an airflow rate of 24.0 L/min in place of the previously used 30.3 L/min. Figure 4.5 shows the plot of the adjusted ignition energy for the lower airflow rate for various fueling time lengths. The average adjusted ignition energy is constant near a value of 263 J, with measurements ranging from 202 J to 316 J. Comparing adjusted ignition energy between the flowrates, the lower airflow rate for all filling time lengths showed a larger variation than that of the higher flowrates from Figure 4.4. Reasons for this higher variation are uncertain, however the lower flow rate may have resulted in a less well-mixed fuel vapor/ air mixture, resulting in significant local equivalence ratio variations in the chamber. For the biofuel and Jet A trials, filling airflow rates of 30.3 L/min were used due to the smaller range of ignition energy values, indicating more consistent results and less uncertainty in the measurements.

4.2 Example Data and Calculations

This section gives an example of the data collected and calculations preformed for Jet A at an equivalence ratio of 1.00. The data for other fuels was processed in a similar manner.

4.2.1 Example Data

Thermocouple temperatures, the ignitor current, and the ignitor power were recorded by the DAQ and LabView program for each trial conducted. Figure 4.6 displays

the temperature data during the trial for the each of the four thermocouple locations, coil, above coil, mixture inflow, and case. These thermocouple locations are described in greater detail in Sections 3.2.2 and 3.2.3. Temperatures were recorded once a minute during the heat up phase, described in Section 3.3.1, and continuously at a rate of 1000 Hz during the fueling and ignition phases, described in Sections 3.3.2 and 3.3.3. Times for the beginning of the filling phase as well as the enabling and disabling of the ignitor during the ignition phase are marked with dotted vertical lines. The mixture inflow temperature quickly rose to, and leveled off at, a temperature of 375°C within the first 3 minutes. The temperatures 1 mm above the ignitor, 15 mm above the ignitor, and at the case rose slowly to values of 325°C, 340°C, and 350°C, in approximately 20 minutes, oscillating within ±10°C until the start of the filling phase at 33 minutes.

Figure 4.7 provides a closer view of the filling and ignition phases, previously shown in Figure 4.6. The filling phase began at approximately 1990 seconds into the run. As the fuel was injected into the inflow airstream, the mixture inflow/chamber inlet temperature oscillated between 370°C and 380°C. The temperatures 1 mm above the ignitor, 15 mm above the ignitor, and at the case increased by approximately 50 to 75°C to values of 400°C, 420°C, and 400°C. The fueling phase lasted for 1 minute and stopped at 2050 seconds. Between the end of the fuel injection and enabling of the ignitor, the setup was prepared for ignition, as described in the beginning of the ignition phase, Section 3.3.3. Visible as well in this figure is the sharp 10 to 15°C increase in temperature for the 15 mm above ignitor and case thermocouple locations following the ignition at time 2068.5 seconds. This was expected as the temperature and pressure of a gas rose significantly following combustion.

Figure 4.8 shows a closer view of the period of time the ignitor was active, from 2066 to 2071 seconds. The ignitor current and ignition temperature are also displayed alongside the temperature data. Times for the enabling and disabling of the ignitor (2066.100 s and 2071.000 s) as well as when the camera was triggered (2069.206 s) and when the ignition occurred (2068.502 s) are displayed as vertical lines. While the ignitor was on, the current flowing through the ignitor was recorded, as described in Section 3.2.1, and is displayed in the Figure 4.8 on the second axis. The current increased from 3500 mA to 5500 mA over a period of 3 seconds. The current then slowly decreased to a value of 5250 mA over the following 2 seconds. The temperature of the ignitor was calculated using the current temperature relations discussed in Section 3.2.3. The ignitor temperature is displayed in the figure along with a linear trend line to plot the expected ignitor temperature for the portion of level current, when the ignitor current and temperature were poorly related. Also noteworthy is the slight increase in the mixture temperature at 1 mm above the ignitor immediately following ignition, consistent with the expectation of a temperature increase due to a passing flame.

Images of the combustion captured by the high speed camera are presented in Figure 4.9. These images are in sequential order from left to right, top to bottom. The larger number indicates the image's frame number. Negative values indicate frames recorded before the camera was triggered, at frame number 0. The smaller, lower number indicates the time of the image in seconds, which can be matched to the previous temperatures figures. At a rate of 500 frames per second, there is 2 millisecond interval between each frame. The reflective tabs on the left side of the images were 1 cm in height and spaced 1 cm apart vertically. These tabs were used to measure the flame front and

ember travel distances. The flame is first visible in frame -352 and moves at a constant rate towards the top and bottom of the combustion chamber. It is also observed that the upper flame front moved significantly quicker than the lower flame front, due to the buoyancy effect of the high temperature flame products. In this trial, an ember is clearly visible near the lower flame front on the right side, beginning at frame -340. The ember moves upward, following the significant bulk flow created by buoyancy forces. Figure 4.10 shows the position of the ember, relative to the bottom of the window with respect to time. The ember accelerates upwards with the flow and reaches a steady velocity beginning at frame -336.

4.2.2 Example Calculations

The flame front and flow velocities, discussed previously in Section 3.2.4, were calculated with the images obtained from the high speed camera. Using the images recorded by the high speed camera, the first flame image is shown to occur at frame number -352. At 500 frames per second, and 2 ms per frame, the ignition occurred 0.704 seconds before the camera was triggered. The camera was triggered at 2069.206 seconds; using Equation 3.10, the first flame appearance was calculated to have occurred at 2068.502 seconds. At the first appearance, the flame had a height of 0.75 cm upward and 0 cm downward relative to the ignitor (approximately 8 cm above the bottom marking on the combustion chamber window). The flame reached the exit, 9.0 cm upward of the ignition surface, at frame -343. Using Equation 3.8 with an initial frame of -352, initial distance of 0.75 cm, final frame of -343, final distance of 9 cm, and a frame rate of 500 fps, the upper flame front velocity was calculated to be 4.58 m/s. Similarly, the lower flame reached the lower portion of the marked window, 8 cm below the ignitor, at a frame

of -321. Again, using Equation 3.8, with an initial frame of -352, initial distance of 0 cm, final frame of -321, final distance of 8.0 cm, and a frame rate of 500 fps, the lower flame front velocity was calculated to be 1.29 m/s. The ember in the lower right hand side following the flame was tracked for 12 frames, -336 to -325 to measure flow velocity upward. The flow velocity (taken to be equal to the ember velocity) was calculated using Equation 3.9 with an initial position of 6.75 at an initial frame of -336, a final position of 12.25 at a frame of -325, with a frame rate of 500 fps. The ember velocity was 2.50 m/s. Velocities of other embers were also calculated, and the average ember/flow velocity was found to be 3.13 m/s, with a standard deviation of 0.78 m/s, which was similar to the 3.29 m/s difference between the upper and lower flame front velocities.

Using the current flowing through the ignitor at the time of ignition, the ignition surface temperature was calculated. At the time of ignition, the ignitor current, plotted in Figure 4.8, was 5.421 A and was increasing with time. Using Equation 3.6, the ignitor surface temperature, described in Section 3.2.3, was calculated to be 660°C. The time interval for ignition, described in Section 3.2.5, was calculated to be 2.402 s using Equation 3.11 with an initial ignitor enabled time of 2066.100 s and an ignition time of 2068.502 s. The measured ignition energy, described in Section 3.2.1, was calculated from the ignitor power and Equation 3.1. Power used by the ignitor was determined by using the ignitor current data displayed in Figure 4.8, between the ignitor enabled and ignition times, multiplied by the assumed wall voltage of 120 V. For this trial, the measured ignition energy was calculated to be 1252.3 J.

Lastly, the ignition energy was adjusted using the process described in Section 3.2.1 to account for energy lost to the ignitor and radiation. First, the measured ignition

energy was corrected for the actual wall voltage of 115V using Equation 3.2. The voltage corrected ignition energy was 1200.1 J. Next, the energy used by the ignitor was calculated. An initial ignitor temperature of 393.7°C was found using Equation 3.6 and the second recorded current value (the first value was an incomplete measure of the current flowing through the ignitor, as the ignitor was turned on halfway through the recording cycle). The energy used by the ignitor was calculated using Equation 3.3 where the mass of the ignitor was 4.65 grams, and the specific heat was 670 J/kg K. Approximately 830.6 Joules were used to heat the ignitor. Following the ignitor energy calculation, the energy lost to radiation was determined. The ignitor temperature was approximated as a linear function of time, using the initial and ignition temperatures as well as the ignition delay to calculate the slope, and a Y-intercept of the initial temperature. The radiation energy was then calculated using Equation 3.4 with the values listed in Section 3.2.1 and a case temperature of 670.8°C. The energy lost to radiation was found to be approximately 55.6 J. Finally, the ignitor and radiation energies were subtracted from the voltage corrected ignition energy of 1200.1 J to find an adjusted ignition energy of 313.9 J.

4.3 Setup verification

In order to ensure that the setup provided accurate and reliable results, trials were conducted with Jet A fuel for a variety of equivalence ratios, and the measurements were compared to those in existing literature.

4.3.1 Ignition Temperature

Kuchta et al. (1965), Kuchta and Cato (1966), and Boettcher (2012) all observed that ignition temperature of hydrocarbon fuels was constant with changing equivalence

ratios for a fuel. Figure 4.11 shows measured variation in ignition temperature of Jet A with equivalence ratios between 0.75 and 2.00. The average ignition temperature decreased slightly from 644±14°C at an equivalence ratio of 0.75 to 607±14°C at an equivalence ratio of 2.00. Overall, the ignition temperature did not vary significantly with changes in equivalence ratio, in agreement with previous works.

As noted by Kuchta et al. (1965), Kuchta and Cato (1966), and Botteri et al. (1979), the ignitor surface area affects the ignition temperature of a fuel air mixture. Figure 4.12 shows the plotted results of Kuchta et al. (1965), relating ignitor size and ignition temperature for JP-6 and Hexane fuels, which were most similar to Jet-A. As the ignition surface area decreased, the ignition temperature increased. For the surface area of the ignitor used in this present work, 17.8 cm^2, the ignition temperature was expected to be approximately 640°C to 670°C. The calculated ignition temperatures for Jet A, shown in Figure 4.11, ranged between 607±14°C to 644±14°C, in agreement with previously published values by Kuchta et al. (1965) for similarly sized ignitors and fuels.

4.3.2 Flame Velocities

Boettcher (2012) measured the flame velocities of n-hexane as a surrogate fuel for Jet A. The vertical flame velocities for n-hexane peaked at an equivalence ratio between 1.2 and 1.3, with a velocity of 5.5 m/s. At equivalence ratios of 0.75 and 2.00 the upper flame velocities were approximately 2.2 m/s. The upper flame velocities for Jet A in the current work are presented in Figure 4.13. The measured upper flame front velocities peaked at an equivalence ratio of 1.3 with a velocity of 6.08 m/s. At equivalence ratios of 0.75 and 2.00 the upper flame front velocities were 2.81 m/s and 1.76 m/s. These are similar to the values published by Boettcher (2012), reproduced in Figure 4.14. The

slightly higher velocities in the current study are expected as flame velocity has a temperature dependence of $T^{1.55}$. The mixture in the current study was heated to near 673 K, which was larger than the mixture temperature 2 cm above the glow plug used by Boettcher, 600 K. For the same equivalence ratio it is then expected that the current study will have a larger flame velocity.

Due to buoyancy effects, a larger upper flame front velocity was observed, in both the current work and by Boettcher (2012), compared to the lateral/lower flame front velocities. The lateral flame velocities observed by Boettcher, displayed in Figure 4.14, peaked at an equivalence ratio of 1.2 at a velocity of 3.0 m/s. Figure 4.13 displays the lower flame front velocities measured in the current work, which peaked at an equivalence ratio of 1.2 to 1.4 with a velocity of 1.88 m/s, which is 62.7% of the lateral velocity measured by Boettcher (2012). Although the velocities themselves weren't in agreement, most likely due to a difference in orientation, the equivalence ratio at which the velocities were at a maximum were similar. The lower flame front velocity may have been subject to stronger buoyancy effects, resulting in a lower velocity compared to the lateral direction.

4.3.3 Ignition Energy Trends

Lewis and von Elbe (1961) and Lee et al. (2001) noted a concave upward parabolic trend in spark ignition energy for hydrocarbon fuels. Lee et al. (2001) measured the minimum ignition energy of Jet A, with laser generated sparks, to be 2 mJ at a pressure of 1 atm, temperature of 60°C, and estimated equivalence ratio of 1.98. A comparison between the ignition energies measured by Lee and the adjusted ignition energies in this study for Jet A are shown in Figure 4.15. The ignition energies are normalized using the

ignition energy at stoichiometric conditions to reduce the difference in magnitude between the spark and hot surface ignition methods. The normalized ignition energy of Jet A in the current study decreased from 1.0, at stoichiometric conditions, in a parabolic fashion to 0.2 as the equivalence ratio approached 2.0. Similarly, the normalized ignition energy measured by Lee decreased in a parabolic fashion from 1.0 at stoichiometric conditions to 0.7 at an equivalence ratio of 2.0. The trend displayed by the normalized ignition energy values in the current study agreed with the trend found by Lee and coworkers for spark ignition.

4.4 Results and Discussion

4.4.1 General Observations

Figure 4.16 displays a comparison between the brightness of each fuel at an equivalence ratio of 1.3. Jet A was the brightest fuel, while the biofuels were all slightly dimmer. Figure 4.17 through Figure 4.20 show the high speed images captured at various equivalence ratios for each fuel. Flames at lower equivalence ratios were light blue in color. The flames became a darker blue at higher equivalence ratios. The brightest flames occurred between the equivalence ratios of 1.30 and 1.50. At the more extreme equivalence ratios of 0.5, 1.75, and 2.00, the flame was observed to propagate slowly and was extremely dim. Occasionally, at the higher equivalence ratios of 1.75 and 2.00, the flame did not extend more than one or two centimeters downward before being extinguished.

The biofuel flames appeared dimmer than the Jet A ignition at similar equivalence ratios. After biofuel ignition at each equivalence ratio, the inside of the window was found to be obscured by a brown deposit. Figure 4.21 shows the deposit buildup after testing all

nine equivalence ratios. This required cleaning maintenance through the use of a scotch bright pad and stove top cleaner. Vigorous scrubbing was required to remove the deposits. These types of deposits were not noticed during Jet A trials and could present a problem to engines using biodiesels with glow plugs or spark ignitors. Other studies also noticed significant deposits when biofuels were used in engines (Agarwal, 2007).

Figure 4.22 through Figure 4.25 show the images captured by the high speed camera at an equivalence ratio of 1.3 for each of the fuels tested. The flame front moved outward in a linear fashion from the center of the combustion chamber near the ignitor. The upper flame front velocity was higher than the lower flame front velocity, due to the buoyancy effect caused by the high flame temperature. The lower flame front velocity was found to be similar to the laminar flame speed of a fuel.

4.4.2 Lower Flame Front Velocity

The flame front velocities were calculated using images captured by the high speed camera during combustion. Velocities for the various fuels and equivalence ratios are displayed in Figure 4.26. The flame front velocities were parabola-shaped in a downward fashion. Jet A, CME, and SME peaked at an equivalence ratio of 1.30. PME reached a maximum flame front velocity at an equivalence ratio of 1.40. The biodiesels were generally within a margin of uncertainty from each other in terms of flame velocities. Jet A had a higher flame velocity (1.88 m/s, Φ=1.30) than the biodiesels (1.60 m/s, Φ=1.30) at equivalence ratios between 0.75 and 1.75. The biodiesels had similar velocities, within 0.2 m/s of each other. The uncertainties for the lower flame front velocities averaged ±0.45 m/s. For equivalence ratios ranging between 0.75 and 1.50, the

uncertainties averaged 0.32 m/s. At higher equivalence ratios, the uncertainties increased to ±0.9 m/s.

Gómez-Meyer et al. (2012) measured the laminar flame velocities of diesel as well as SME and CME for equivalence ratios of 1.0, 1.1, and 1.2. Both SME and CME were noted to be not significantly different and peaked at an equivalence ratio of 1.1 with laminar flame velocities of 1.07 m/s and 1.10 m/s. These velocities were compared with the lower flame front velocities for SME and CME in the current study, which are displayed in Figure 4.27. The maximum lower flame velocities for SME and CME in the current study peaked at an equivalence ratio of 1.3 with velocities of approximately 1.60 m/s. This was due to of the larger temperature in the current study and the flame velocity temperature dependence of $T^{1.5}$, increasing the reaction rate and flame front velocity. However, at an equivalence ratio of 1.0, the current study measured a lower flame front velocity for SME and CME of 1.10 m/s, which is in agreement with the values for laminar flame velocity observed by Gómez-Meyer et al. (2012), approximately 1.0 m/s.

4.4.3 Upper Flame Front Velocity

The average upper flame front velocities were plotted in Figure 4.28. Similar to the lower flame front velocities, the upper flame front velocities were parabolic in nature, peaking at an equivalence ratio of 1.30 for Jet A, CME, and SME. PME peaked at an equivalence ratio of 1.40. Jet A had a higher flame front velocity from equivalence ratios 0.75 to 1.50. Average upper flame front velocity uncertainties were 1.07 m/s. For equivalence ratios between 0.75 and 1.50, the average uncertainty was ±0.83 m/s. Jet A had the highest flame front velocity at a value of 6.08 m/s at an equivalence ratio of 1.30,

followed by SME at a velocity of 5.02 m/s (82.6% of Jet A) and CME and PME at a velocity of 4.70 m/s (77.3% of Jet A).

Upper flame front velocities were significantly higher than the lower flame front velocities. The differences in the upper and lower flame front velocities were due to the large buoyancy effect, caused by high temperature flame which caused a decrease in density of the combustion products. This caused the products to rise, carrying the flame front with it. To quantify the buoyancy effect, the bulk vertical flow rate was measured by the movements of glowing embers which followed the flame front. An example of these embers is displayed in Figure 4.29. The velocities of these embers were calculated using the same method as the flame front velocities, and represented the mixture flow following the flame front. Table 4.1 shows the calculated flame velocities and ember velocities for an individual trial of Jet A at various equivalence ratios. The difference in the upper and lower flame front velocities was similar to the ember velocity, indicating that the difference between the two velocities was due primarily to a bulk flow in the upward direction, caused by the buoyancy effect.

4.4.4 Ignition Temperature

The ignition temperatures, as calculated by the ignitor current at the instance of ignition, are plotted in Figure 4.30 for each fuel and equivalence ratio. The difference in ignition temperature between fuels was not significant within experimental uncertainty. At an equivalence ratio of 1.00, Jet A had an ignition temperature of 643°C. CME and SME had a slightly lower ignition temperature of 635°C, and PME had a slightly higher ignition temperature of 646°C. The uncertainty for ignition temperature measurements was ±20.08°C. Ignition temperature decreased slightly with equivalence ratio for all fuels

from an average of 644°C at equivalence ratio 0.75 to 613°C at an equivalence ratio of 2.00. The ignition temperature's loose dependence on equivalence ratio was also noted by Kuchta et al. (1965), Kuchta and Cato (1966), and Boettcher (2012) in their studies with hydrocarbon fuels. The similarity in ignition temperature between Jet A and the biodiesels does not follow the trend noticed by Zabetakis et al. (1954) and Kuchta et al. (1965) of increasing ignition temperature with increasing molecular weight of the fuel.

4.4.5 Time Interval for Ignition and Measured Ignition Energy

Variations in the time interval for ignition, with respect to equivalence ratio and fuel, are displayed in Figure 4.31. Time intervals for ignition decreased as the equivalence ratio increased for each fuel tested. Each fuel required a similar length of time at an equivalence ratio of 0.75, of 2.62 s. Generally, Jet A and PME had the longest time interval, followed by CME and finally SME. The time interval for ignition reached a minimum at an equivalence ratio of 2.00 for each fuel, with a delay of 2.0 s for Jet A, CME, and PME, and 1.8 s for SME. Uncertainties for the time interval for ignition averaged ±0.22 s for a 95% confidence value. Using a relationship noted by Laurendeau, the reaction rate of a fuel is exponentially related to the initial fuel mass fraction and mixture density (Laurendeau, 1982). Table 4.2 through Table 4.5 contain the density, specific heat, and initial mass fractions of both the fuel and oxidizer for each of the fuels and equivalence ratios tested. For each fuel, as the equivalence ratio increased, so did the density and fuel mass fraction. As a result, the reaction rate also increased with equivalence ratio. Higher reaction rates imply a quicker heat release and lower time interval for ignition with increased equivalence ratio.

Variations in the measured ignition energy are displayed in Figure 4.32. Measured ignition energy varied with equivalence ratio and fuel in the same fashion as the time interval for ignition. This was expected, as a smaller time interval for ignition results in a smaller range for integration in Equation 3.1 and a lower ignition energy. In general, the measured ignition energy decreased with increasing equivalence ratio, from approximately 1320 J, at an equivalence ratio of 0.75, to 1000 J for Jet A, CME, and PME, and 923 J for SME at an equivalence ratio of 2.00. The average uncertainty for 95% confidence for measured ignition energy was ±117 J. Because the ignitor temperature ramped up at a constant rate, the time interval for ignition and measured ignition energy were coupled and depended on the initial temperature of the ignitor.

The initial fuel air mixture temperature, as measured by the thermocouple 1 mm above ignitor when the ignitor was first enabled, is plotted in Figure 4.33. Initial mixture temperature increased slightly with increasing equivalence ratio. The increase in temperature is expected to be because of the increase in energy flow rate into the chamber volume. At an equivalence ratio of 0.75 the initial mixture temperature was 378°C. This increased in a linear fashion with equivalence ratio to an initial mixture temperature of 414°C at an equivalence ratio of 2.00. SME generally had the highest initial mixture temperature, with 400°C at an equivalence ratio of 1.00. Jet A and CME had a slightly lower mixture temperature of 389°C. Finally, PME generally had the lowest initial mixture temperature at 380°C for an equivalence ratio of 1.00. The average uncertainty of the initial mixture temperature measurements, was ±15°C. A higher initial mixture temperature heated up the ignitor and influenced the time interval for ignition. Figure 4.34 displays the initial temperature of the ignitor, measured from the first instance it was

enabled, with respect to equivalence ratio for all the tested fuels. The initial ignitor temperature followed the general trend of the initial mixture temperature, increasing with equivalence ratio. The temperature for Jet A increased from 362°C at an equivalence ratio of 0.75 to 385°C at an equivalence ratio of 2.00. PME had initial temperature similar to that of Jet A. CME and SME averaged an initial ignitor temperature of 4.5°C and 17.1°C above the initial ignitor temperature of Jet A. A larger initial ignitor temperature would require less time to heat the ignitor to the ignition temperature.

4.4.6 Adjusted Ignition Energy

The adjusted ignition energy was used to account for the energy lost through radiation or from heating up the ignitor. Values for the adjusted ignition energy are plotted in Figure 4.35, with respect to equivalence ratio, for each fuel. The adjusted ignition energy has a parabolic shape, with a minimum near an equivalence ratio of 2.00. At an equivalence ratio of 0.75, the adjusted ignition energy was approximately 334 J for Jet A, CME, and PME. SME had a higher ignition energy of 354 J. These decreased from an equivalence ratio of 0.75 to an equivalence ratio of 1.30 and leveled off at an average adjusted ignition energy value of 270 J. The average uncertainties, for a confidence value of 95%, were ±43 J. For an equivalence ratio of 2.00, the ignition energy of CME had an uncertainty of ±96 J.

4.4.7 Ignition Energy Discussion

Lewis and von Elbe (1961) noted a relationship between the equivalence ratio where spark ignition energy was a minimum and the number of carbon atoms in a fuel. The minimum spark ignition energy equivalence ratio for hydrocarbon fuels, observed by Lewis and von Elbe, is plotted in Figure 4.36, along with the minimum laser spark ignition

energy equivalence ratio found by Lee et al. (2001) for Jet A. A logarithmic relationship best fit the relationship between the number of carbon atoms and the minimum ignition energy equivalence ratio. Extrapolating to the higher number of carbon atoms, it is expected that the biodiesels SME, CME, and PME will reach a minimum for ignition energy at larger equivalence ratios, near 2.25. Additionally, through Lee's work, in agreement with the empirical trends observed by Lewis and von Elbe, it is expected that Jet A will reach a minimum ignition energy near an equivalence ratio of 2. The decrease in ignition energy with equivalence ratio and leveling off near equivalence ratio of 2.00 indicate an agreement between the observations in current and previous studies with regards to the equivalence ratio at which ignition energy is at a minimum.

The flame velocity of a fuel is related to the reaction rate (Turns, 2000). Since laminar flame velocity of the biofuels was also similar for all the biofuels, it is expected that they will have similar reaction rates. However, the flame velocities of the biofuels are only 70-83% of the flame velocities of Jet A for the same equivalence ratio and 80-90% of the flame velocities of diesel (Gomez-Meyer et al., 2012). With slower flame velocities, the biodiesels are expected to have slower reaction rates and lower heat release rates compared to diesel and Jet A. The reaction rate of a fuel is inversely related to the required ignition energy (Turns, 2000). A lower flame velocity indicates a lower reaction rate and a higher required ignition energy. As the flame velocity of the biofuels was lower than that of Jet A, it was expected that they would have a lower ignition energy for the same equivalence ratio.

In addition to the flame velocity, the thermal properties of the mixture also played a significant role in the required ignition energies. As the ignitor heated up, a temperature

gradient developed between the ignitor and the wall. A representation of this temperature gradient can be seen in Figure 4.37. The mixture temperature is expected to decrease sharply away from the ignitor, leveling out towards the walls. As the ignitor temperature increases, the temperature gradient increases, as the heat is unable to diffuse into the surrounding mixture quick enough. Ignition occurs when a sufficient amount of energy is provided to the mixture layer near the ignitor and is unable to diffuse throughout the remainder of the mixture. Factors such as buoyancy also play a role in moving energy away from the ignitor, increasing the required amount of energy to reach ignition.

The equivalence ratios tested were all below the minimum ignition energy equivalence ratios of the fuels. For equivalence ratios 0.75 to 2.00, the trends noted by Lewis and von Elbe predict a larger ignition energy for the biodiesels compared to Jet A, as the equivalence ratio for the minimum ignition energy is higher for biodiesels than Jet A. This is supported by the flame velocities of Jet A and the tested biodiesels, and their theoretical effect on ignition energy.

Table 4.1: Flame and ember velocities at various equivalence ratios for a trial of Jet A

Equivalence Ratio	Upper Flame Front Velocity (m/s)	Lower Flame Front Velocity (m/s)	Difference Between Upper and Lower Flame Front Velocities (m/s)	Ember Velocities (m/s)
1.0	3.4	1.2	2.2	2.1
1.1	5.0	1.6	3.4	3.5
1.2	5.0	1.5	3.5	3.5
1.3	6.3	1.9	4.4	4.3
1.4	6.3	2.1	4.2	4.3
1.5	5.7	1.8	3.9	3.8

Table 4.2: Physical and thermal properties of Jet A/air mixtures at 670 K

Equivalence Ratio	Mixture Density (kg/m^3)	Constant Pressure Specific Heat (J/kg K)	Fuel Mass Fraction	Oxygen Mass Fraction
0.75	0.547	1208.2	0.050	0.222
1.00	0.555	1248.6	0.065	0.218
1.10	0.558	1264.5	0.071	0.217
1.20	0.561	1280.1	0.077	0.215
1.30	0.564	1295.5	0.083	0.214
1.40	0.566	1310.7	0.089	0.212
1.50	0.569	1325.7	0.094	0.211
1.75	0.577	1362.5	0.108	0.208
2.00	0.584	1398.1	0.122	0.205

Table 4.3: Physical and thermal properties of CME/air mixtures at 670 K

Equivalence Ratio	Mixture Density (kg/m^3)	Constant Pressure Specific Heat (J/kg K)	Fuel Mass Fraction	Oxygen Mass Fraction
0.75	0.553	1178.4	0.057	0.220
1.00	0.562	1209.3	0.074	0.216
1.10	0.566	1221.3	0.081	0.214
1.20	0.569	1233.2	0.087	0.213
1.30	0.573	1244.9	0.094	0.211
1.40	0.577	1256.4	0.101	0.210
1.50	0.580	1267.7	0.107	0.208
1.75	0.590	1295.4	0.123	0.205
2.00	0.599	1322.1	0.138	0.201

Table 4.4: Physical and thermal properties of SME/air mixtures at 670 K

Equivalence Ratio	Mixture Density (kg/m^3)	Constant Pressure Specific Heat (J/kg K)	Fuel Mass Fraction	Oxygen Mass Fraction
0.75	0.553	1179.6	0.057	0.220
1.00	0.562	1210.8	0.074	0.216
1.10	0.566	1223.0	0.081	0.214
1.20	0.570	1235.0	0.088	0.213
1.30	0.573	1246.8	0.095	0.211
1.40	0.577	1258.4	0.101	0.209
1.50	0.581	1269.9	0.108	0.208
1.75	0.590	1297.8	0.123	0.204
2.00	0.599	1324.8	0.139	0.201

Table 4.5: Physical and thermal properties of PME/air mixtures at 670 K

Equivalence Ratio	Mixture Density (kg/m^3)	Constant Pressure Specific Heat (J/kg K)	Fuel Mass Fraction	Oxygen Mass Fraction
0.75	0.553	1191.7	0.057	0.220
1.00	0.562	1226.7	0.075	0.216
1.10	0.566	1240.3	0.082	0.214
1.20	0.569	1253.7	0.088	0.212
1.30	0.573	1266.9	0.095	0.211
1.40	0.577	1280.0	0.102	0.209
1.50	0.580	1292.8	0.108	0.208
1.75	0.590	1324.1	0.124	0.204
2.00	0.599	1354.3	0.139	0.201

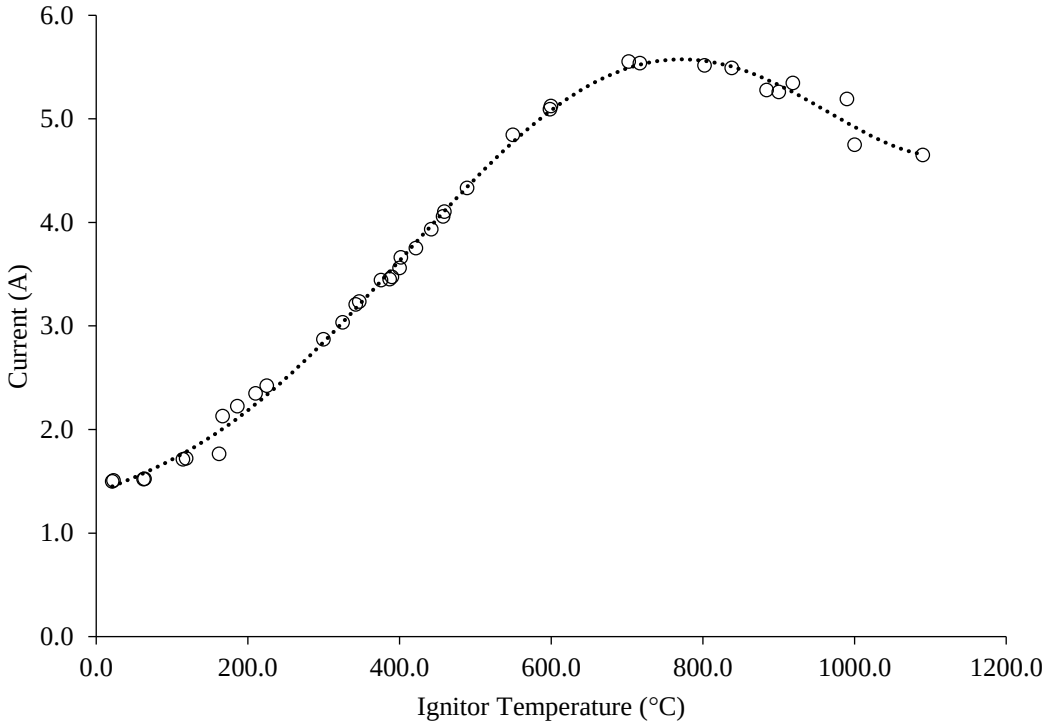

Figure 4.1: Ignitor current at various temperatures

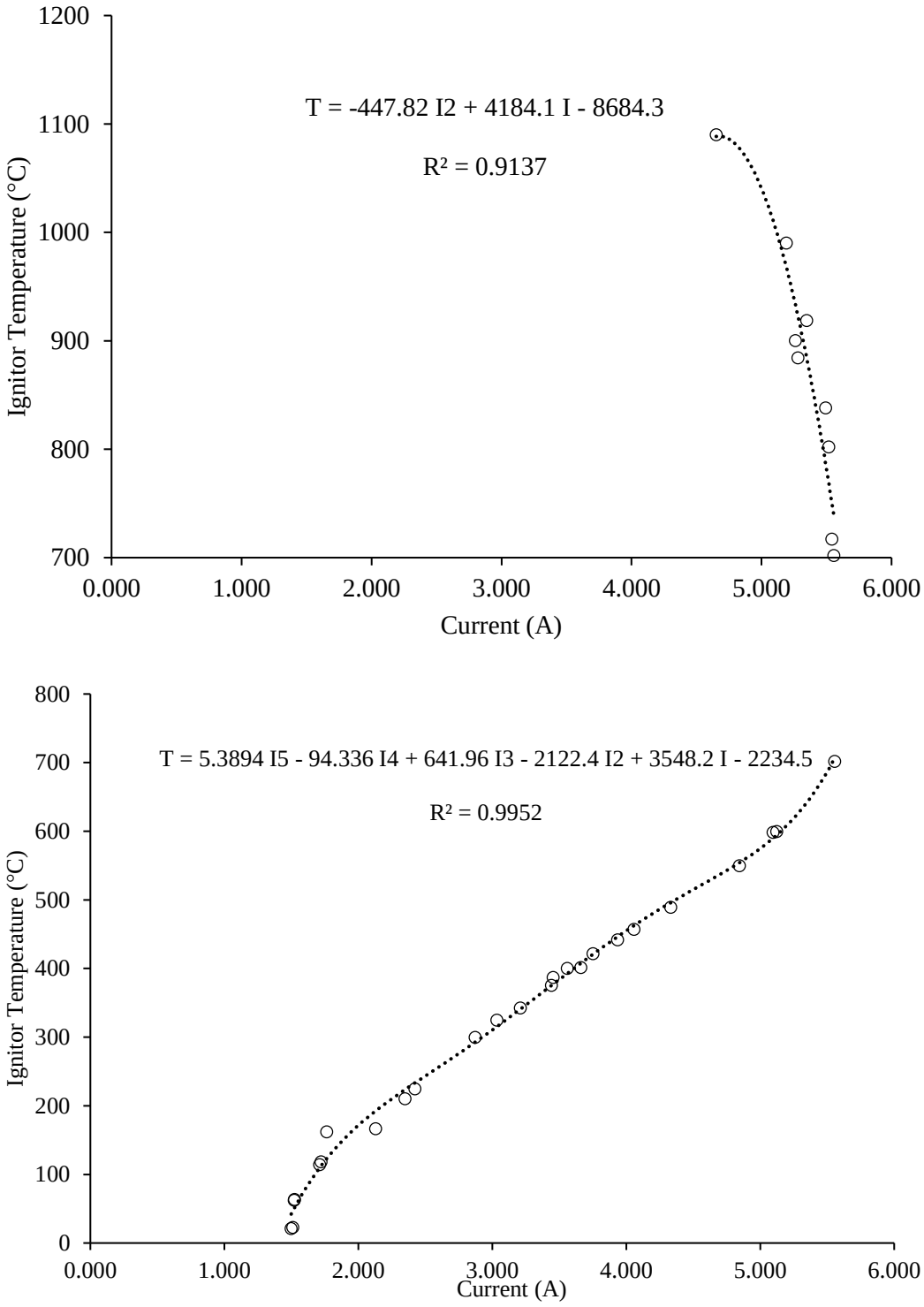

Figure 4.2: Ignitor temperatures as a function of current and change in current with time

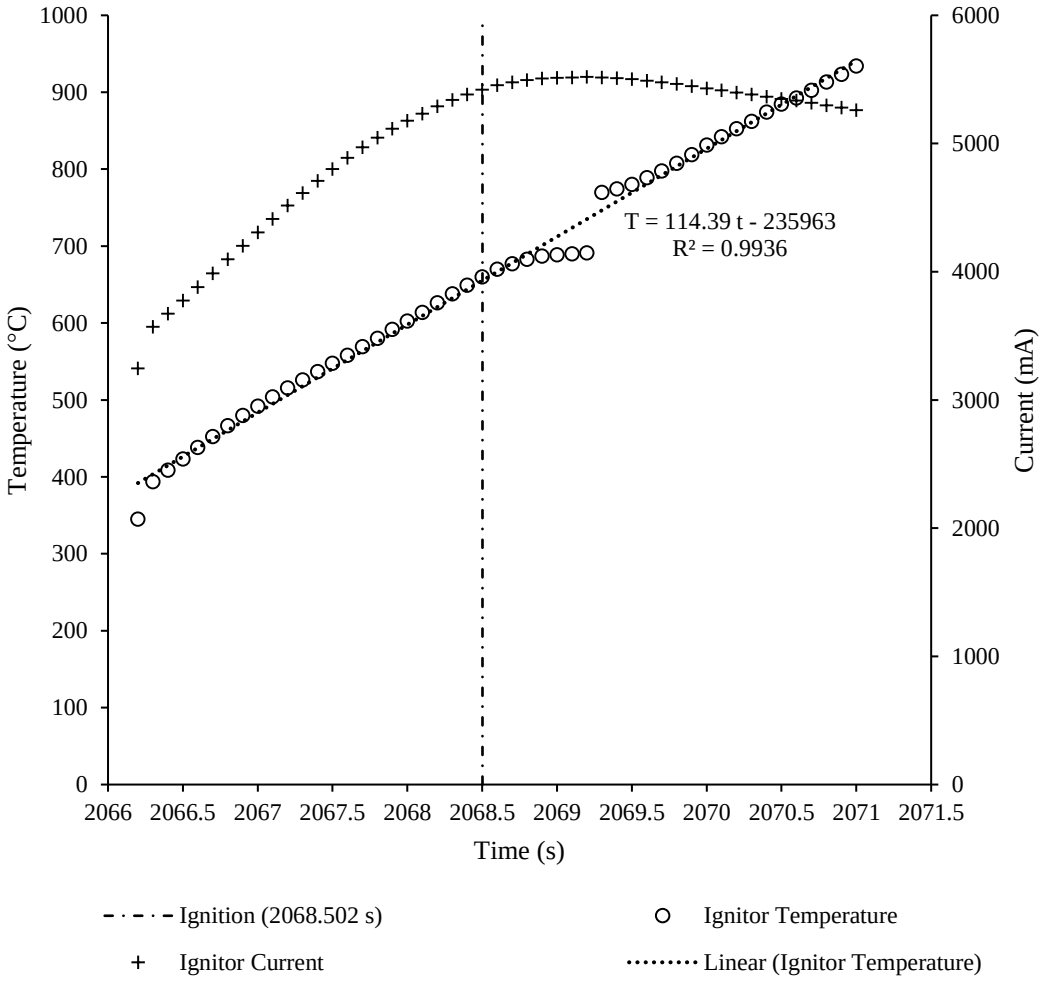

Figure 4.3: Ignitor temperature varying with time

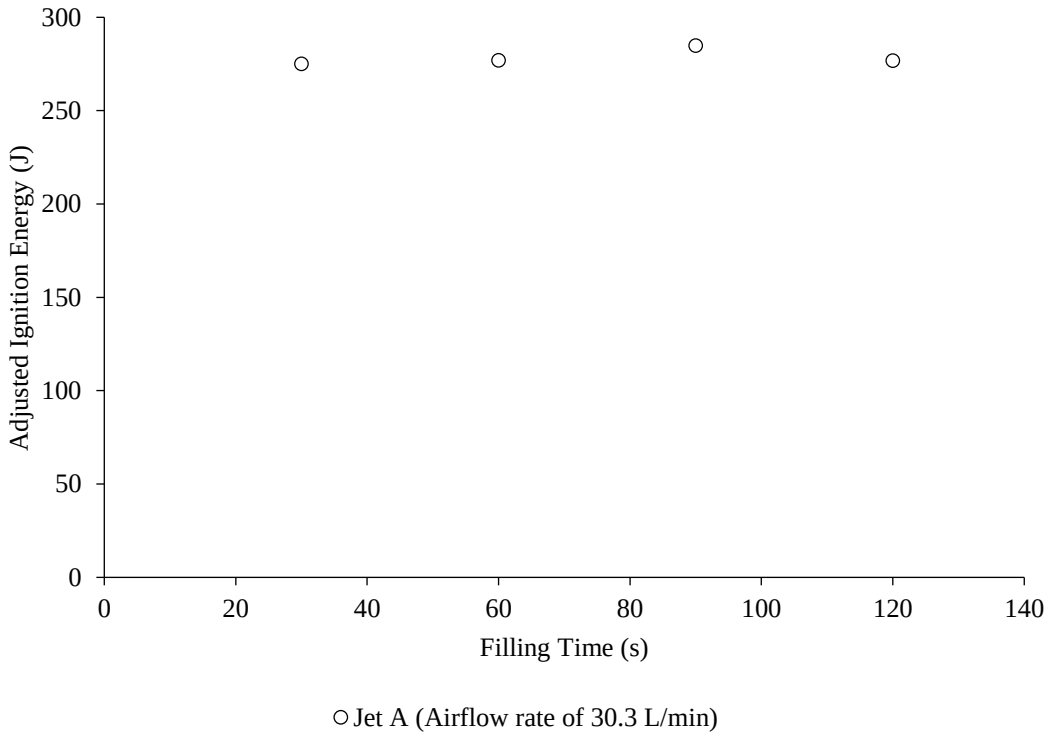

Figure 4.4: Adjusted ignition energy for Jet A, equivalence ratio 1.00, for varying fueling times at a fueling airflow rate of 30.3 L/min

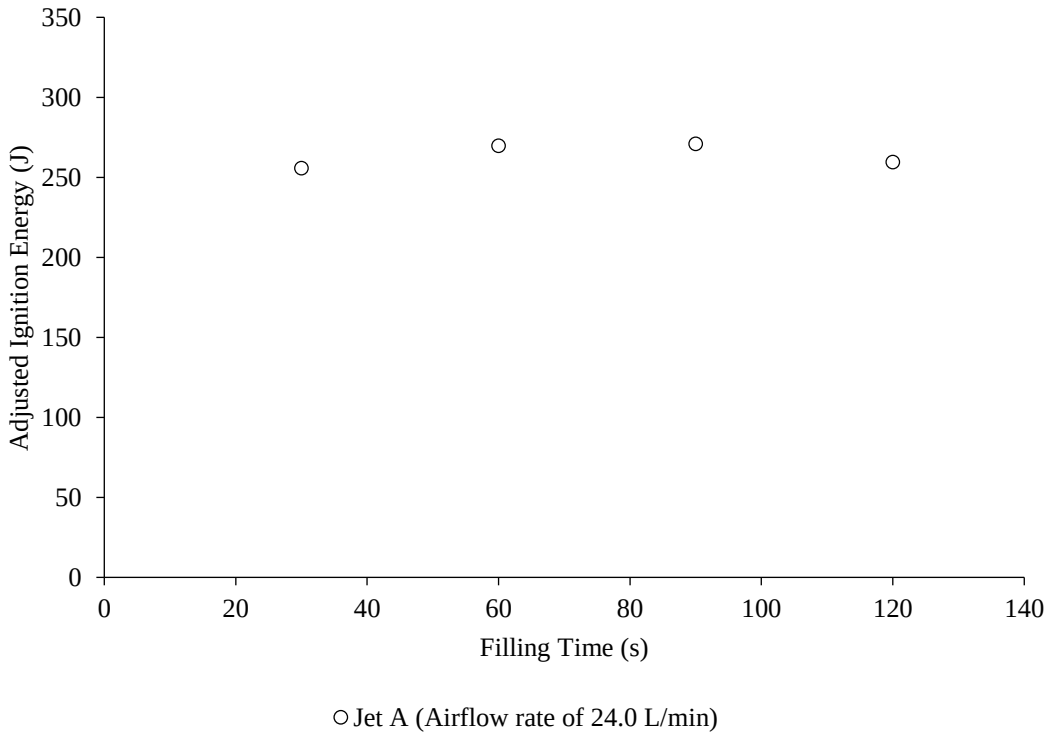

Figure 4.5: Adjusted ignition energy for Jet A, equivalence ratio 1.00, for varying fuel times at a fueling airflow rate of 24 L/min

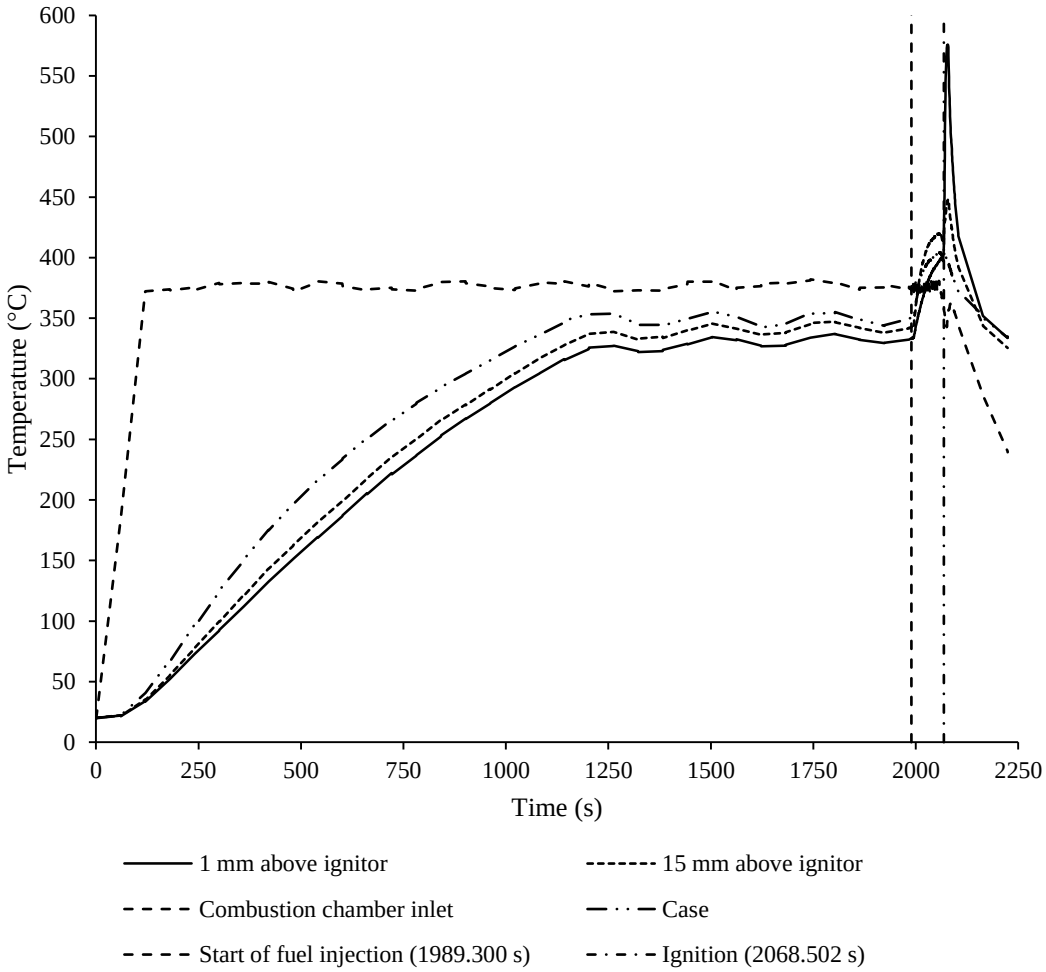

Figure 4.6: Temperatures recorded from a complete trial of Jet A at an equivalence ratio of 1.00

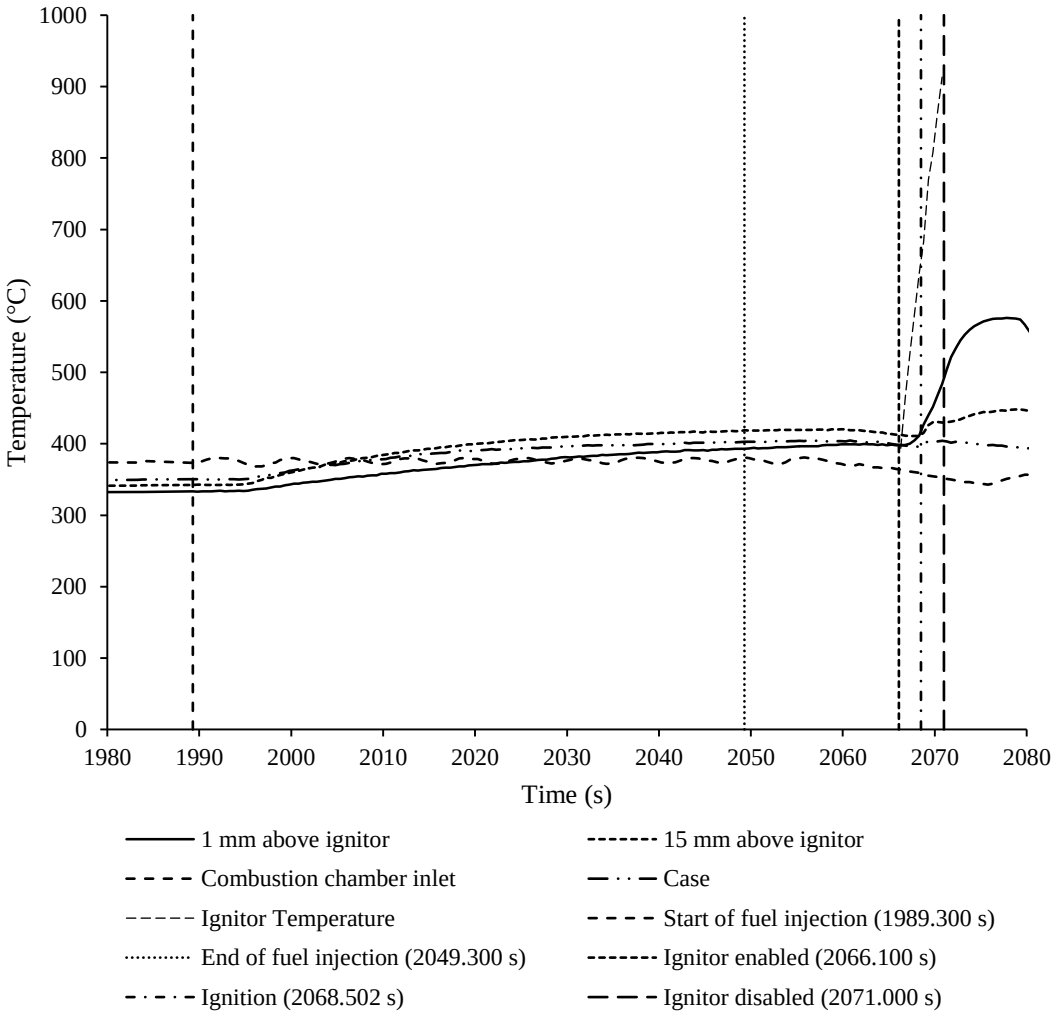

Figure 4.7: Temperatures during the fueling and ignition phases of a trial of Jet A at an equivalence ratio of 1.00

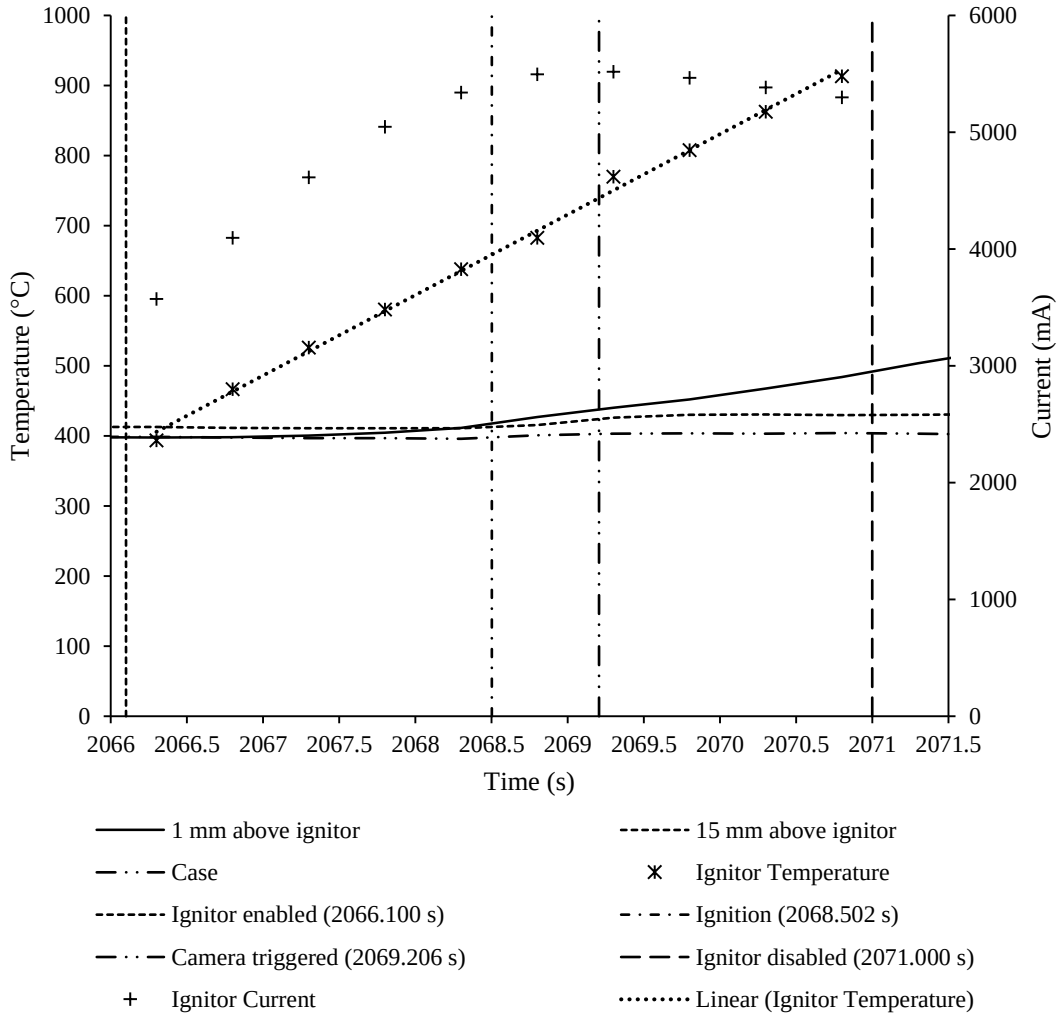

Figure 4.8: Temperature during the ignition phase of a trial of Jet A at an equivalence ratio of 1.00

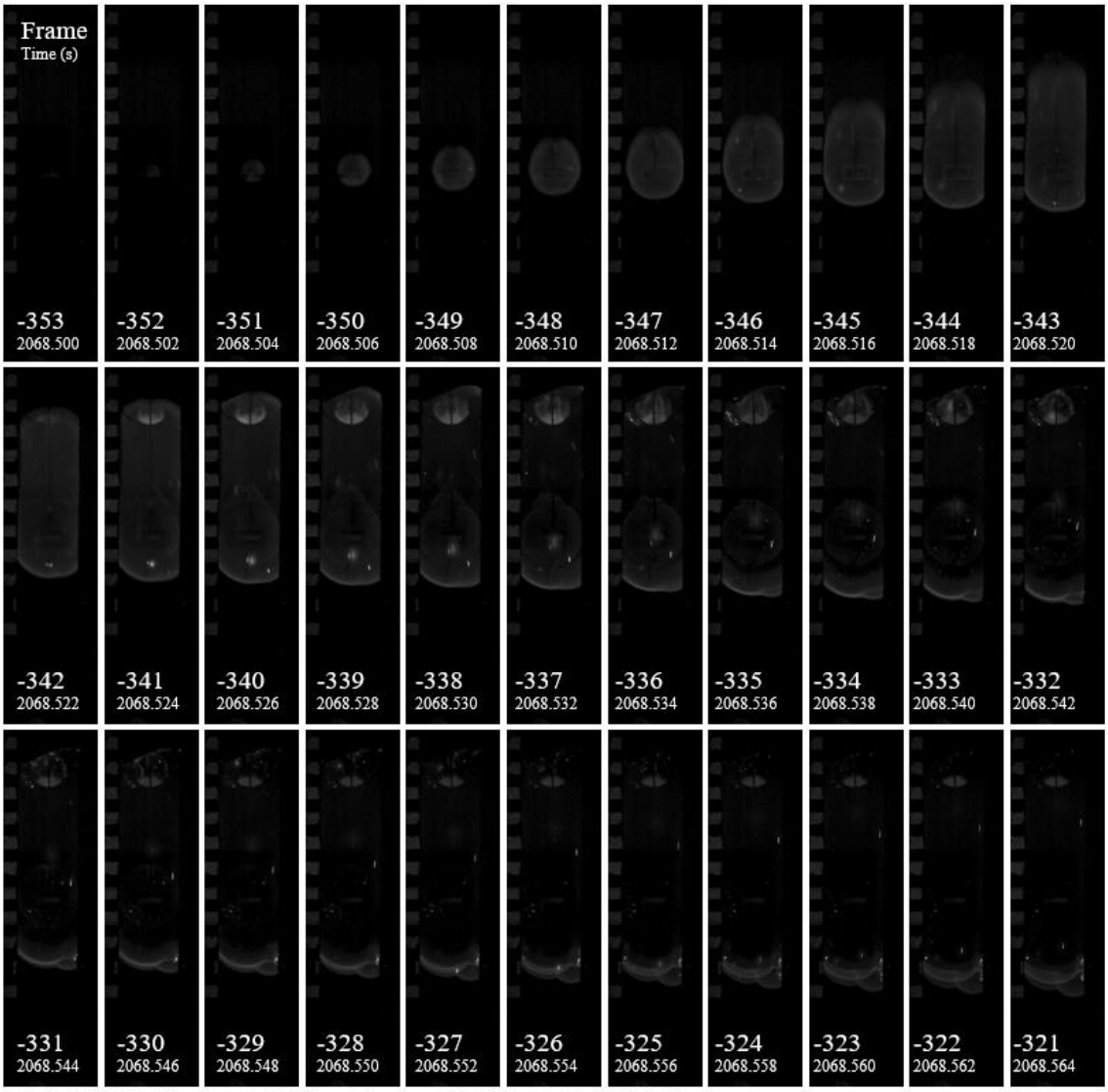

Jet A, Φ 1.00, Exposure 1997 µs, Gamma 1.7, Frame Rate 500 fps

Figure 4.9: Images captured by the high speed camera during a trial of Jet A at an equivalence ratio of 1.00

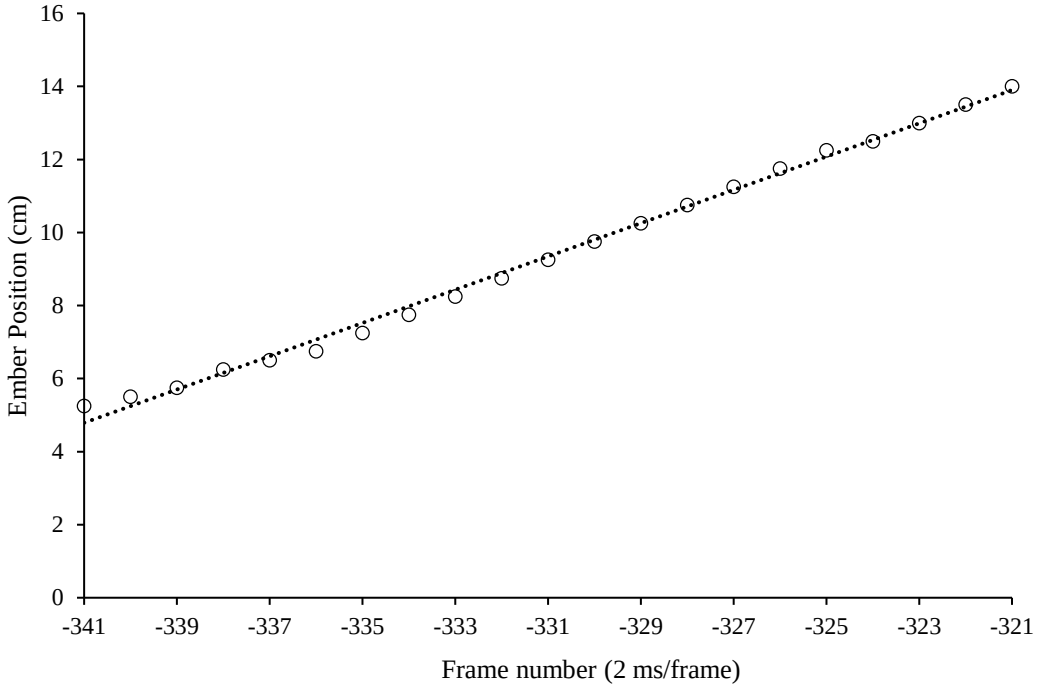

Figure 4.10: Ember position with respect to frame number for an ember in a trial of Jet A at an equivalence ratio of 1.00

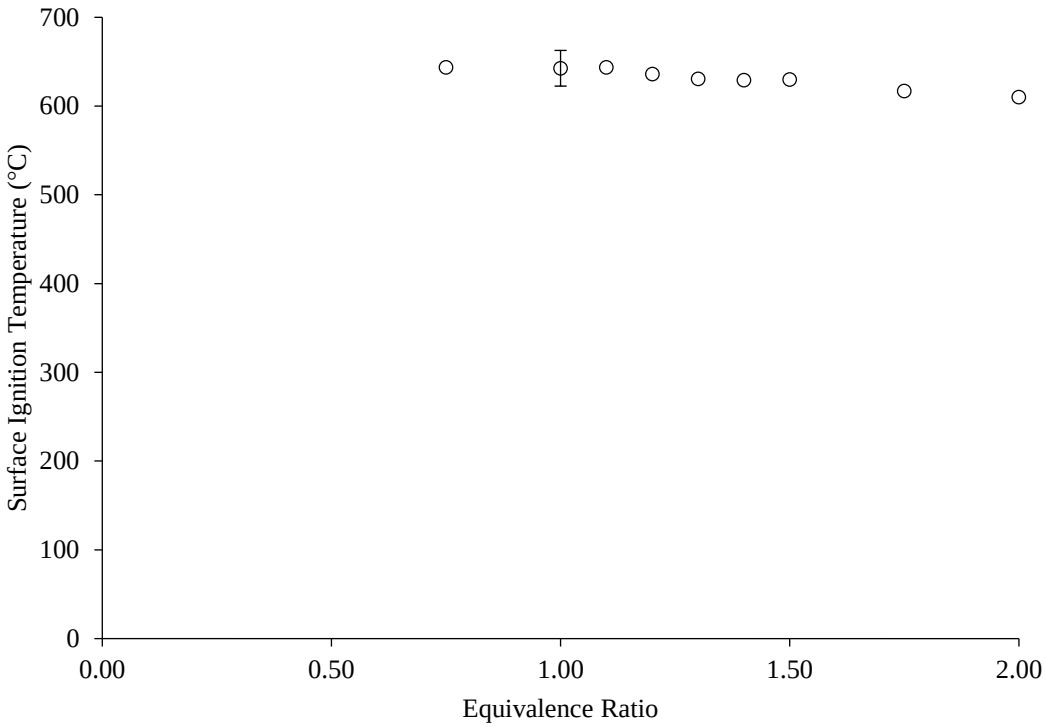

Figure 4.11: Plot of Jet A ignition temperature with respect to equivalence ratio

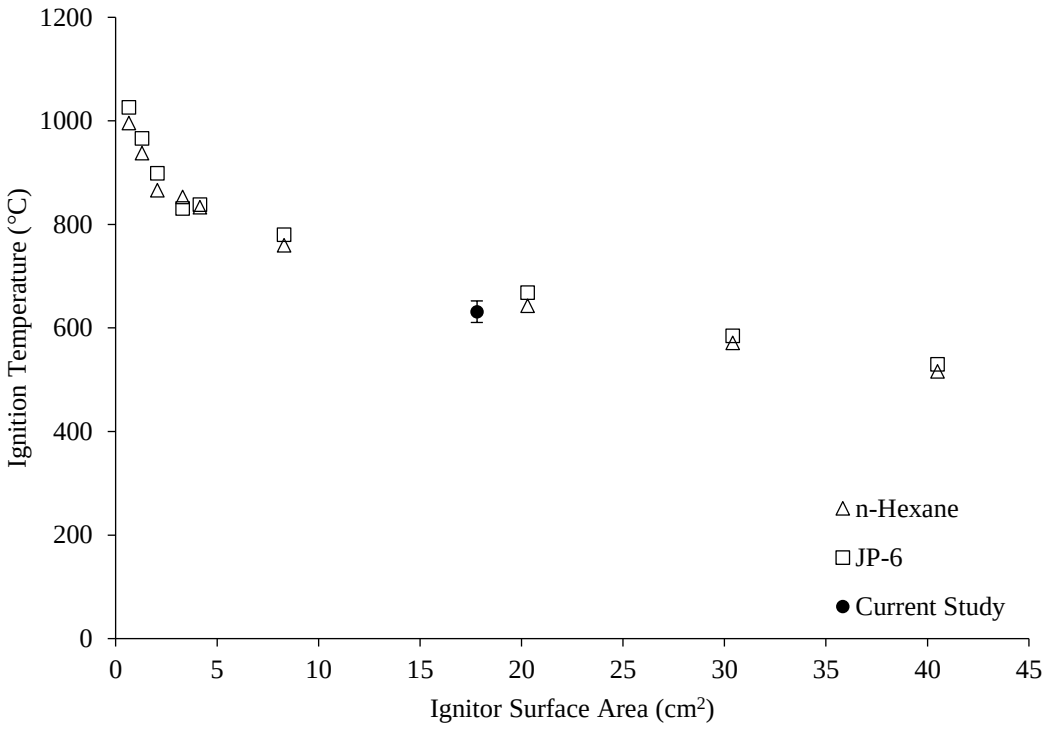

Figure 4.12: Variation in ignition temperature with ignitor size, Kuchta et al. (1965)

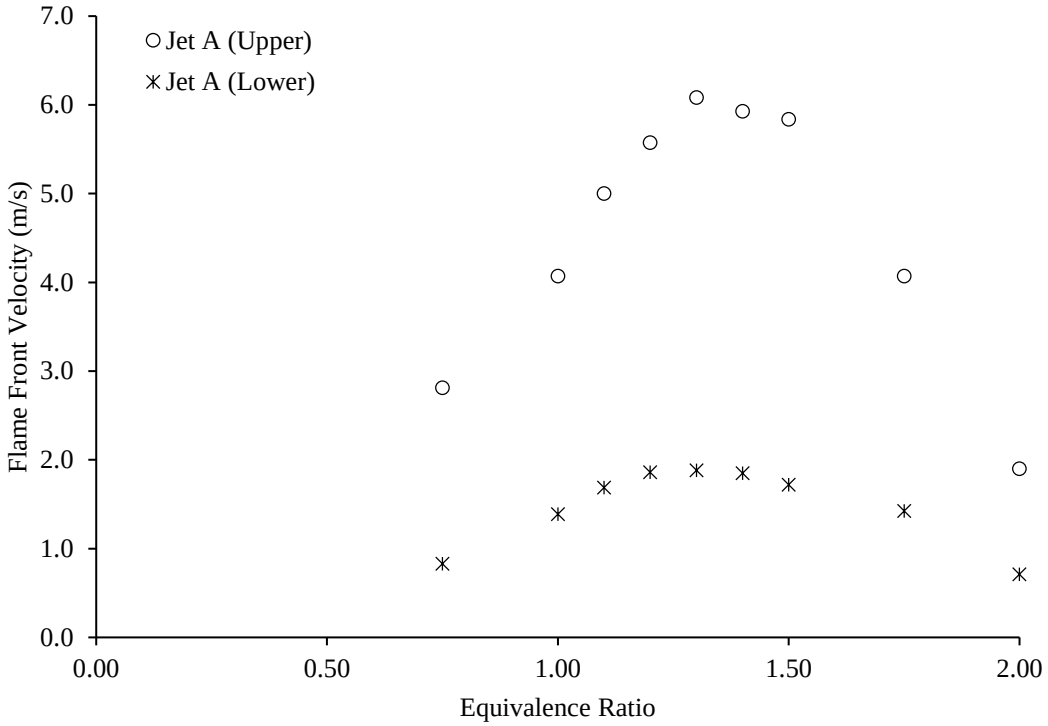

Figure 4.13: Upper and lower flame front velocities of Jet A at various equivalence ratios

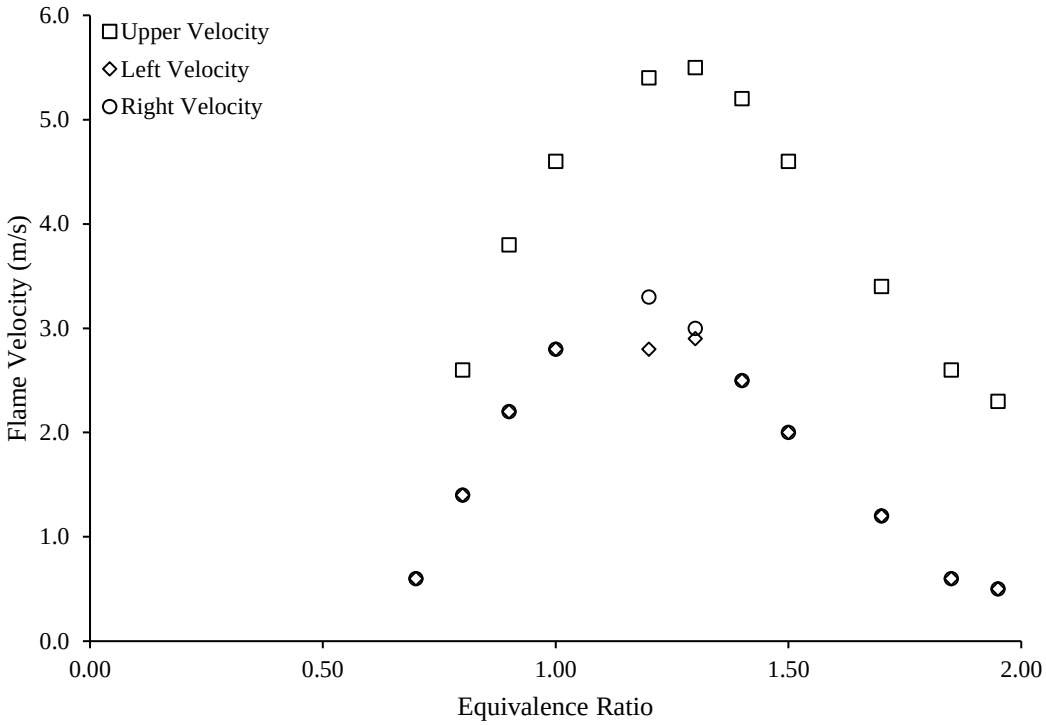

Figure 4.14: Flame velocity data for n-hexane as measured by Boettcher (2012)

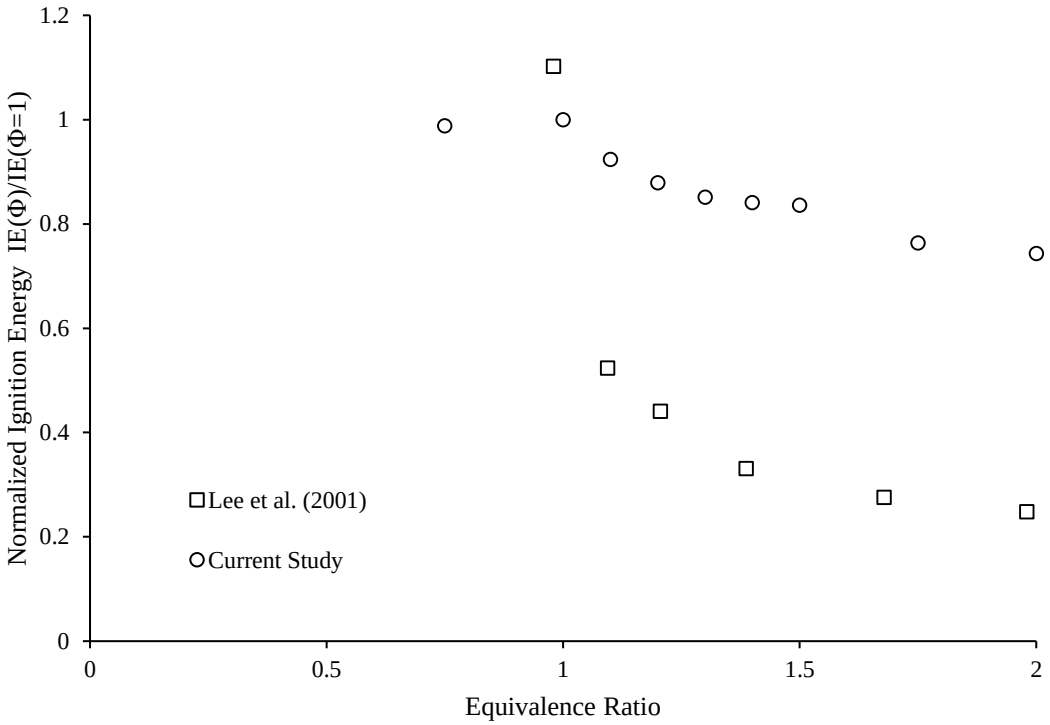

Figure 4.15: Normalized ignition energy of Jet A for the current study and Lee (2001)

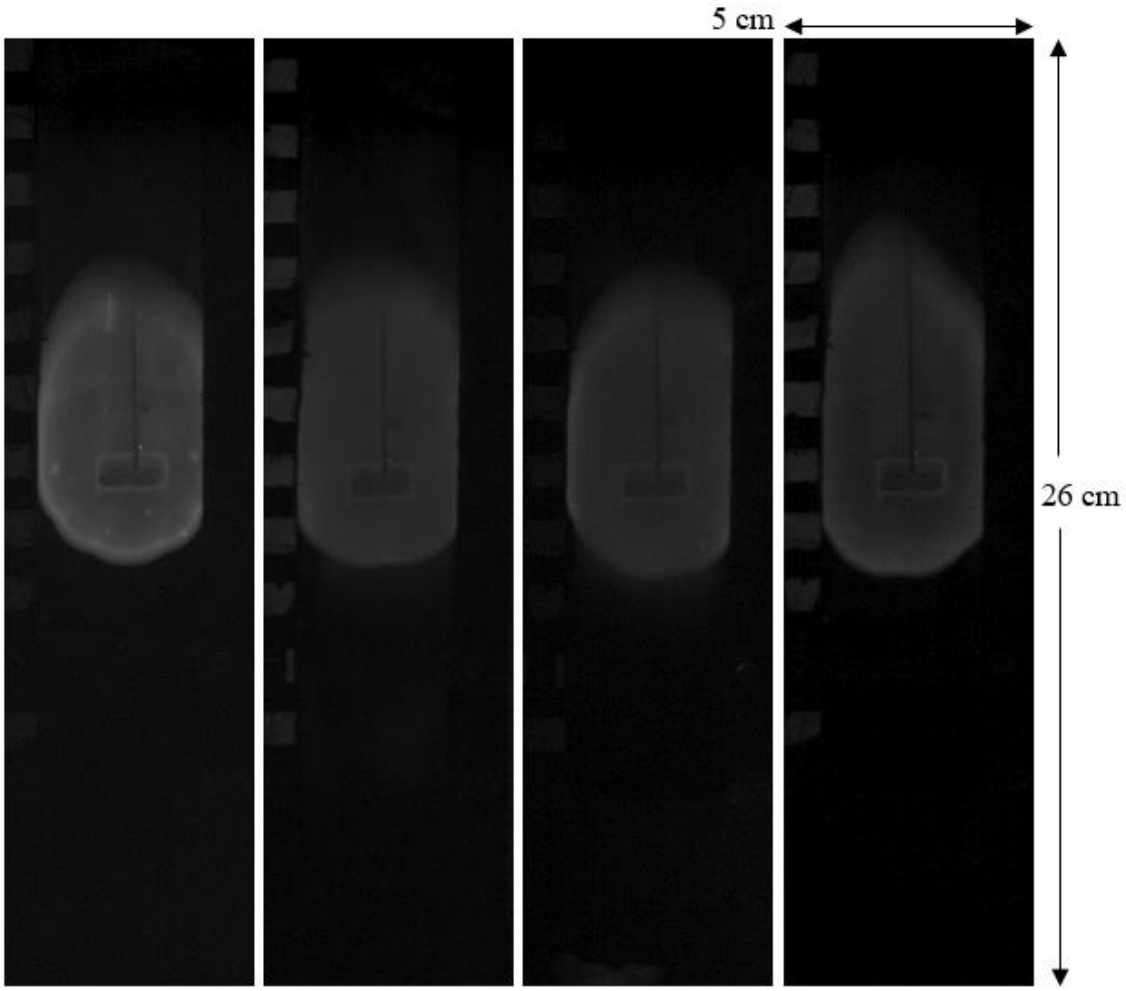

Φ 1.3, Exposure 1997 µs, Gamma 1.7, Frame Rate 500 fps

Figure 4.16: Flames of Jet A, CME, SME, and PME, at an equivalence ratio of 1.3

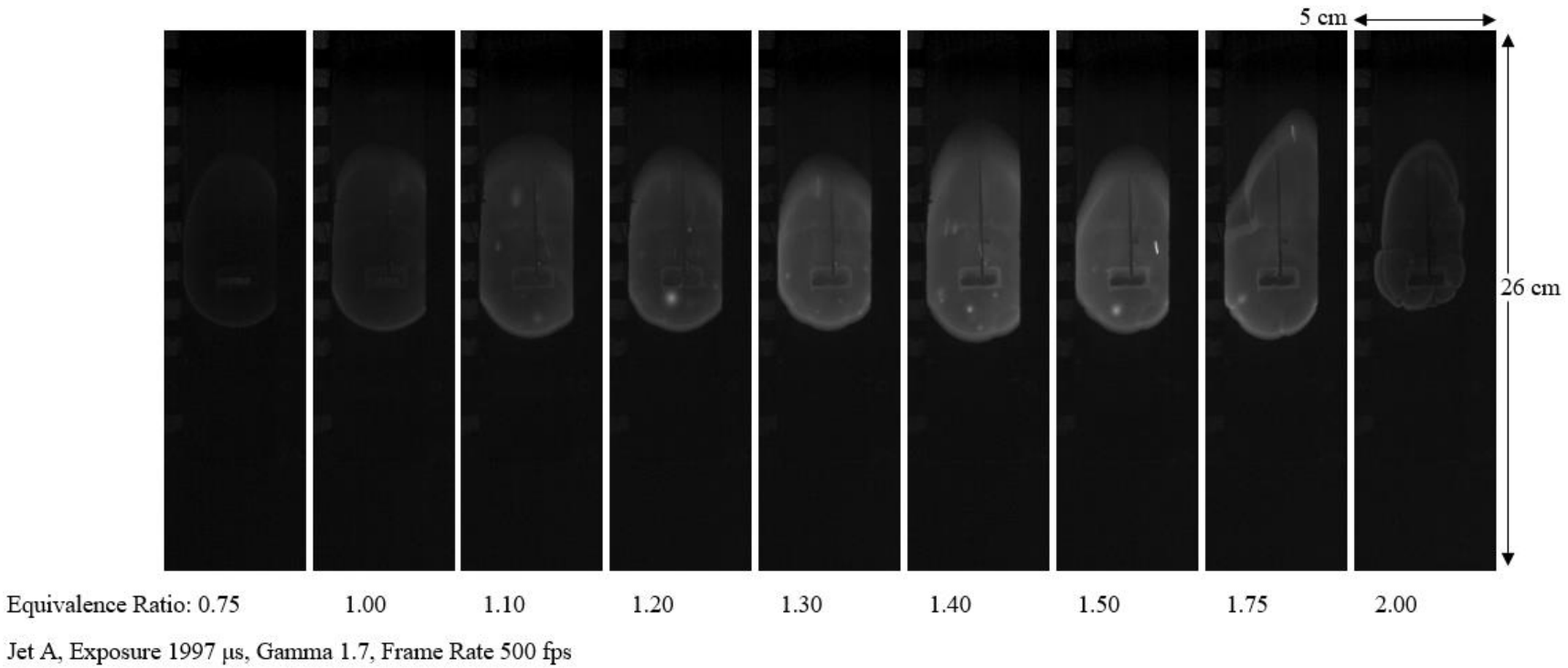

Figure 4.17: Images of Jet A flames at various equivalence ratios

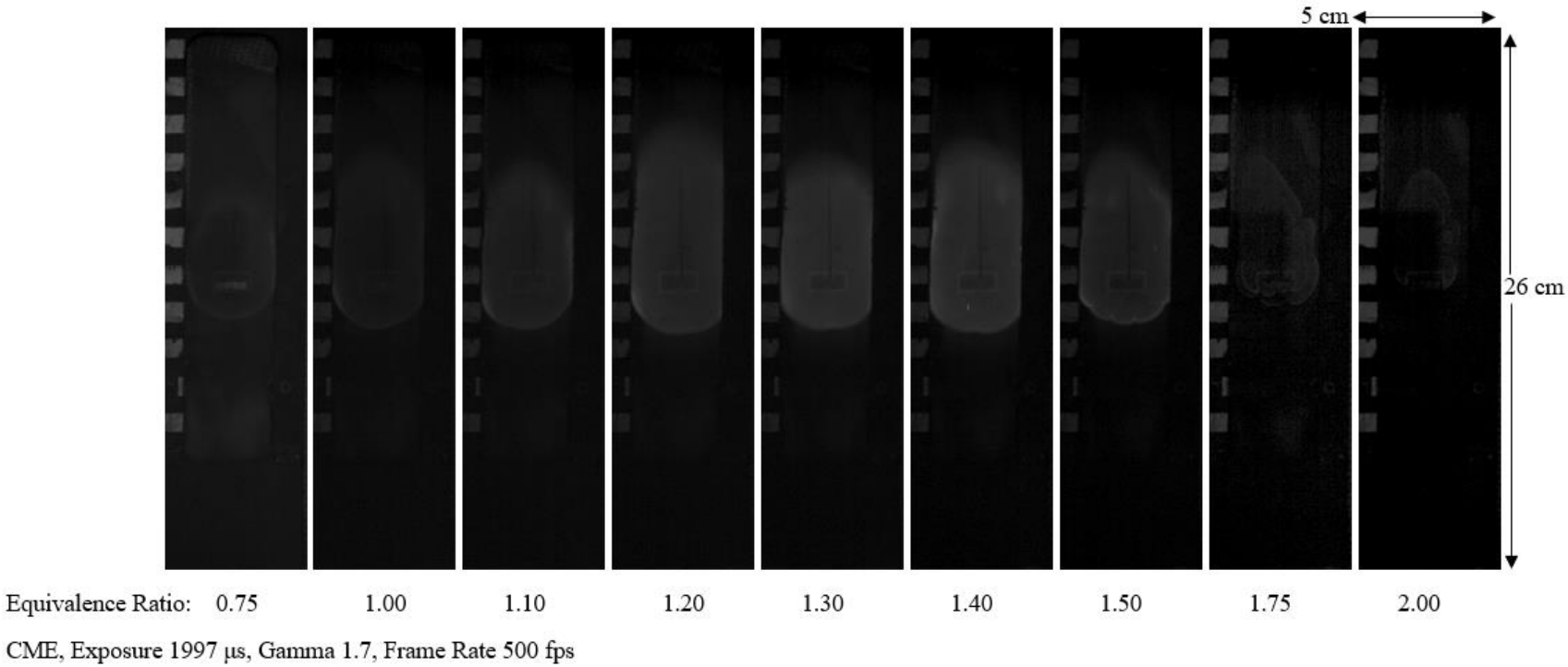

Figure 4.18: Images of CME flames at various equivalence ratios

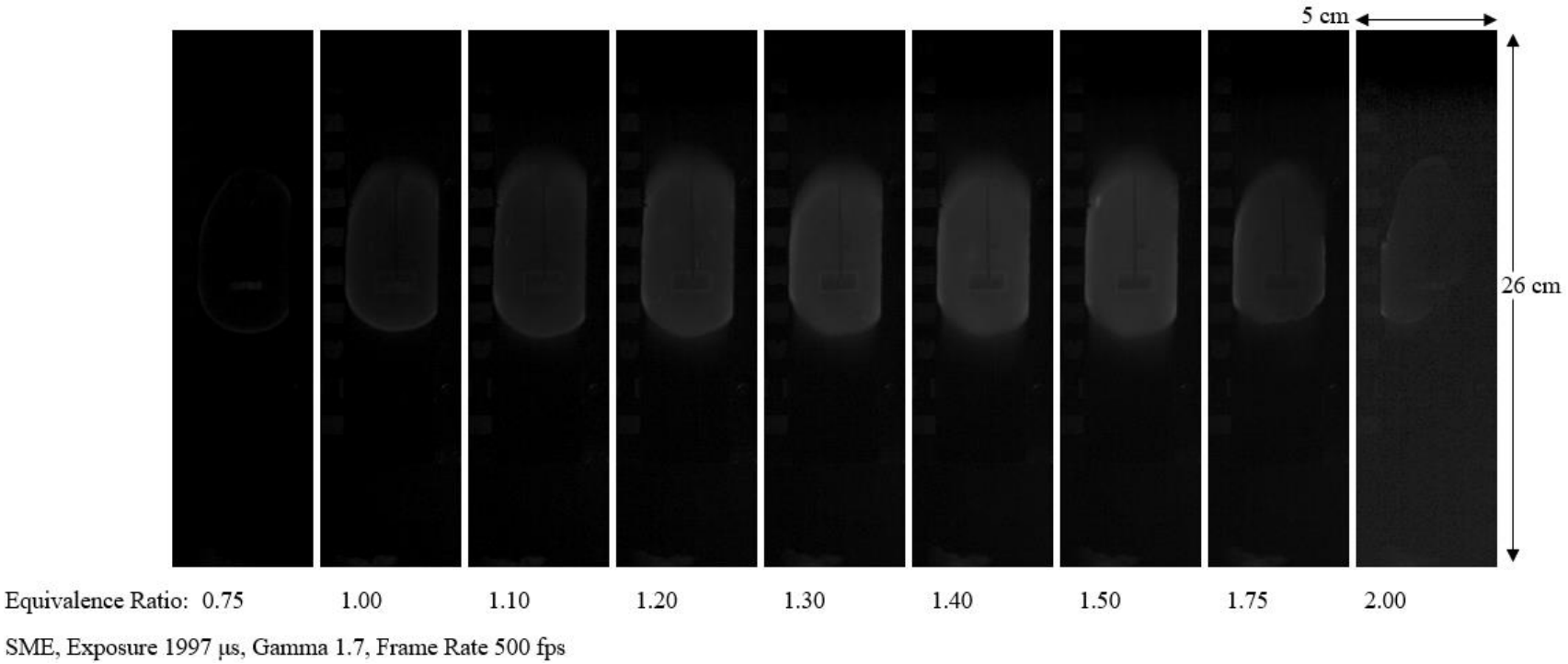

Figure 4.19: Images of SME flames at various equivalence ratios

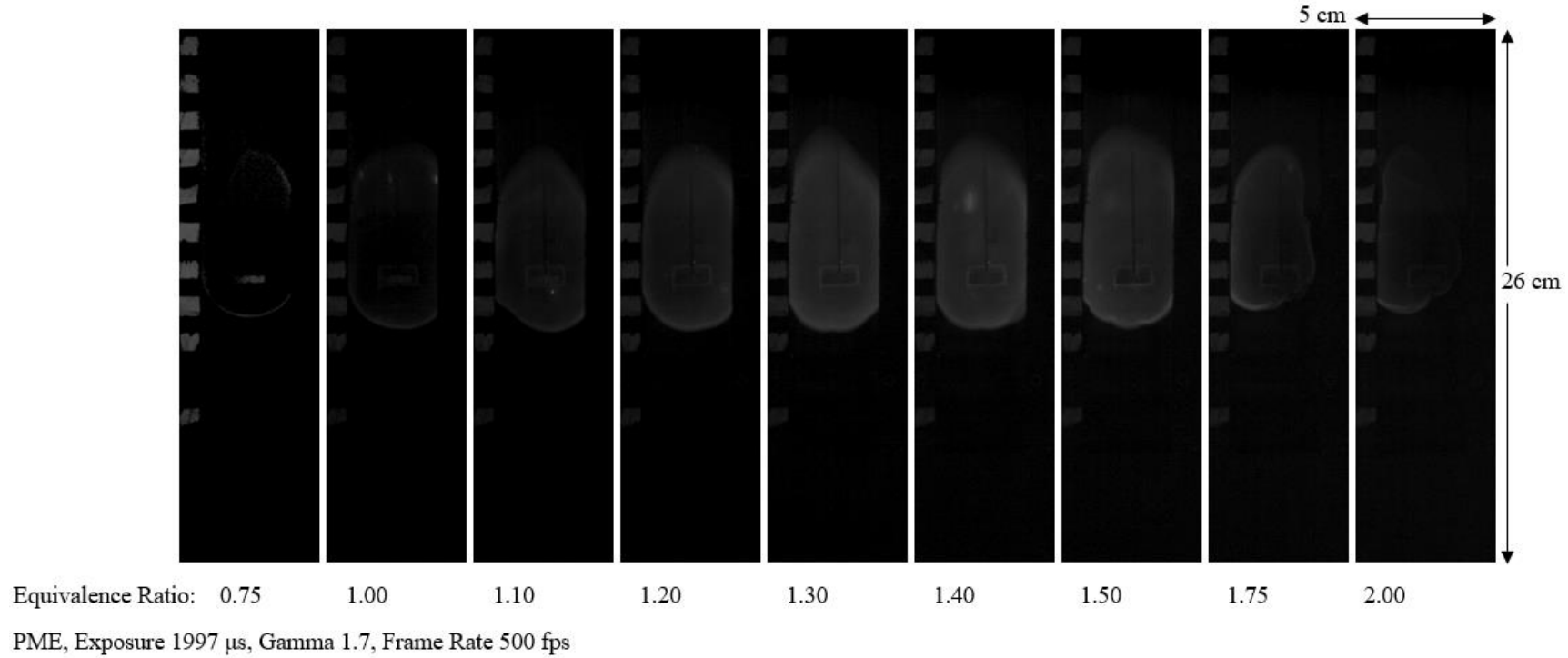

Figure 4.20: Images of PME flames at various equivalence ratios

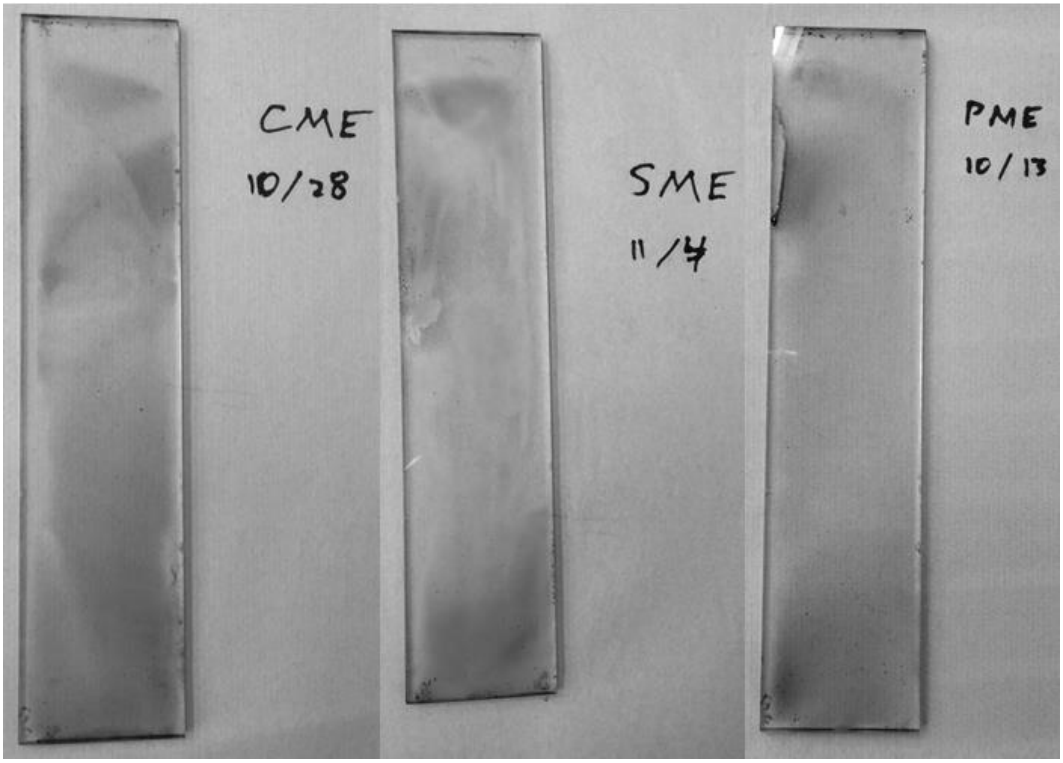

Figure 4.21: Residue left behind by CME, SME, and PME

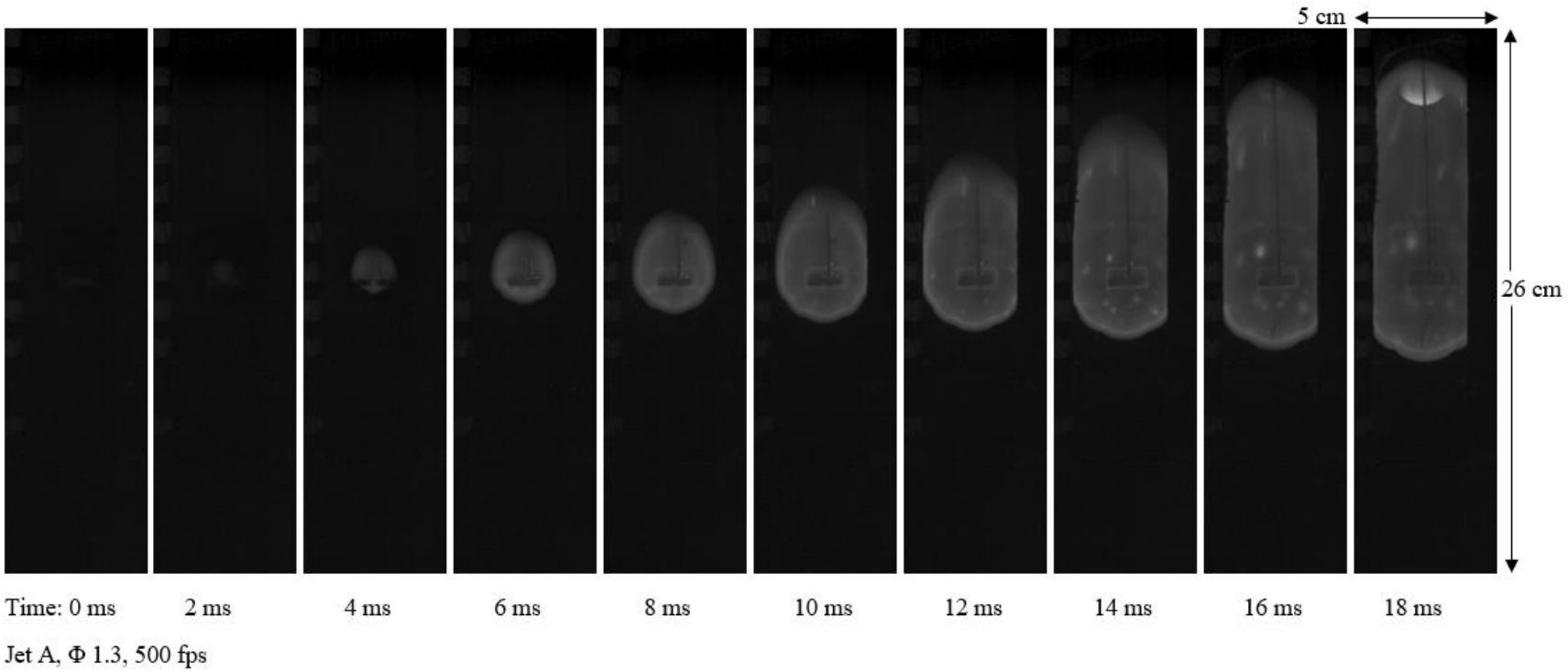

Figure 4.22: Images of Jet A flame at an equivalence ratio of 1.3

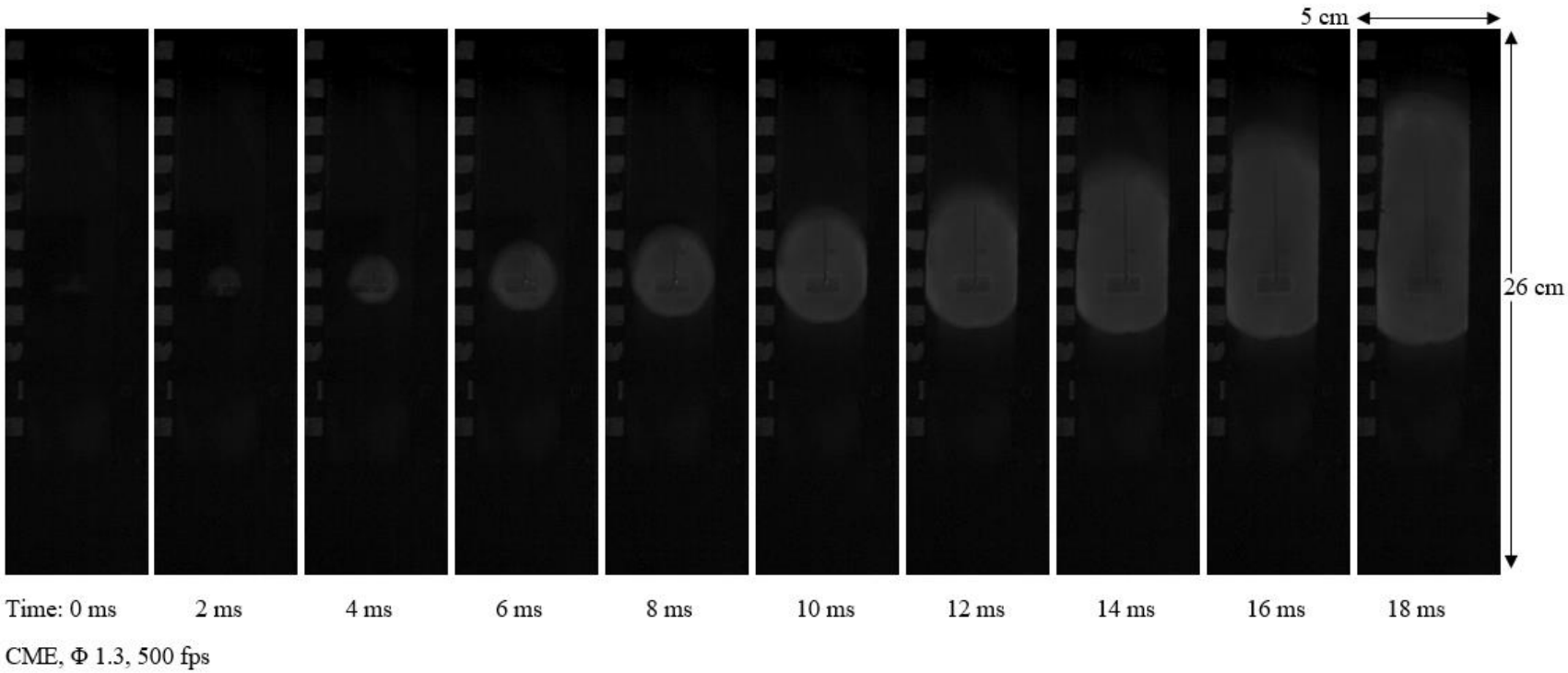

Figure 4.23: Images of CME flame at an equivalence ratio of 1.3

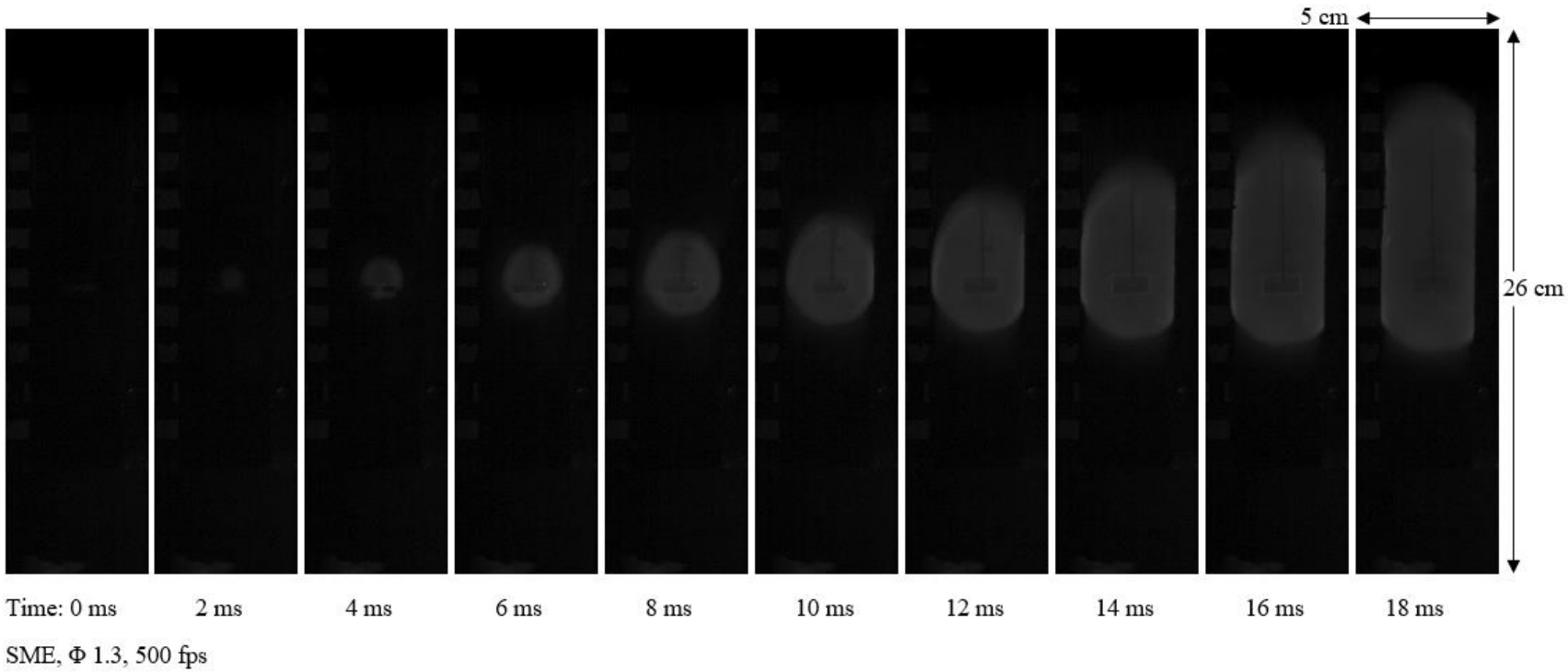

Figure 4.24: Images of SME flame at an equivalence ratio of 1.3

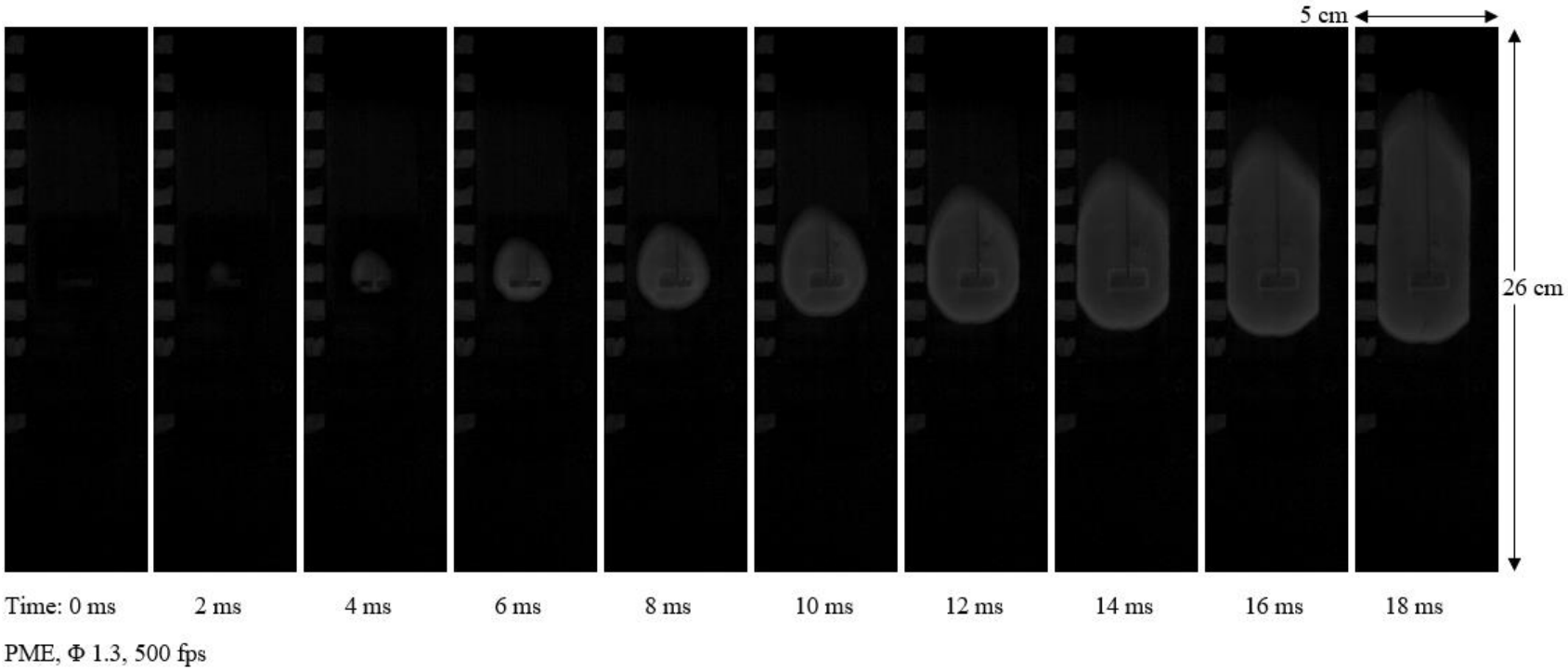

Figure 4.25: Images of PME flame at an equivalence ratio of 1.3

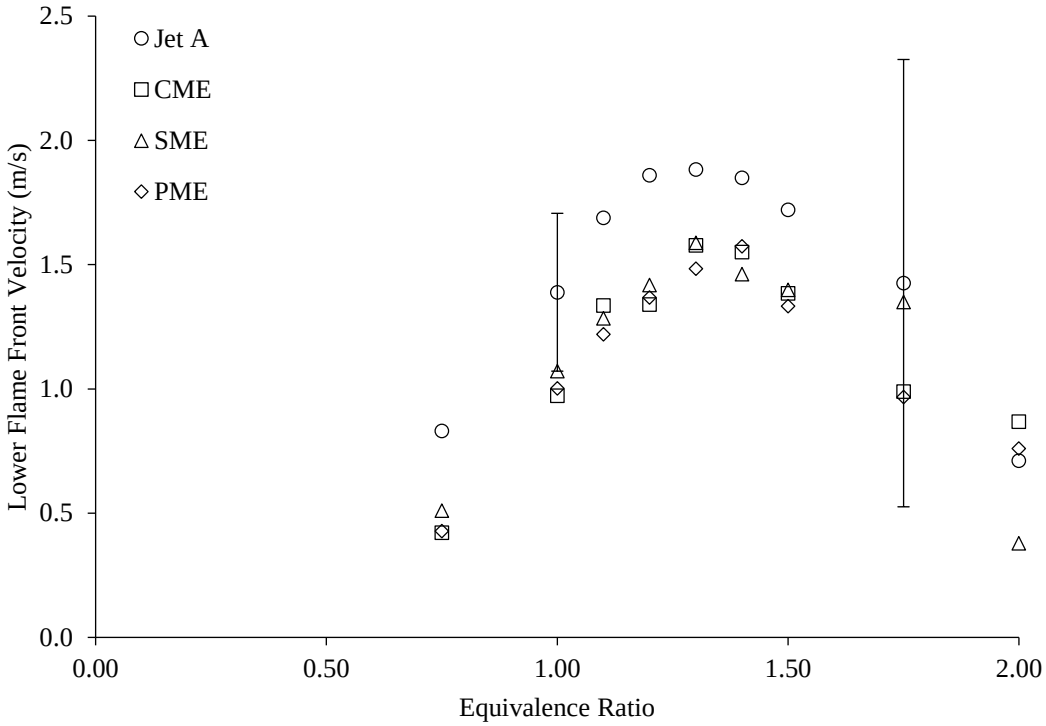

Figure 4.26: Lower flame front velocity with respect to equivalence ratio for all tested fuels

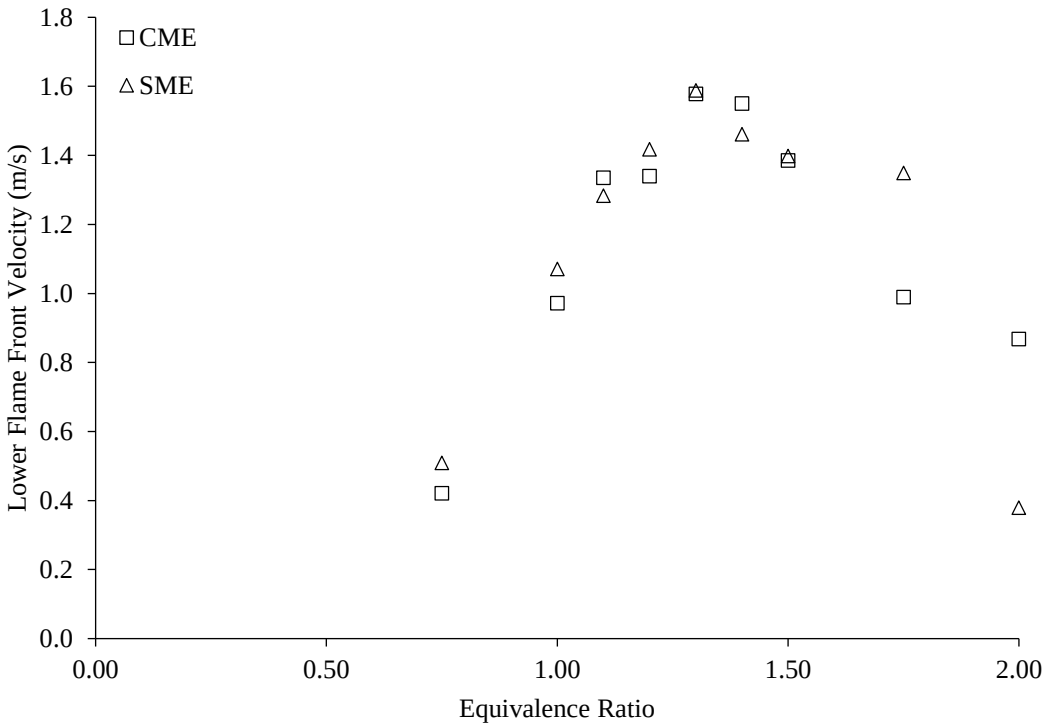

Figure 4.27: Lower flame front velocities of CME and SME

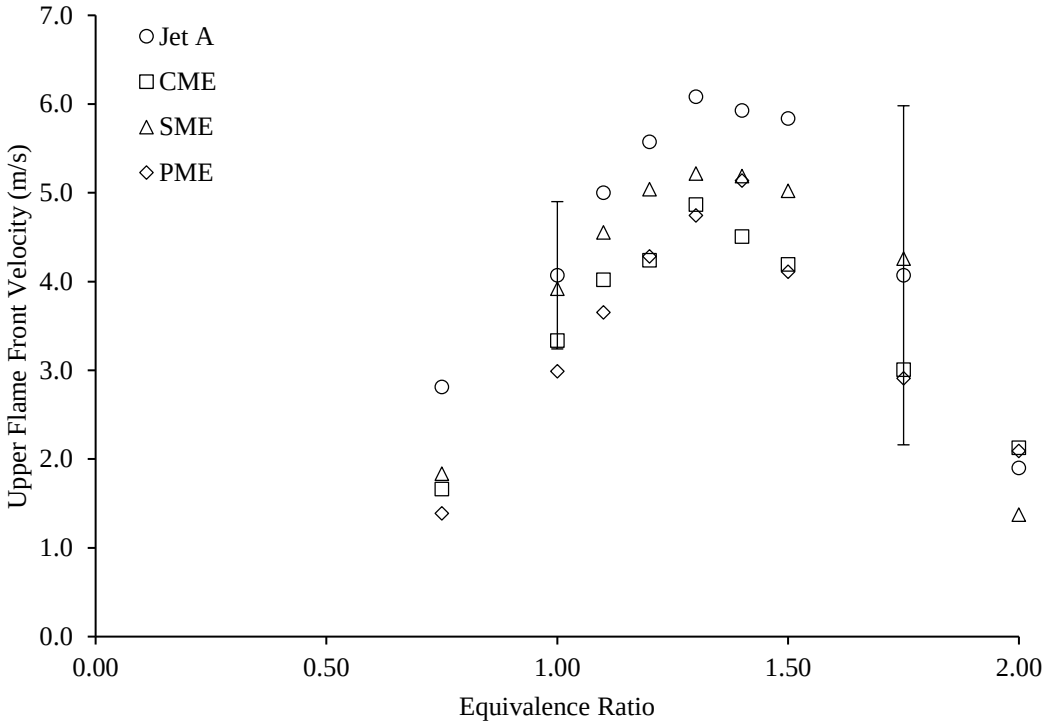

Figure 4.28: Upper flame front velocity with respect to equivalence ratio for all tested fuels

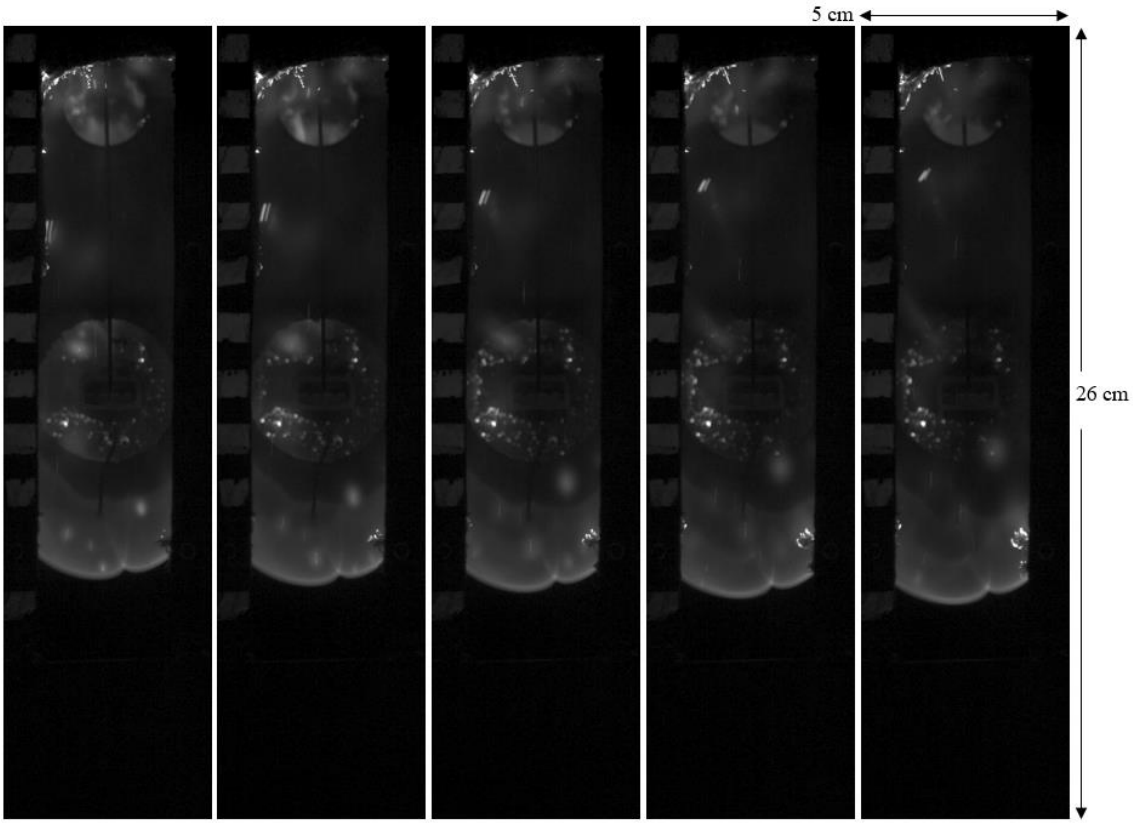

Figure 4.29: Images of sparks following the flame of Jet A at an equivalence ratio of 1.4

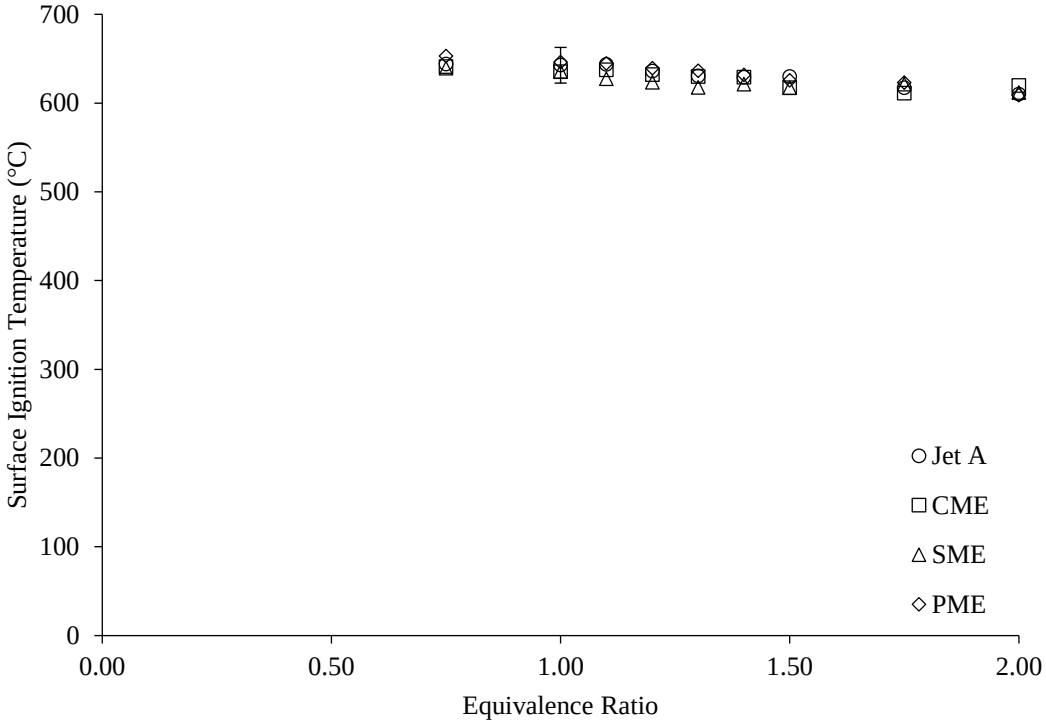

Figure 4.30: Ignition temperature with respect to equivalence ratio for all tested fuels

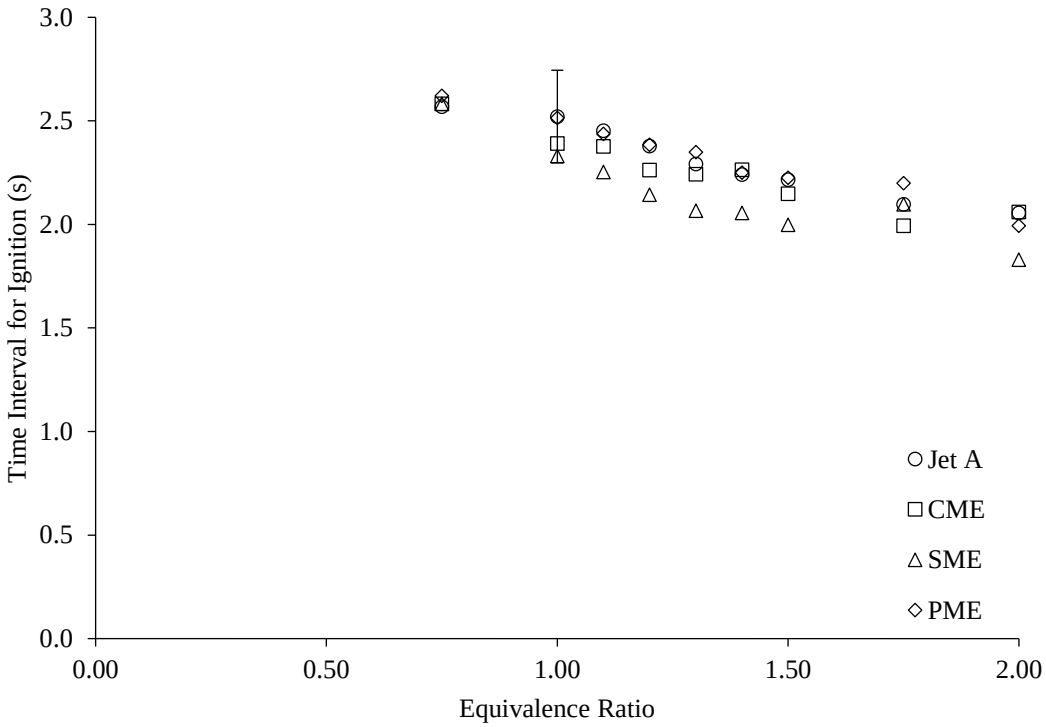

Figure 4.31: Time interval for ignition with respect to equivalence ratio for all tested fuels

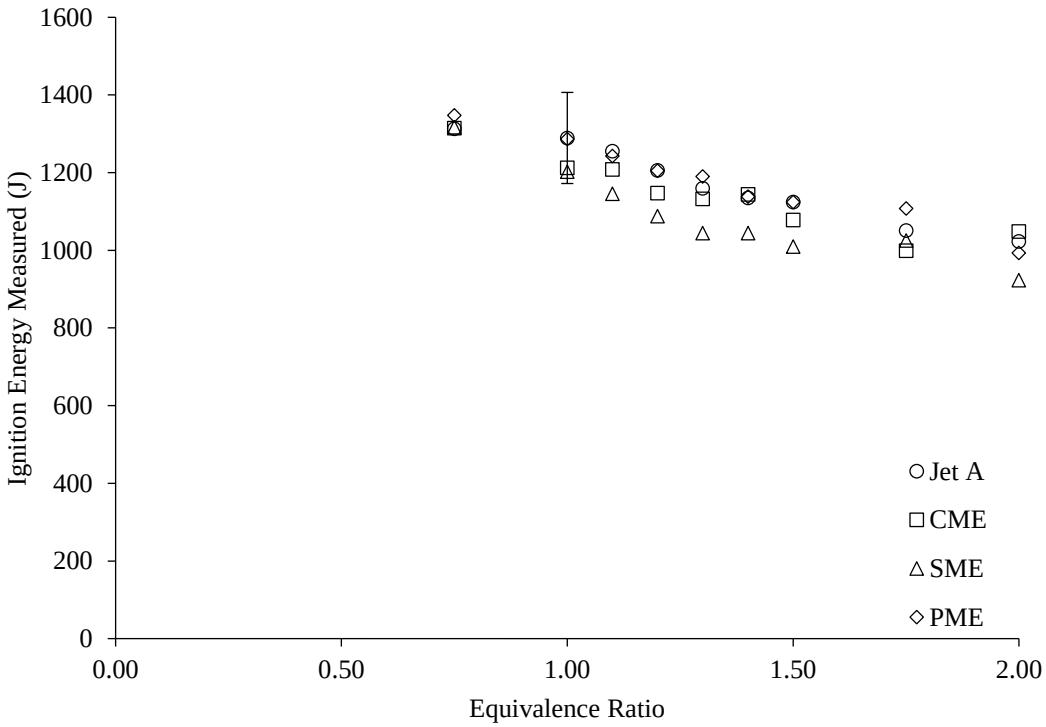

Figure 4.32: Measured ignition energy with respect to equivalence ratio for all tested fuels

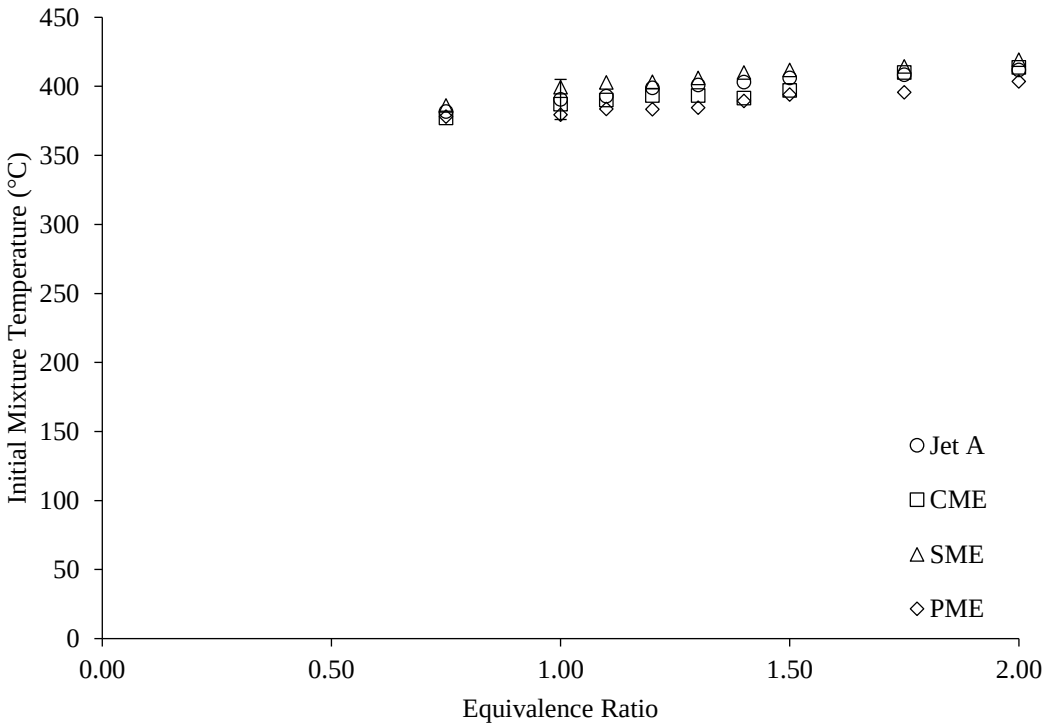

Figure 4.33: Initial mixture temperature with respect to equivalence ratio for all tested fuels

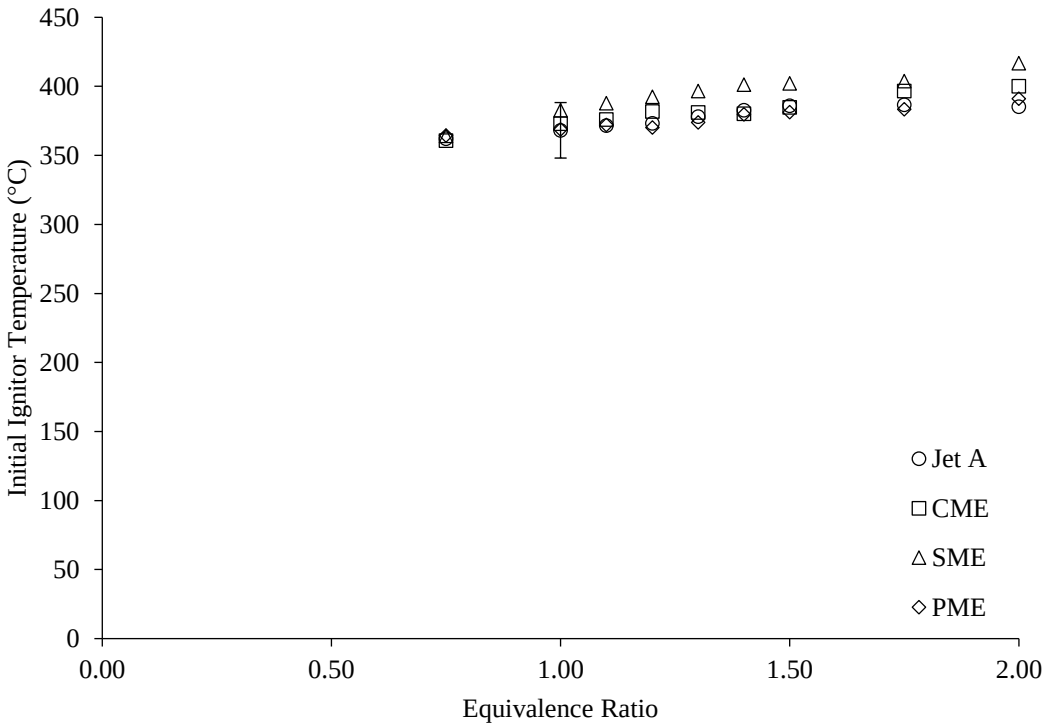

Figure 4.34: Initial ignitor temperature with respect to equivalence ratio for all tested fuels

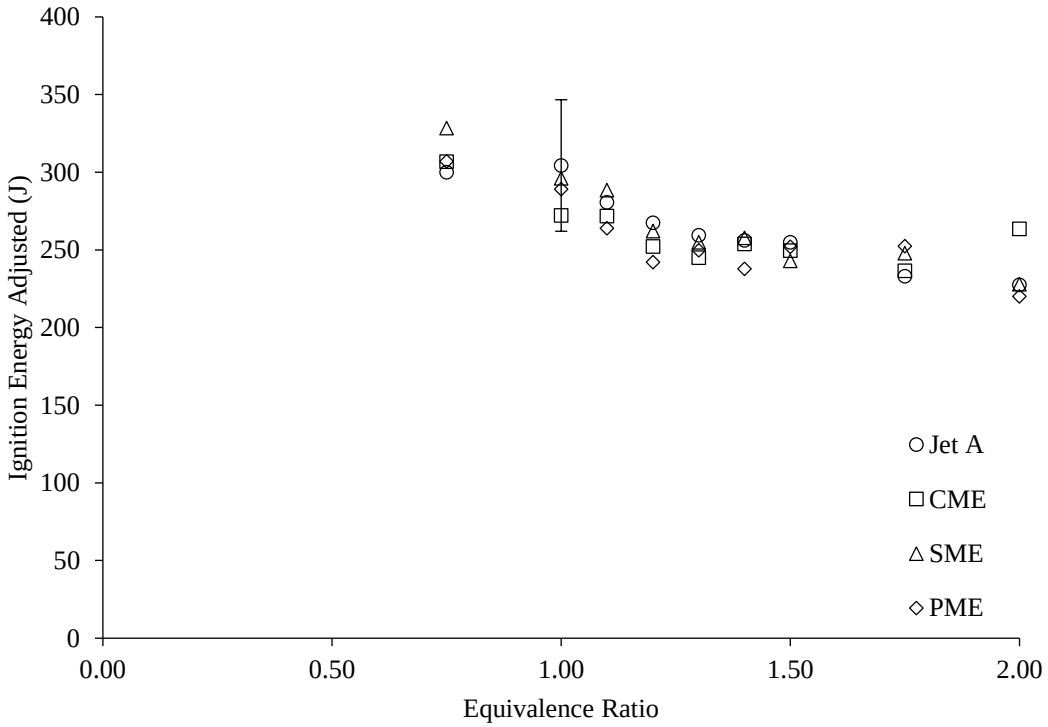

Figure 4.35: Adjusted ignition energy plotted with respect to equivalence ratio for all tested fuels

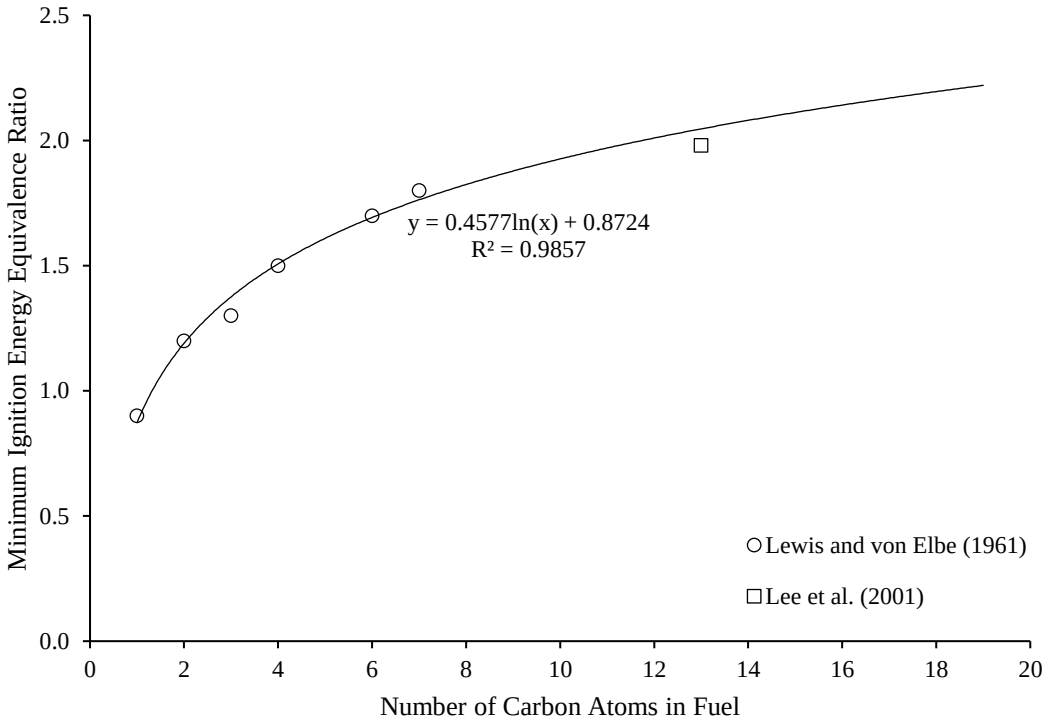

Figure 4.36: Equivalence ratio at which ignition energy is at a minimum, plotted with respect to the number of carbon atoms in the fuel for various fuels, from Lewis and von Elbe (1961) and Lee et al. (2001) data

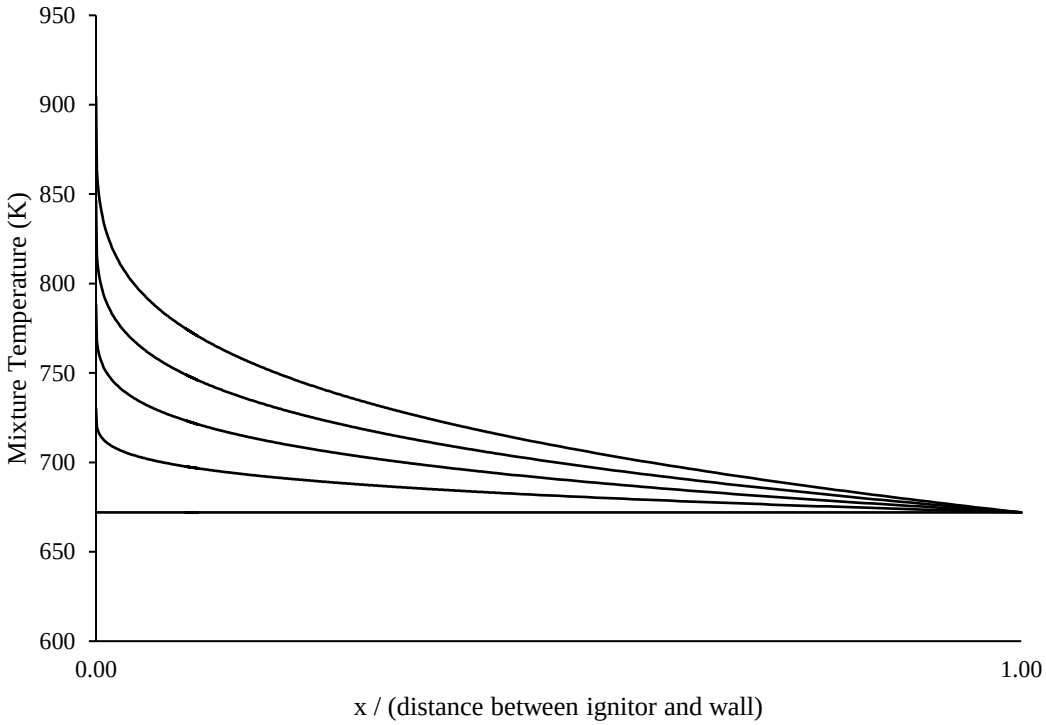

Figure 4.37: Representation of the mixture temperature with respect to distance from the ignitor, for various ignitor temperatures at x=0

Chapter 5: Summary and Conclusions

In summary, a setup was constructed to measure the fundamental ignition properties of traditional hydrocarbon fuels and biofuels. A hot surface ignition method was used with pre-vaporized liquid fuels in a quasi-stagnant environment. The ignitor was a commercially available dryer ignitor which followed a linear temperature ramp of 110 K/s. A 1.6 L steel rectangular prism, with heated and insulated walls as well as a viewing window, was used as the combustion chamber. Various fuels were tested, including Jet A, CME, SME, and PME, at various equivalence ratios, ranging from 0.75 to 2.00. Properties which were measured included the ignition temperature, ignition energy, time interval for ignition, and flame front velocity. Ignition energy was measured by monitoring the current and voltage supplied to the ignitor. Ignition temperature was determined using a relationship between the ignitor current and surface temperature. Time interval for ignition was measured as the time between the ignitor start and the first visual appearance of the flame. A high speed camera at a frame rate of 500 fps was used to measure the flame front velocities as they moved both upwards and downwards.

Based on the measurements and results, the following conclusions were drawn:

- The surface ignition temperatures did not change significantly for Jet A and biofuels with equivalence ratios, similar to trends observed with other fuels in the literature; the surface ignition temperature was about 630°C in the present setup.
- Values of time interval for ignition were similar between Jet A and biofuels, decreasing with equivalence ratios. Time interval for ignition values ranged between 2.62 s and 1.83 s for equivalence ratios between 0.75 and 2.00. As the

mixture density and fuel mass fraction increased, the mixture reactivity increased, reducing the time interval for ignition.

- Similar to the time interval for ignition, the ignition energy was similar between Jet A and biofuels, decreasing with equivalence ratio. After adjustments for energy lost to radiation or heating the ignitor, the minimum ignition energy occurred at values of approximately 250 J at equivalence ratios of 1.3 to 2.0. These values were six orders of magnitude greater than values published for spark ignition of similar fuels, due to the amount of fuel being heated, the high temperature of a spark, and natural convection effects on thermal energy diffusion. Ignition energies decreased due to a decrease in time interval for ignition and an increase in reaction rate, as indicated by the flame velocity increase and time interval for ignition decrease.
- Flame velocities peaked at equivalence ratios of 1.3-1.4 with maximum velocities of 6.08 m/s upwards and 1.88 m/s downwards for Jet A. The biofuels had flame velocities of 70-83% of that of Jet A Upper flame front velocities were larger due to significant buoyancy effects cause by the high temperature flame. Biofuels had a lower flame front velocity (70-83% of Jet A) due to slower reaction rates. The flame velocities measured were larger than similar studies found in literature due to higher temperatures in the current study and the dependence of flame velocity on temperature.

5.1 Recommendations

The following recommendations are made regarding future research related to the current study:

- Study the ignition properties of biodiesel and petroleum fuel blends.
- Measure the flame temperature using a fast response thermocouple.
- Determine the effects of ignitor size and heat ramp characteristics on ignition energy and time interval for ignition.

References

Agarwal, A. K., (2007) “Biofuels (alcholos and biodiesel) applications as fuels for internal combustion engines,” *Progress and Energy and Combustion Science,* vol. 33, pp. 233-271, 2007.

Balakrishnan, A., Parthasarathy, R., and Gollahalli, S., “Combustion Characteristics of Partially Prevaporized Palm Methyl Ester and Jet A Fuel Blends,” *Journal of Energy Resources Technology,* vol. 138, N. pag., 2016.

Balakrishnan, A., Parthasarathy, R. N., and Gollahalli, S. R., “Effects of degree of fuel unsaturation on NOx emission from petroleum and biofuel flames,” *Fuel,* vol. 182, pp. 798-806, 2009.

Boettcher, P. A., (2012) “Thermal Ignition,” Ph.D. Thesis, California Institute of Technology, Pasadena, California, USA.

Botteri, B. P., Gerstein, M., Horeff, T., and Parker, J., “Aircraft Fire Safety,” Advisory Group for Aerospace Research and Development, North Atlantic Treaty Organization, 1979.

Colwell, J. D., and Reza, A., “Hot Surface Ignition of Automotive and Aviation Fluids,” *Fire Technology,* vol. Second Quarter, no. 41, pp. 105-123, 2005.

Coordinating Research Council, “Aviation Fuel Properties,” Atlanta, 1983.

Gieck, K., and Gieck, R., *Engineering Formulas 6th Edition*, Heilbronn: McGraw-Hill, Inc, 1990.

Gomez-Meyer, J. S., Gollahalli, S. R., Parthasarathy, R. N., and Quiroga, J. E., "Laminar flame speed of soy and canola biofuels," *Ciencia, Technologia y Futuro,* vol. 4, no. 5, pp. 76-83, 2012.

Hashimoto, N., Ozawa, Y., Mori, N., Yuri, I., and Hisamatsu, T., "Fundamental combustion characteristics of palm methyl ester (PME) as alternative fuel for gas turbines," *Fuel,* vol. 87, no. 15-16, pp. 3373-3378, 2008.

Kahn, R. S., Kobayashi, S., Beuthe, M., Gasca, J., Greene, D., Lee, D. S., Muromachi, Y., Newton, P. J., Plotkin, S., Sperling, D., Wit, R., and Zhou, P. J., "Transport and its Infrastructure. In Climate Change 2007: Mitigation," Contribution of Working Group III to the Fourth Assessment Report of the Intergovernmental Panel on Climate Change [B. Metz, O.R. Davidson, P.R. Bosch, R. Dave, L.A. Meyer (eds)], Cambridge University Press, Cambridge, United Kingdom and New York, NY, USA., 2007.

Klopfenstein, W., "Effect of molecular weights of fatty acid esters on cetane numbers as diesel fuels," *Journal of American Oil Chemists' Society,* vol. 62, no. 6, pp. 1029-1031, 1985.

Ko, Y., Anderson, R. W., and Arpaci, V. S., "Spark Ignition of Propane-Air Mixtures Near the Minimum Ignition Energy: Part I. An Experimental Study," *Combustion and Flame,* vol. 83, pp. 75-87, 1991.

Kuchta, J. M., Bartkowiak, A., Spolan, I., and Zabetakis, M. G., "Flammibility Characteristics of High Temperature Hydrocarbon Fuels," Bureau of Mines, Pittsburgh, PA, 1961.

Kuchta, J. M., Bartkowiak, A., and Zabetakis, M. G., "Hot Surface Igition Temperatures of Hydrocarbon Fuel Vapor-Air Mixtures," *Journal of Chemical and Engineering Data,* vol. 10, no. 3, pp. 282-288, 1965.

Kuchta, J. M., and Cato, R. J., "Hot Gas Ignition Temperatures of Hydrocarbon Fuel Vapor-Air Mixtures," US Department of the Interior, Bureau of Mines, 1966.

Laurendeau, N. M., "Thermal Ignition of Methane-Air Mixtures by Hot Surfaces: A Critical Examination," *Combustion and Flame,* vol. 46, pp. 29-49, 1982.

Lee, T. W., Jain, V., and Kozola, S., "Measurements of Minimum Ignition Energy By Using Laser Sparks for Hydrocarbon Fuels in Air: Propane, Dodecane, and Jet-A Fuel," *Combustion and Flame,* vol. 125, pp. 1320-1328, 2001.

Lewis, B., and Von Elbe, G., *Combustion, flames, and explosions of gases,* New York: Academic Press, 1961.

Love, N. D., Parthasarathy, R. N., and Gollahalli, S. R., "Effect of Iodine Number on NOx Formation in Laminar Flames of Oxygenated Biofuels," *International Journal of Green Energy,* vol. 6, no. 4, pp. 323-332, 2009.

Macdonald, J. A., and Cansdale, J. T., "Spontaneous Ignition of Aircraft Fuel," RAE Technical Report, 1972

McCrometer, "SK McCrometer," 1996. [Online]. Available: mccrometer.com. [Accessed 12 February 2017].

Melguizo-Gavilanes, J., Boeck, L. R., Mevel, R., and Shepherd, J. E., "Hot Surface Ignition of Stoichiometric Hydrogen-Air Mixtures," *International Journal of Hydrogen Energy,* 2016.

Myronuk, D. J., "Dynamic, Hot Surface Ignition of Aircraft Fuels and Hydraulic Fluids," 1980.

Phuoc, T. X., and White, F. P., "Laser-Induced Spark Ignition of CH4/Air Mixtures," *Combustion and Flame,* vol. 119, pp. 203-216, 1999.

Pulkrabek, W., *Engineering fundamentals of the internal combustion engine*, Pearson Prentice Hall, 2004.

Rae, D., Singh, B., and Danson, R., "Safety Mines Res. Rept. No 224," 1964.

Sharon, H., Karuppasamy, K., Soban Kumar, D. R., and Sundaresan, A., "A test on DI diesel engine fueled with methyl esters of used palm oil," *Renewable Energy,* vol. 47, pp. 160-166, 2012.

Sheperd, J. E., Krok, J. C., and Lee, J. J., "Spark Ignition Energy Measurements in Jet A," 1999.

Turns, S. R., *An Introduction to Combustion*, McGraw-Hill, 2000.

United States Emvironmental Protection Agency, "Greenhouse Gas Emissions," 14 February 2017. [Online]. Available: https://www.epa.gov/ghgemissions/overview-greenhouse-gases. [Accessed 4 April 2017].

Wang, W., Gowdagiri, S., and Oehlschlaeger, M. A., "The high-temperature autoignition of biodiesels and biodiesel components," *Combustion and Flame,* vol. 161, pp. 3014-3021, 2014.

Wong, K.-F. V., *Intermediate Heat Transfer*, New York: Marcel Dekker, Inc, 2003.

Zabetakis, M. G., Furno, A. L., and Jones, G. W., "Minimum Spontaneous Ignition Temperatures of Combustibles in Air," *Industrial and Egineering Chemistry,* no. October, pp. 2173-2178, 1954.

Appendix A: Nomenclature

A	Surface area of the ignitor
C	Specific heat of the ignitor
E_{adj}	Adjusted ignition energy
$E_{C\ (specific\ heat\ of\ the\ ignitor)}$	Energy related to the specific heat of the ignitor
$E_{ignition}$	Ignition energy
$E_{R\ (radiation)}$	Energy related to the radiation from the ignitor
E_{115V}	Ignition energy corrected for voltage at 115 V
E_{120V}	Ignition energy measured assuming 120 V
fps	Frames per second
h_1	Height of the flame or ember at the first appearance
h_2	Height of the flame or ember at the last appearance
I	Ignitor current
m	Mass of the ignitor heating element
$n_{ignition}$	Frame number of the first observed flame
n_1	Frame number of the first appearance of the flame or ember
n_2	Frame number of the last appearance of the flame or ember
$P_{ignitor}$	Ignitor power output
T_{case}	Temperature of the combustion chamber interior wall
T_i	Temperature of ignitor
$t_{ignition}$	Time of ignition
$t_{recording\ started}$	Time of high speed camera trigger
$t_{0\ (ignitor\ enabled)}$	Time of ignitor enabled
ΔT	Temperature difference of the ignitor between times $t_{0\ (ignitor\ enabled)}$ and $t_{ignition}$
$\Delta t_{for\ ignition}$	Time interval for ignition
$V_{flame\ front}$	Flame front velocity
V_{gas}	Gas velocity
σ	Stefan-Boltzmann constant
Φ	Equivalence ratio